International Scientific-Technical and Production Journal

# The Paton WELDING JOURNAL

January 2004 # 1

English translation of the monthly «Avtomaticheskaya Svarka» (Automatic Welding) journal published in Russian since 1948

**Founders:** *E.O. Paton Electric Welding Institute of the NAS of Ukraine*
*International Association «Welding»*

**Publisher:** *International Association «Welding»*



***Address:***
*E.O. Paton Electric Welding Institute,*
*International Association «Welding»,*
*11, Bozhenko str., 03680, Kyiv, Ukraine*
*Tel.: (38044) 227 67 57*
*Fax: (38044) 268 04 86*
*E-mail: journal@paton.kiev.ua*
*http://www.nas.gov.ua/pwj*

State Registration Certificate
KV 4790 of 09.01.2001

***Subscriptions:***
$460, 12 issues per year,
postage and packaging included.
Back issues available.



## CONTENTS

# EFFECT OF HEAT OF ALUMINIUM ALLOY MELTING ON SHAPE AND SIZES OF WELD POOL

V.A. KARKHIN[1], A.S. ILIIN[1], V.V. PLOSHIKHIN[2] and A.A. PRIKHODOVSKY[2]
[1]St.-Petersburg State Polytechnik University, St.-Petersburg, Russia
[2]New Materials Bairout GmbH, Germany

An algorithm is developed for solving the quasi-stationary temperature problem taking into account the heat of melting and solidification, based on the method of sources (Green function). The case of welding thin aluminium plate is used to demonstrate that the melting heat has a significant influence on the shape and dimensions of the weld pool and solid-liquidus zone. It is noted that the thermal efficiency of the process of melting $\eta_t$ of a plate by a linear source can be much higher than 0.4839 with allowance for the melting heat. Known simplified methods with allowance for melting heat may lead to significant errors in $\eta_t$ determination. A comparison of calculated and experimental shape of the weld pool is given.

***Keywords:*** *fusion welding, equation of heat conductivity, melting heat, weld pool, calculation, method of sources*

When the thermal processes are analyzed, the known analytical solutions of the temperature problem, which do not take into account the effect of heat of phase transitions, are usually used [1–3]. The advantage of these solutions is the generalization and simplicity of realization, while the drawback is the significant error in results of calculation in the high-temperature region. If the heat of phase transitions in solid state is relatively low and it can be neglected, then the share of a melting heat in total heat of molten metal can reach 40 % and more (for example, in case of aluminium alloys). Numerical methods can make allowance for heat of melting and solidification (crystallization) [4–6]. However, the published results of investigations have, as a rule, a particular nature, therefore, it is difficult to reveal the general laws and to answer the question: when is it possible not to make an allowance for melting heat and what error of calculation is here?

The aim of the present investigation was to analyze the effect of heat of melting and solidification on temperature fields in butt welding of thin aluminium plates and to evaluate the error of calculation of sizes and shape of weld pool at indirect allowance and non-allowance for melting heat.

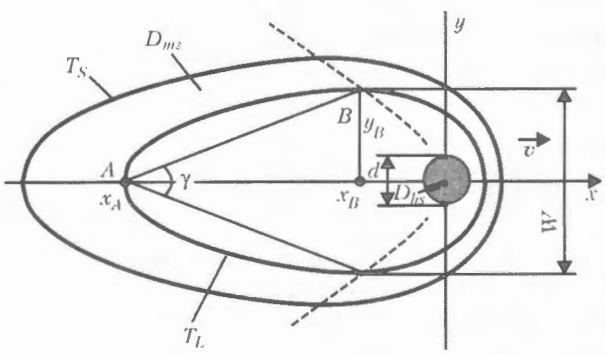


**Figure 1.** Scheme of weld pool and heat source (dash lines separate the zone of heating from zone of cooling; see designations in text)

**Solution of temperature problem with allowance for melting heat.** Let us formulate the temperature problem at the following assumptions: a body represents a homogeneous unlimited plate without temperature drop across its thickness $h$ (temperature field is two-dimensional); properties of the material (heat conductivity $\lambda$, specific heat capacity $c$, density $\rho$ and coefficient of surface heat transfer $\alpha$) do not depend on temperature $T$; temperature interval of the phase transition is known, heat of solidification is equal to melting heat, and the heat of transformations in solid phase is not taken into account; heat source is moved straightline along axis $x$ at constant rate $v$ (Figure 1); in movable system of coordinates $x$, $y$ connected with a heat source, the temperature field is not changed (field is quasi-stationary); there are no convective flows in a molten pool; heat exchange with environment is occurred by Newton law; temperature of medium is constant and equal to initial temperature $T_0$. Then the equation of energy balance in the movable system of coordinates has a form

$$\lambda\nabla^2 T + v\rho\frac{\partial H}{\partial x} - \frac{2\alpha}{h}(T - T_0) + \frac{q_2}{h} = 0, \qquad (1)$$

where $\nabla^2 = \partial^2/\partial x^2 + \partial^2/\partial y^2$ is the Laplace operator; $q_2$ is the density of effective power of surface source; $H$ is the enthalpy.

By distinguishing melting heat $H$ from enthalpy $\Delta H$ (Figure 2):

$$H(T) = c(T - T_0) + \Delta H(T), \quad 0 \le \Delta H(T) \le L, \qquad (2)$$

where $L$ is the total heat of melting.

Substituting equation (2) to (1), we shall obtain

$$\lambda\nabla^2 T + v\rho c\frac{\partial T}{\partial x} - \frac{2\alpha}{h}(T - T_0) + \frac{q_2}{h} + v\rho\frac{\partial \Delta H}{\partial x} = 0. \qquad (3)$$

This differential equation is non-linear (due to last term, which depends on temperature non-linearly)

and can be converted by using method of sources (Green function) into an integral equation which is solved with a preset accuracy by the method of iterations:

$$T^{(i)}(x, y) - T_0 = \iint_{D_{hs}} q_2(\xi, \eta) f(x, y, \xi, \eta) d\xi d\eta + \tag{4}$$

$$+ v\rho h \iint_{D_{mz}} \frac{\partial \Delta H^{(i)}}{\partial x}(\xi, \eta) f(x, y, \xi, \eta) d\xi d\eta,$$

where

$$f(x, y, \xi, \eta) = \frac{1}{2\pi\lambda h} \exp\left[-\frac{v(x-\xi)}{2a}\right] K_0 \times$$

$$\times \left(\beta \frac{v\sqrt{(x-\xi)^2 + (y-\eta)^2}}{2a}\right); \quad \beta = \sqrt{1 + \frac{8a\alpha}{c\rho h v^2}}.$$

Here, $D_{hs}$ is the area of heat source action ($q_2 \neq 0$); $D_{mz}$ is the area of solid-liquid phase ($\partial\Delta H / \partial x \neq 0$) (see Figure 1); $i$ is the number of iteration; $f$ is the Green function (temperature in point $x$, $y$ from movable linear source of a unit power, acting in point $\xi$, $\eta$); $a$ is the temperature conductivity; $K_0$ is the McDonald function; $\beta$ is the criterion of effect of heat dissipation on movable temperature field. Function $K_0$ is infinite in point $x = \xi$, $y = \eta$, therefore, the integration near this singular point is recommended to be calculated numerically using the Gauss method in a polar system of coordinates [7].

Let us construct the iteration process by taking the algorithm from [8] as a base:

1) on $i$-th iteration $\Delta H^{(i)}$ is determined by distribution of $\partial\Delta H^{(i)} / \partial x$ successively and temperature $T^{(i)}$ is calculated by equation (4);

2) on next $(i+1)$-th iteration, $\Delta H^{(i+1)}$ is calculated with allowance for limitations:

$$\begin{aligned} \Delta H^{(i+1)} &= \Delta H^{(i)} + \omega c[T^{(i)} - T(\Delta H^{(i)})]; \\ \Delta H^{(i+1)} &= \max[0, \Delta H^{(i+1)}]; \\ \Delta H^{(i+1)} &= \min[L, \Delta H^{(i+1)}], \end{aligned} \tag{5}$$

where $\omega$ is the iteration parameter, $\omega > 0$; $T(\Delta H)$ is the inverse function ($T$ is the melting heat function $\Delta H$). The fulfillment of condition of phase transformation $T = T(\Delta H)$ follows from similarity of iteration process ($\Delta H^{(i+1)} = \Delta H^{(i)}$).

It should be noted that heat of solidification can differ from heat of melting, for example, when weld pool is alloyed with a filler material. It can be taken into account in equations (4) and (5). It is not difficult to take into account the effect of plate limitation in width using a method of reflection [2].

**Example.** Let us consider the temperature field in laser welding of aluminium alloy containing 0.5 % Si. Its properties and conditions of the laser welding are given below.

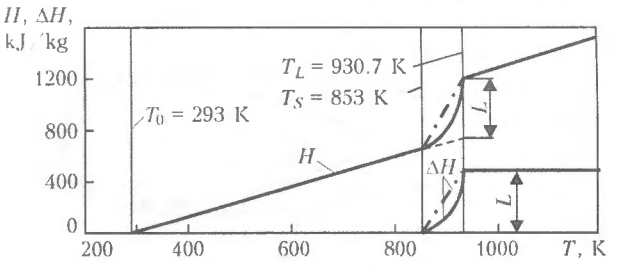


**Figure 2.** Temperature relationships of enthalpy $H$ and melting heat $\Delta H$ for aluminium alloy Al–0.5Si (dot-dash lines — simplified relationships)

**Properties of aluminium alloy Al–0.5Si and laser welding condition**

| | |
|---|---|
| Heat conductivity $\lambda$, W/(m·K) | 215 |
| Density $\rho$, kg/m$^3$ | 2710 |
| Specific heat capacity $c$, J/(kg·K) | 1085 |
| Solidus temperature $T_S$, K | 853 |
| Liquidus temperature $T_L$, K | 930.7 |
| Heat of melting $L$, kJ/kg | 460 |
| Coefficient of heat transfer $\alpha$, W/(m$^2$·K) | 50 |
| Thickness of plate $h$, mm | 1.5 |
| Effective power $q_{net}$, W | 1450 |
| Diameter of heat spot $d$, mm | 0.5 |
| Welding speed $v$, mm/s | 46.67 |
| Initial temperature $T_0$, K | 293 |

Heat conductivity was determined by a laser method. Using the program Thermo-Calc [9] and database [10] the temperature of solidus $T_S$ and liquidus $T_L$, and also $c$ and $\Delta H(T)$ were calculated. In this case, the Gulliver–Scheil model was used [11], and also the complete chemical homogeneity of liquid phase and absence of diffusion in solid phase were assumed. Dimensionless melting heat

$$\Lambda = \frac{L}{c(T_L - T_0)}$$

was 0.6648, that corresponded to 40 % of melting heat in total heat of metal at $T_L$. Effective power was determined by the solution of an appropriate inverse problem of heat conductivity [12, 13]. Low value of Prandtl criterion ($Pr < 0.01$) indicates that heat in the liquid phase is spread mainly due to the heat conductivity.

At high speed of welding the aluminium alloy the weld pool is elongated (Figure 3, *a*). Length of the pool (isotherms of liquidus) and especially the width of solid-liquid zone in a tail part of the pool are sensitive to the type of temperature relationship of melting heat $\Delta H(T)$. At non-linear relationship $\Delta H(T)$ the temperature gradient ahead of front of solidification is low (Figure 3, *b*), the pool has a more elongated shape, and the width of a solid-liquid zone is more narrow than that at simplified linear relationship $\Delta H(T)$ (Figure 3, *a*).

It is seen in comparison of calculated isotherms of liquidus with experimental data, presented in Figure 4, that the non-linear relationship of melting heat corresponds better to a sharp shape of a tail part of the weld pool (visible «flakes» on weld surface). Similar calculated drop-like shape of the weld pool is obtained in laser welding of aluminium alloy Al–0.4Mg–1.2Si at 117 mm/s speed, if the non-linear

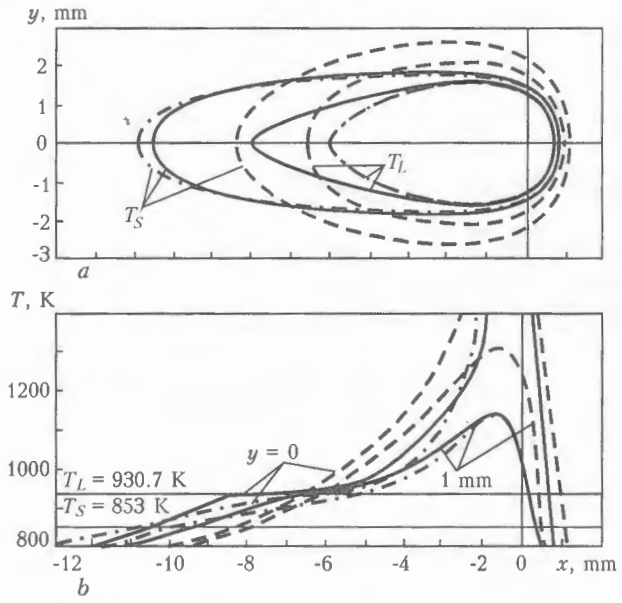


**Figure 3.** Effect of melting heat of weld pool shape (*a*) and distribution of temperature (*b*) in welding of aluminium alloy (solid curves — non-linear relationship $\Delta H(T)$; dot-dash curves — linear $\Delta H(T)$; dash curves — melting heat is not taken into account, $\Delta H(T) = 0$)

dependence of a share of liquid phase on temperature is taken into account [5].

It should be noted that the type of relationship $\Delta H(T)$ can be very complicated (it depends on distribution of liquation elements and type of equilibrium phase diagram, jump is possible at temperature of eutectic formation). Any relationship $\Delta H(T)$ can be taken into account in (4) by formula

$$\partial \Delta H/\partial x = (\partial \Delta H/\partial T)\,(\partial T/\partial x).$$

Variation of the iteration parameter $\omega$ in (5) showed that the highest rate of convergence (tens of iterations when at the last iteration the temperature in any point is changed not more than by 0.01 K), is provided at $\omega = 0.6$–$1.2$ (the higher non-linearity $\Delta H(T)$, the lower $\omega$).

**Effect of melting heat on weld width.** Melting heat leads to a significant decrease in the weld pool width. This does not almost depend on the type of function $\Delta H(T)$ (see Figure 3, *a*): weld width is 3 mm at linear relationship $\Delta H(T)$ and 3.04 mm at non-linear relationship. Weld width $W$ does not also depend on diameter of uniformly distributed source $d$, if $W > 2d$. For example, the change of $d$ from 0.5 to 0 leads to the decrease in $W$ by 2 %. By the same reason, the concentrated linear source ($d = 0$) and linear relationship $\Delta H(T)$ are taken furtheron.

In welding, the random deviations of weld sizes from preset values are inevitable. For the systems of welding process control, it is necessary to obtain the dependences of weld sizes on parameters of control (power of source and welding speed). Allowance for a latent heat of melting makes difficult and delays the obtaining of these dependencies. Question arises: in what cases is possible to neglect the latent heat? It is seen in Figure 5 that the change of power values in the ranges of 20 % leads to directly proportional change in weld width, moreover, the sensitivity factor $\partial(W/W_0)/\partial q_{net}$ (angle of straight line inclination) depends on melting heat negligibly (here $W_0$ — weld width at mean power). For example, melting heat of aluminium alloy decreases the sensitivity factor by 2 %. At the same time, the sensitivity factor as regards to speed $\partial(W/W_0)/\partial v$ is not constant and also little depends on the melting heat (see Figure 5). Hence, it follows that the melting heat can be neglected in calculation of sensitivity factors. This conclusion is also valid for the three-dimensional case [6].

**Effect of melting heat on thermal efficiency factor.** The main characteristic of effective use of input energy is the thermal efficiency factor (thermal effec-

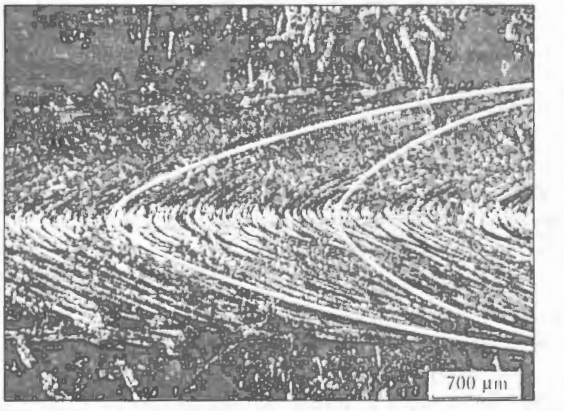


**Figure 4.** Appearance of weld in laser welding of aluminium alloy at 46.67 mm/s speed. Isotherms of liquidus calculated with allowance for linear (*right isotherm*) and non-linear (*left isotherm*) temperature relationship of melting heat are shown on the weld

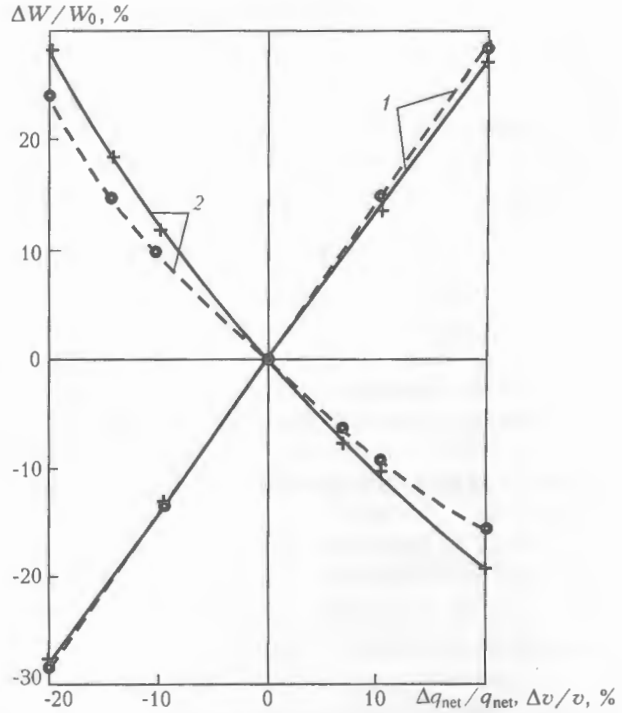


**Figure 5.** Dependence of relative change of weld width $\Delta W/W_0$ on relative change in effective power $\Delta q_{net}/q_{net}$ (*1*) and speed $\Delta v/v$ (*2*) in welding of aluminium alloy (solid curves — melting heat is taken into account; dash curves — it is not taken into account; middle points correspond to width $W_0$ and welding conditions given above)

tiveness) of the penetration process, $\eta_t$. This value expresses the relation of heat, consumed for metal heating up to $T_L$, to effective (supplied) power $q_{net}$ [2]:

$$\eta_t = \frac{vA_L\rho H(T_L)}{q_{net}},$$

where $A_L$ is the area of cross-section of zone heated up to $T_L$. For case of welding the plate and accepted relationship $H(T)$ (see Figure 2) we have

$$\eta_t = \frac{vWh\rho[c(T_L - T_0) + L]}{q_{net}}. \quad (6)$$

Let us analyze the effect of melting heat on thermal efficiency factor in welding of heat-insulated plates ($\beta = 1$). All curves in Figure 6 were obtained in varying the power $q_{net}$ (the rest conditions are above-given).

Curve *2* was plotted as a result of solution of non-linear problem (3) using the above-mentioned method (equations (4) and (5)). It is seen that the value $\eta_t$ can much exceed $(\pi e/2)^{-1/2} = 0.4839$. Additional varying of speed within the wide range (10–50 mm/s at $\varepsilon_1 = 5$–30) does not almost change the value of thermal efficiency factor.

Solution (3) is associated with definite difficulties due to the last non-linear term $\partial\Delta H/\partial x$, which takes into account the melting heat. Question arises: is it possible to omit this term (to take $\partial\Delta H/\partial x = 0$), and to take into account the melting heat in the remained linear equation approximately using one of the variants – by changing the coefficients in the equation (properties of material) or by changing the supplied energy $q_2$? Let us evaluate the error of these two approximate methods with allowance for melting heat.

Let us change the heat capacity in the first variant in (3) from $c$ by $\overline{c} = c + L/(T_L - T_0)$ and heat conductivity $\lambda$ by $\overline{\lambda} = \lambda + a\rho L/(T_L - T_0)$ so, that temperature conductivity $a$ and, consequently, Peclet criterion Pe were not changed ($a = \lambda/(c\rho) = \overline{\lambda}(\overline{c}\rho)$ and $\text{Pe} = vx/a = \text{const}$). It should be noted that this change is similar to taking into account the melting heat in total heat of metal at $T_L$. In other words, $\overline{c}(T_L - T_0) = H(T_L)$, where $H(T_L)$ is the preset enthalpy at $T_L$ (see Figure 2). Then (3) will have the form

$$\overline{\lambda}\nabla^2 T + v\rho\overline{c}\frac{\partial T}{\partial x} - \frac{2\alpha}{h}(T - T_0) + \frac{q_2}{h} = 0. \quad (7)$$

If the source is linear concentrated ($d = 0$) and located at the beginning of coordinates, then the following expression is the solution of equation (7):

$$T(x, y) - T_0 = q_{net} f(x, y, 0). \quad (8)$$

This solution allows plotting of function $\eta_t$ from argument

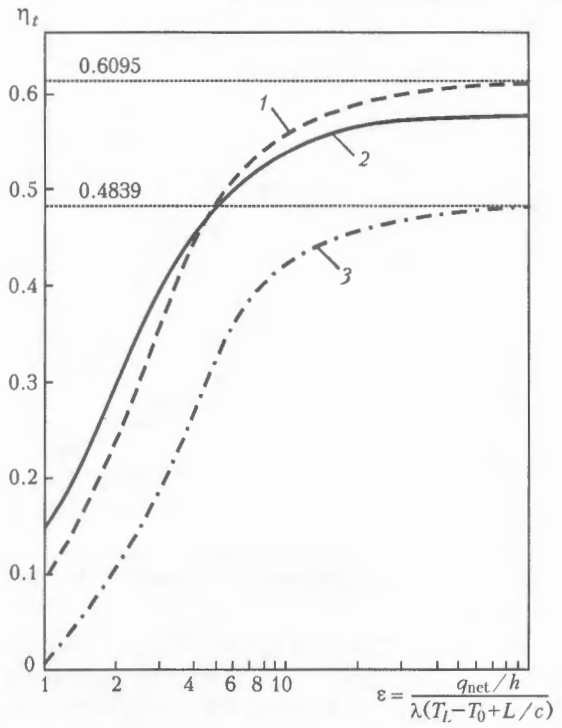


**Figure 6.** Effect of melting heat on thermal efficiency factor of process of penetration in welding of heat-insulating plates of aluminium alloy using a linear source: *1*, *3* – solution of linear problem at the condition of changing, respectively, effective power and properties; *2* – solution of non-linear problem by (4)

$$\varepsilon = \frac{q_{net}/h}{\overline{\lambda}(T_L - T_0)} = \frac{q_{net}/h}{\lambda(T_L - T_0 + L/c)}.$$

Curve *3* in Figure 6 does not depend on speed and is single for all the materials with different values of melting heat. This approach is used in [2].

In the second variant let us supply the energy, used for melting metal and distributed over the front of melting to the center of source, i.e. let us change power $q_{net}$ by $q_{net} - vWh\rho L$ and use equation (8). Furtheron, we shall determine the weld width using the iteration method and thermal efficiency factor by (6) (Figure 6, curve *1*).

Value of asymptote at such approach can be found analytically, using a scheme of a rapidly moving linear source. Weld width at the absence of heat dissipation is determined by formula

$$W \approx \frac{q_{net}/(vh)}{\sqrt{\pi e/2}\,c\rho(T_L - T_0) + \rho L}.$$

Substituting this expression into (6) we shall obtain

$$\eta_t = \frac{1 + \Lambda}{\sqrt{\pi e/2} + \Lambda}.$$

It follows from this formula that the values of thermal efficiency factor increase with increase in $\Lambda$ (for example, due to preheating temperature $T_0$). Value of asymptote for aluminium alloy is 0.6095.

It is seen from Figure 6 that curves *1–3* are not coincided. Accuracy of the second approach (curve *1*)

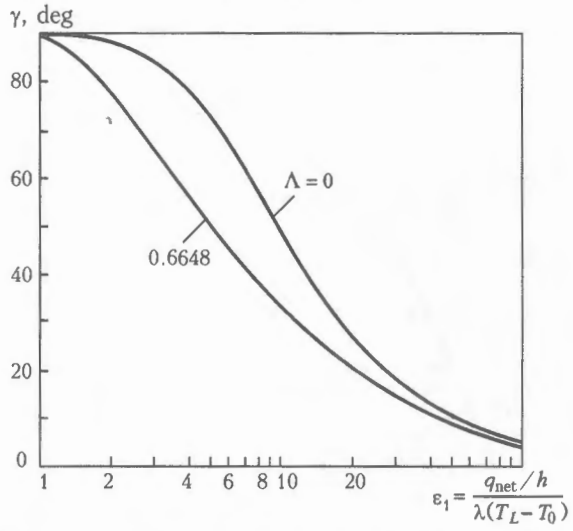


**Figure 7.** Effect of melting heat on angle of solidification front in welding of heat-insulating plates from aluminium alloy using a linear source

is much higher. The first approach gives clearly the lowered results (curve *3*). It should be outlined that additional increase in thermal efficiency factor can be realized by distributed-thermal source in a transverse direction.

**Effect of melting heat on the shape of solidification front.** Grained structure of weld metal is defined by a shape of crystallization front having an angle γ [14] (see Figure 1):

$$\gamma = 2 \operatorname{arctg} \frac{y_B}{x_B - x_A}. \qquad (9)$$

From the condition $T(x_B, y_B) = T_L$ and $\partial T / \partial x(x_B, y_B) = 0$ it is possible to find the coordinate of point $B$, and from $T(x_A, 0) = T_L$ — the coordinate of point $A$ and, consequently, angle $A$ by (9).

Angle of crystallization front γ is lower, the higher is the source power (Figure 7). Melting heat has a significant influence on decrease in values γ (ratio of pool width to the length of the pool tail part).

It should be noted that the method developed can make allowance for heat of any phase transitions (for example, $\alpha \leftrightarrow \gamma$ transformations in steel). Similar calculated method can be developed for analysis of three-dimensional temperature field with allowance for melting heat. The principal differences will be in the form of differential equation (3) and solution (4) (differed by Green functions $f$).

## CONCLUSIONS

1. The offered algorithm of solution of quasi-stationary equation of heat conductivity using analytical method of sources can take into account the effect of heat of melting and solidification on the temperature fields in welding.

2. Melting heat decreases the weld width. Relative change in weld width by varying the supplied energy of welding speed within 20 % depends on melting heat negligibly. Here, the dependence on energy has a linear nature, while that on speed is non-linear.

3. The type of temperature relationship of melting heat has a great influence on width of solid-liquid zone and shape of front of solidification of liquid metal. Thus, in laser welding of aluminium alloy Al–0.5Si at 47 mm/s speed the weld pool has a drop-like shape.

4. With allowance for melting heat the value of thermal efficiency factor of the process of plate penetration by a linear source can exceed significantly 0.4839. Known simplified methods of allowance for melting heat can lead to significant errors. Among them, the more precise is the method, associated with decrease in effective (supplied) power for a value used for metal melting.

5. With increase in heat of solidification the angle of solidification front is decreased.

6. Correlation between the calculated and experimental shape of the weld pool is satisfactory.


1. Rosenthal, D. (1935) Etude theorique du regime thermique pendant la soudure a l'arc. *II Congres National des Sciences*. Bruxelles.
2. Rykalin, N.N. (1951) *Calculations of thermal processes in welding*. Moscow: Mashgiz.
3. Makhnenko, V.I., Kravtsov, T.G. (1976) *Thermal processes in mechanized surfacing of parts of circular cylinders type*. Kiev: Naukova Dumka.
4. Kou, S. (1981) Simulation of heat flow during the welding of thin plates. *Metallurgical Transact. A*, **12A**, 2025–2030.
5. Bergmann, H.W., Hilbinger, R.M. (1998) Numerical simulation of centre line hot cracks in laser beam welding of aluminium close to the sheet edge. In: *Mathematical modelling of weld phenomena 4*. Ed. by H. Cerjak. London.
6. Tosello, I., Tissot, F.X., Barras, M. (1998) Modelling of weld behaviour for the control of the GTA process by computer aided welding. *Ibid*.
7. Ramachandran, P.A. (1994) Boundary element methods in transport phenomena. In: *Computational mechanics publications*. London: Elsevier.
8. Prakash, C., Samonds, M., Singhal, A.K. (1987) A fixed grid numerical methodology for phase problems involving a moving heat source. *Int. J. Heat and Mass Transfer*, 30(**12**), 2690–2694.
9. Andersson, J.O., Helander, T., Hoglund, L. (2002) Thermo-Calc&DICTRA, computational tools for materials science. *Calculation of Phase Diagrams*, **26**, 273–312.
10. *GOST 507 – Final Report*: Thermochemical database for light metal alloys. Vol. 2. Ed. by I. Ansara, A.T. Dinsdale, M.H. Rand. Europ. Com.
11. Saunders, N., Miodownik, A.P. (1998) Calculation of phase diagrams. In: *A comprehensive guide*. Pergamon Materials Series. Oxford: New York. Tokyo: Elsevier.
12. Karkhin, V.A., Plochikhine, V.V., Ilyin, A.S. et al. (2002) Inverse modelling of fusion welding processes. In: *Mathematical modelling of weld phenomena 6*. Ed. by H. Cerjak. London: Maney Publ.
13. Karkhin, V.A., Ploshikhin, V.V., Bergman, Kh.V. (2002) Simulation of thermal and solidification processes in laser welding of aluminium plates. *The Paton Welding J.*, **8**, 10–14.
14. Plochikhine, V., Bergmann, H.W. (2001) Correlation between the welding parameters and the grain structure for the fast moving high power line heat source in a thin plate. In: *Mathematical modelling of weld phenomena 5*. Ed. by H. Cerjak. London.

# CONSUMABLE-ELECTRODE PULSED-ARC WELDING WITH AUTOMATIC STABILIZATION OF MODE PARAMETERS

**P.P. SHEJKO, A.M. ZHERNOSEKOV** and **Yu.O. SHIMANOVSKY**
E.O. Paton Electric Welding Institute, NASU, Kiev, Ukraine

The paper gives the results of studying the developed two-loop system for automatic stabilization of average values of arc voltage and welding current in consumable-electrode pulsed-arc welding by regulation of the parameters of the power source pulses and electrode wire feed rate, respectively. Separate and combined influence of the disturbing production factors (change of electrode extension, lowering of mains voltage) on the process of consumable-electrode pulsed-arc welding of low-alloyed steels and quality of weld metal has been studied.

***Keywords:*** *consumable-electrode pulsed-arc welding, disturbing factors, carbon structural steels, process stabilization, average values of arc voltage, average values of welding current, feedbacks, mode parameters, weld quality*

Consumable-electrode pulsed-arc welding in Ar-based gas mixtures is effectively applied in many manufacturing sectors of industrialized countries. This process allows reducing electrode metal spatter, as well as performing welding in any positions in space, welding of sheet metal and multipass welding. High mechanical properties of weld metal should be noted in welds produced by consumable-electrode pulsed-arc welding, which is due to structure refinement with formation of acicular ferrite in it [1–7].

Under the production conditions the consumable-electrode pulsed-arc welding process is exposed to various disturbing factors [8, 9], which change the main energy parameters of welding, namely average values of welding current $I_{av.w}$ and arc voltage $U_{av.a}$, this leading to instability of geometrical dimensions of welds and appearance of defects in them.

PWI developed a new variant of construction of the system of stabilization of consumable-electrode pulsed-arc process [9]. The paper gives the results of investigations of the influence of the developed two-loop system for automatic stabilization of average values of arc voltage and welding current with regulation of the parameters of current pulses of the power source and rate of electrode wire feed, respectively, on the stability of quality parameters of the consumable-electrode pulsed-arc process, both at the impact of individual disturbing factors (variation of electrode extension, mains voltage, edge misalignment), and at their simultaneous integrated impact. A pulsed power source of I-169 type with a smooth adjustment of pulse parameters developed at PWI was used. Welding head of SGU-7 type with BARS-2V control system was applied in this case. Beads were deposited on plates of steel St3 10 and 20 mm thick in a mixture of Ar + 18 % $CO_2$ with Sv-08G2S wire of 1.2 mm diameter, welding speed being 21 m/h.

Conducted experimental studies yielded dependencies between the main energy parameters of consumable-electrode pulsed-arc process ($U_{av.a}$, $I_{av.w}$) and the disturbing factor the most often active under the production conditions, namely variation of elec-

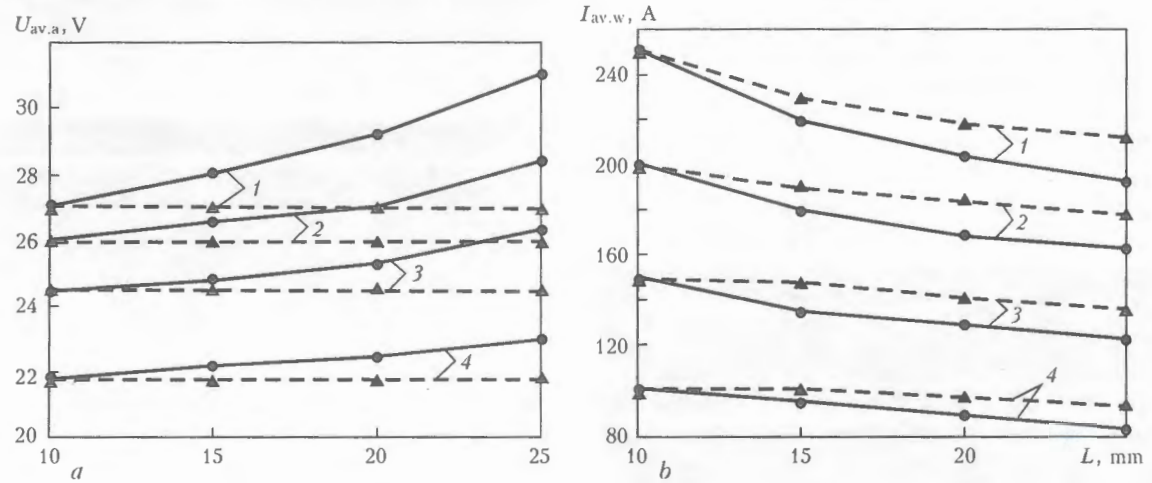


**Figure 1.** Dependence of average values of arc voltage $U_{av.a}$ (*a*) and welding current $I_{av.w}$ (*b*) (modes *1–4*) on electrode extension $L$ = = 10–25 mm in consumable-electrode pulsed-arc welding of steel St3 in gas mixture of Ar + 18 % $CO_2$ with Sv-08G2S wire of 1.2 mm diameter without the stabilization system (●) and with voltage and current stabilization (▲)

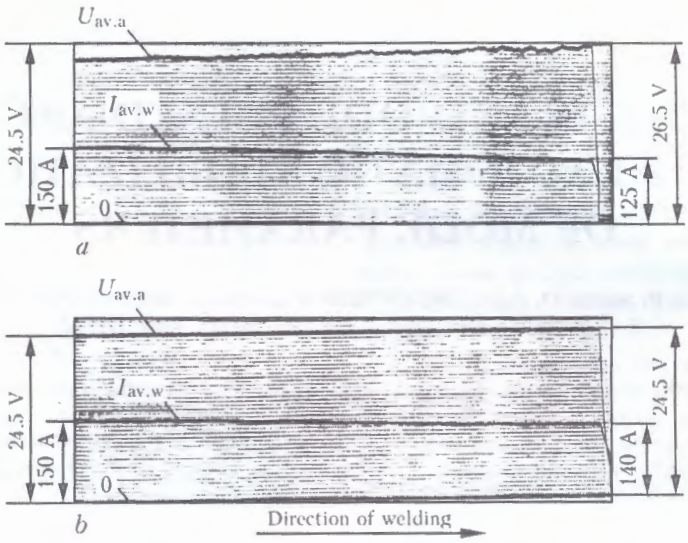


**Figure 2.** Oscillograms of average values of welding current $I_{av.w}$ and arc voltage $U_{av.a}$ at variation of electrode wire extension in the range of 10–25 mm without the stabilization system (*a*) and with stabilization of voltage and current (*b*)

trode wire extension $L$. A family of these curves, obtained at different values of $U_{av.a}$, $I_{av.w}$, $L$ in consumable-electrode pulsed-arc welding without the stabilization system and with it, is shown in Figure 1. In the Figure curves *1* (●) show the nature and limits of variation of $U_{av.a}$, $I_{av.w}$ values without application of a stabilization system (initial values are $U_{av.a}$ = = 27 V; $I_{av.w}$ = 250 A). In this case the welding current is reduced to 195 A. As is seen from Figure 1, $U_{av.a}$ variation was 4 V, and $I_{av.w}$ = 55 A at maximum electrode wire extension of 25 mm. Curves *1* (▲) illustrate the same dependencies under the same initial conditions, but with use of the system of automatic stabilization. $U_{av.a}$ values practically did not change, and $I_{av.w}$ values changed by not more than 35 A at $L$ = 25 mm.

The same dependencies $U_{av.a} = f(L)$, $I_{av.w} = f(L)$ were also obtained for other initial values of $U_{av.a}$ and $I_{av.w}$ (see Figure 1). Nature of the dependencies is similar to the case of $U_{av.a}$ = 27 V, $I_{av.w}$ = 250 A. At operation in lower modes, the accuracy of stabilization in increased.

Figure 2 gives oscillograms of $I_{av.w}$ and $U_{av.a}$ of the consumable-electrode pulsed-arc process at variation of electrode wire extension $L$ in the range of 10–25 mm. Duration of current pulses was $3.4 \cdot 10^{-3}$ s, their repetition rate being 68 Hz. As is seen from Figure 2, *a*, increase of electrode wire extension leads to increase of arc voltage and lowering of welding current. Variation of arc voltage increases noticeably by the end of the process, because of a significant voltage drop across the electrode wire extension, which is characteristic for steel wires [10]. Use of feedbacks allows reducing the influence of electrode wire extension, stabilizing the set values of $U_{av.a}$ and reducing the drop of $I_{av.w}$ values (Figure 2, *b*).

Appearance of welds made by the above mode is given in Figure 3. The weld in Figure 3, *a* formed non-uniformly along its length, and has a region of pores coming to the surface, located at the weld end. This is due to increase of arc voltage, which is indicative of arc elongation at increase of electrode wire extension. The weld in Figure 3, *b*, made using the stabilization system, features absence of pores and other defects, stable width and uniform formation along the entire length.

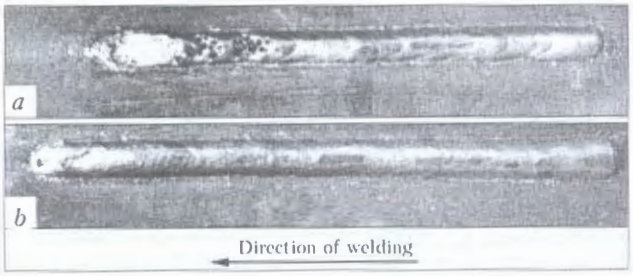


**Figure 3.** Appearance of welds in bead deposition by consumable-electrode pulsed-arc welding at variation of electrode extension in the range of 10–25 mm (*a*, *b* – see Figure 2)

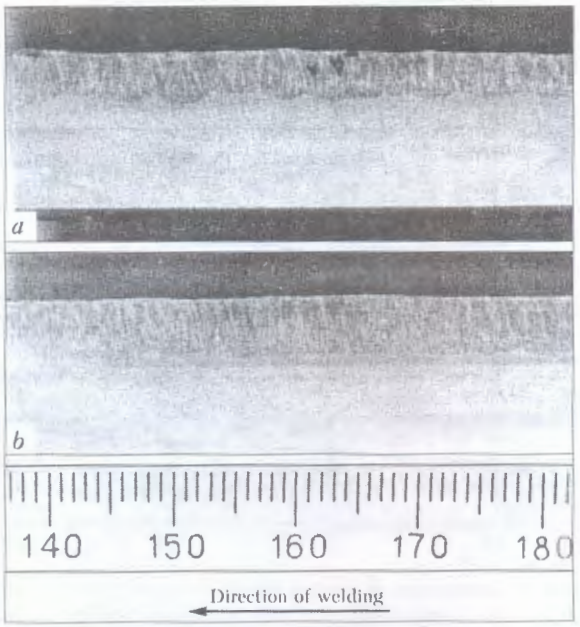


**Figure 4.** Variation of penetration depth in welds made by consumable-electrode pulsed-arc welding process at increase of electrode wire extension (*a*, *b* – see Figure 2)

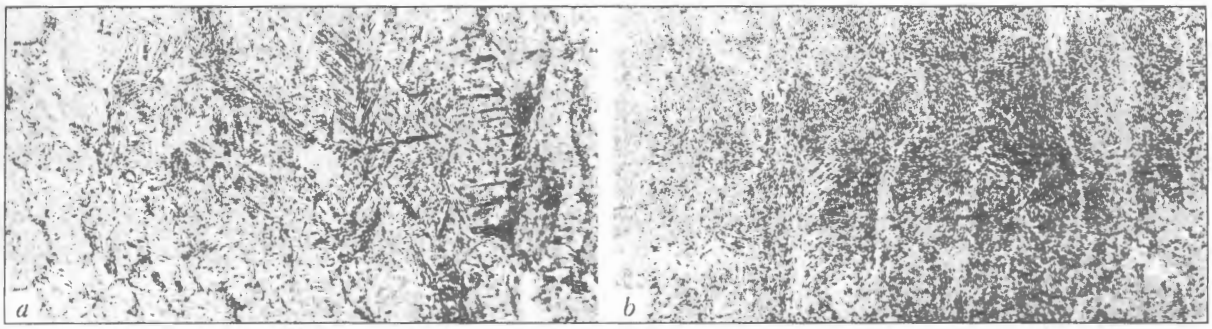

**Figure 5.** Microstructure of the section in the center of weld metal (closer to deposit end) made by the consumable-electrode pulsed-arc welding (*a*, *b* — see Figure 2) (×200)

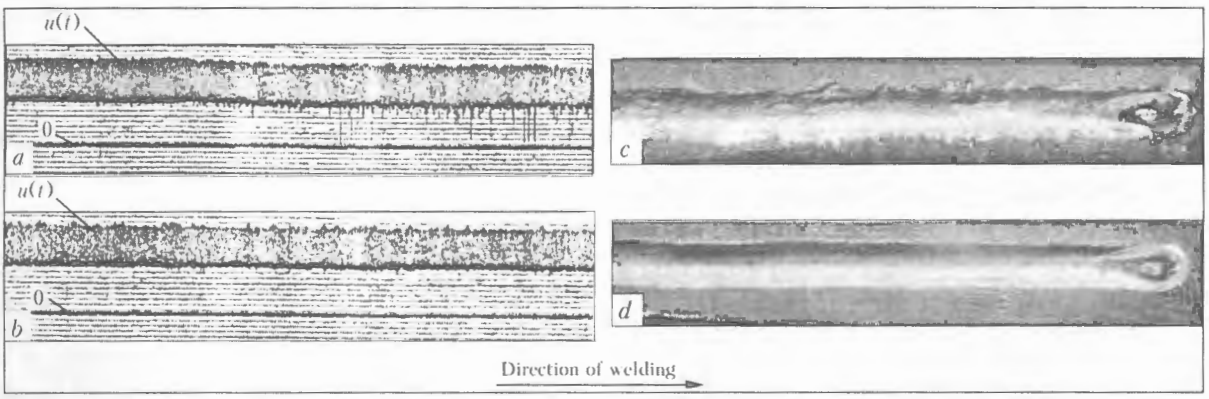


**Figure 6.** Oscillograms of current values (*a*, *b*) of arc voltage $u(t)$ and appearance of welds (*c*, *d*) made by the process of consumable-electrode pulsed-arc welding at a smooth drop of voltage from 380 to 350 V without a stabilization system (*a*, *c*) and with voltage and current stabilization (*b*, *d*)

Figure 4 shows longitudinal sections of welds, given in Figure 3. From Figure 4, *a* it is seen that the penetration depth is unstable, and its variation depends on electrode wire extension. In this case, lacks-of-penetration or burns-through are found, as well as defects of the type of internal pores. A particularly important result of this work for welding under production conditions is the fact that application of the developed system of automatic stabilization allows stabilizing the penetration depth along the entire weld length and eliminating weld defects at the change of electrode wire extension (Figure 4, *b*).

Metallographic and X-ray studies have been conducted, which suggested that at increase of electrode extension by more than 50 % of the rated value, the probability of appearance of defects of the type of cracks, lacks-of-penetration, unstable weld width and penetration depth increases significantly. In addition, the amount of martensite component in the weld metal is also increased (Figure 5, *a*) and the grain point in the HAZ drops to 5 (according to GOST 5639–82), this leading to higher hardness of weld metal and its lower viscosity. At increase of electrode wire extension by 80 % and more, the probability of development of coarse defects of the type of pores becomes higher (see Figure 3, *a*).

At operation of the stabilization system uniform ripple and smooth transition to the base metal are noted even at extension variation by more than 80 % (see Figure 3, *b*). Microstructural components in this case are fine and uniform along the entire weld length, and consist of upper and lower bainite with ferrite regions (see Figure 5, *b*). Grain point in the HAZ is equal to 8 (GOST 5639–82).

The influence of variation of mains voltage on the process of consumable-electrode pulsed-arc welding was studied, using a potential regulator, which performs smooth adjustment of output voltage, which was used as input voltage of the pulsed power source

Variation of process mode parameters at lowering of mains voltage

| *Mains voltage, V* | *Arc voltage, V* | *Welding current, A* | *Pulse repetition frequency, Hz* |
|---|---|---|---|
| 380 | 26.0 | 220 | 92 |
| 350 | 23.5 | 230 | 68 |

*Note.* Duration of current pulses was $3.2 \cdot 10^{-3}$ s.

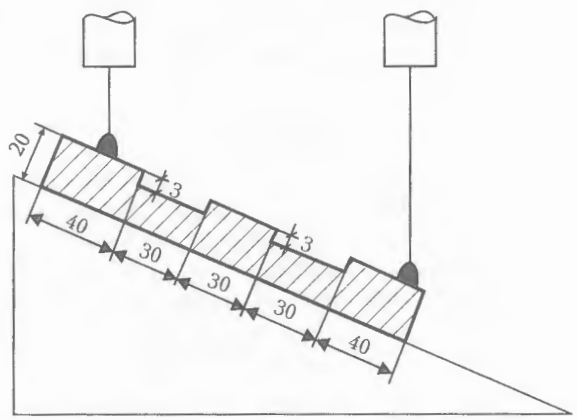


**Figure 7.** Schematic of bead deposition at simultaneous action of several disturbing factors

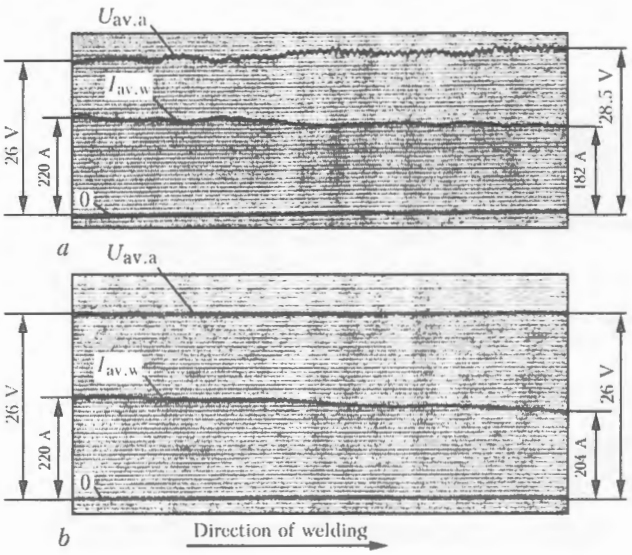


**Figure 8.** Oscillograms of $I_{av.w}$ and $U_{av.a}$ in bead deposition by the schematic in Figure 7 (*a*, *b* — see Figure 2)

I-169. The Table shows changes of deposition modes at lowering of the mains voltage. Figure 6 *a* and *b* gives oscillograms of current values of arc voltage $u(t)$ at smooth lowering of mains voltage from 380 to 350 V. As is seen from Figure 6, *a*, lowering of the mains voltage leads to lowering of arc voltage and development of short-circuits, i.e. violation of the transfer process by the principle of «1 pulse–1 drop». Appearance of welds, deposited at lowering of mains voltage, is shown in Figure 6, *c* and *d*. The bead in Figure 6, *c* forms a coarse-ripple surface with considerable variation of weld width and increased level of spatter. Application of the system of stabilization eliminates the short-circuits, related to a drop of mains voltage (Figure 6, *b*), which allows producing fine-ripple beads uniform over the entire length with a smooth transition to the base metal and without metal drop sticking (Figure 6, *d*).

Simultaneous action of several disturbing factors was studied, namely of variation of electrode wire extension in the range of 10–25 mm, decrease of mains voltage to 350 V, edge misalignment of up to 3 mm in consumable-electrode pulsed-arc welding according to a schematic in Figure 7. Initial welding conditions were as follows: mains voltage of 350 V; arc voltage of 26 V; welding current of 220 A; duration of current pulses of $3.2 \cdot 10^{-3}$ s, pulse repetition rate of 87 Hz; welding speed of 21 m/h.

Figure 8 shows oscillograms of average values of arc voltage and welding current in consumable-electrode pulsed-arc welding by the schematic given in Figure 7. As is seen from Figure 8, *a*, at integrated action of the above disturbing factors without the stabilization system, variation of $I_{av.w}$ and $U_{av.a}$ values increases significantly. This results in considerable spatter and sticking of metal drops, non-uniform weld width and its poor formation, formation of rolls and non-uniform transition from the weld to the base metal (Figure 9, *a*).

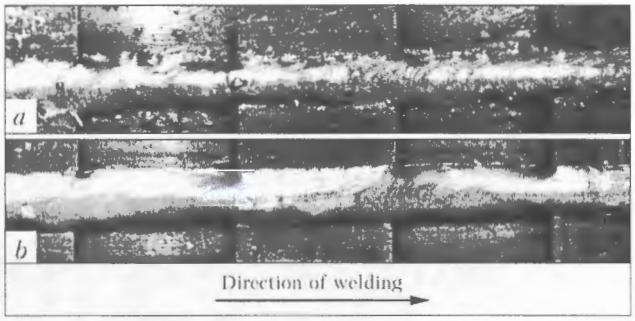


**Figure 9.** Appearance of welds in bead deposition by the schematic in Figure 7 at simultaneous action of several disturbing factors (*a*, *b* — see Figure 2)

At automatic stabilization of average values of arc voltage and welding current, using the developed two-loop system, it is possible to produce welds with good formation even at simultaneous impact of a number of disturbing factors (Figure 9, *b*).

## CONCLUSIONS

1. Application of the developed system of automatic stabilization of $U_{av.a}$ and $I_{av.w}$ for consumable-electrode pulsed-arc welding process at variation of electrode wire extension allows avoiding defects of the type of pores, lacks-of-fusion, non-uniform formation of welds, and provides stability of penetration depth.

2. Stabilization system allows compensating for drop of arc voltage, caused by lowering of mains voltage, eliminating short-circuits and resulting disturbance of drop transfer of metal and reducing spatter and metal drop sticking, as well as improving the quality of weld formation.

3. At simultaneous integrated action of several disturbing factors the developed two-loop system allows producing welds with stable geometry and without spattering or defects.


1. Rimsky, S.T., Svetsinsky, V.G., Shejko, P.P. et al. (1993) Consumable-electrode pulsed-arc welding of low-alloy steels in argon + $CO_2$ mixture. *Avtomatich. Svarka*, **2**, 38–41.
2. Shejko, P.P., Zhernosekov, A.M., Shevchuk, S.A. (1997) Technological peculiarities of consumable-electrode welding of low-alloy steels with alternate supply of shielding gases. *Ibid.*, **8**, 32–36.
3. Buchinsky, V.N., Voropaj, N.M. (1978) Peculiarities of pulsed-arc welding of steels in argon + $CO_2$ shielding mixture. *Ibid.*, **3**, 42–45.
4. Aiechele, G. (1990) Use of the pulsed technique active-gas metal-arc welding. *Schweissen und Schneiden*, **4**, 62–63.
5. Dorling, D. (1992) Applying pulsed GMA welding to pipeline construction. *Welding J.*, **10**, 39–44.
6. Di Pieetro, D., Young, J. (1996) Pulsed GMAW helps John Deer meet fume requirements. *Ibid.*, 75(**10**), 57–58.
7. Pereira, W.A., Ferraresi, V.A. (2000) Estudo dos parametros que influenciam a instabilidade do cordao em soldagem MIG pulsada automatizada. *Soldagem&Inspecao*, **12**, 25–30.
8. Paton, B.E., Lebedev, V.K. (1966) *Electric equipment for arc and slag welding*. Moscow: Mashinostroenie.
9. Paton, B.E., Shejko, P.P., Zhernosekov, A.M. et al. (2003) Stabilization of the process of consumable-electrode pulsed-arc welding. *The Paton Welding J.*, **8**, 2–5.
10. Lebedev, A.V. (1978) Influence of heat evolution in the extension on self-adjustment of the arc. *Avtomatich. Svarka*, **7**, 10–15.

# INVESTIGATION OF PECULIARITIES OF TRANSPORT OF HYDROGEN IN UNDERWATER FUSION WELDING OF STRUCTURAL STEELS

**V.I. MAKHNENKO, S.Yu. MAKSIMOV** and **T.V. KOROLYOVA**
E.O. Paton Electric Welding Institute, NASU, Kiev, Ukraine

Peculiarities of transport of hydrogen in wet underwater arc welding of a root pass of the butt joint in low-carbon and low-alloy steels are considered using the calculation-experimental method. Effect of the depth of welding and type of a filler metal on the concentration of hydrogen in the weld and HAZ metal is shown.

***Keywords:*** *underwater fusion welding, mathematical modelling, transport of hydrogen, hydrogen concentration, cold cracks*

**Introduction.** In wet underwater welding the electric arc burns in a vapour-gas bubble that consists of 85–92 % of hydrogen [1 etc.]. As the depth of welding increases, the pressure in the bubble grows, this leading to increase in the partial pressure of hydrogen over the weld pool. In turn, this leads to increase in the saturation of molten metal of the drops and weld pool with hydrogen [2 etc.]. The latter may result in an intensive pore formation in the fusion zone (FZ), saturation of the heat-affected zone (HAZ) with hydrogen and, therefore, an increased risk of formation of hydrogen-induced (cold) cracks.

At present porosity is controlled by applying appropriate metallurgical effects on molten metal of the weld pool [3]. However, the possibilities of such an effect on the HAZ are more limited. Therefore, the problem of hydrogen-induced cracks is very topical for this zone.

Experimental evaluation of the kinetics of saturation of the HAZ metal with diffusible hydrogen [4, 5] involves difficulties. That is why it is necessary to use the calculation methods for this purpose. Known are some studies [6–8 etc.] which consider welding performed under conventional atmospheric conditions. The use of such approaches to wet underwater welding requires certain adaptation. So, this article is dedicated particularly to the above issue.

**Statement of the problem and experimental studies of model samples.** Considered is the specific problem of wet underwater welding of butt joints in steels St3 and 17G1S. Chemical compositions of these steels are given in Table 1. Mechanised arc welding of plates 14 mm thick on a permanent metal backing using a flux-cored wire (Figure 1) is performed in layers. Welding of a root pass is of the highest concern in terms of cold cracking of the HAZ metal. Therefore, further on the consideration will be given only to this layer. The following conditions were used in the case under consideration: $I_w$ = 160–180 A, $U_w$ = 30–32 V, $v_w$ = 6 m/h, $\alpha_d$ = 9 g/(A·h), and $T_{med}$ = 20 °C.

**Table 1.** Chemical composition of steels St3 and 17G1S

| Steel grade | Content of elements, wt.% | | | $P_{cm}$ | $H^f_{cr}$, cm³/100 g | $H^r_{cr}$, cm³/100 g |
|---|---|---|---|---|---|---|
| | C | Si | Mn | | | |
| St3 | 0.18 | 0.21 | 0.55 | 0.215 | 32 | 10 |
| 17G1S | 0.16 | 0.45 | 1.50 | 0.250 | 12 | 4 |

Table 1 gives the value of carbon equivalent $P_{cm}$ for the indicated chemical composition calculated using the following formula:

$$P_{cm} = C + \frac{Mn + Cu + Cr}{20} + \frac{Si}{30} + \frac{Mo}{15} + \frac{V}{10} + 5B + \frac{Ni}{60}. \quad (1)$$

This Table also gives critical concentrations of diffusible hydrogen $H_{cr}$, at which there is a risk of cold (hydrogen-induced) cracking of a sample 14 mm thick under free, $H^f_{cr}$, and restrained, $H^r_{cr}$, conditions [4]:

$$\log_{10} H_{cr} = P^{cr}_{\omega} - 12P_{cm}, \quad (2)$$

where $P^{cr}_{\omega}$ is the sensitivity index. Normally $P^{cr}_{\omega}$ is equal to 4.1 and 43.6 for welding in a free and restrained condition, respectively.

As seen, critical values of $H_{cr}$ for the HAZ metal even in welding of low-carbon steel St3 in a restrained condition (which is characteristic of underwater repair operations) are rather low, i.e. equal to about

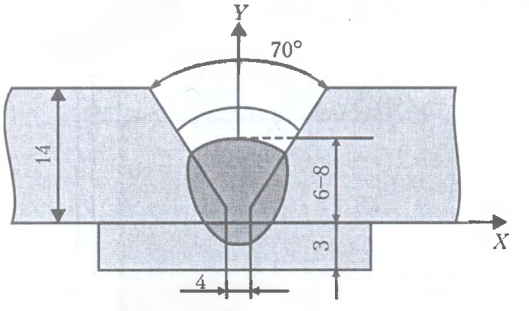


**Figure 1.** Schematic of a welded joint with the root weld

**Table 2.** Results of experimental studies of model samples

| *Welding depth, m* | *Chemical composition of FZ metal* | $H_{dif}$, $cm^3/100$ g | $H_{res}$, $cm^3/100$ g |
|---|---|---|---|
| 0.1 | 0.034C; 0.04Si; 0.07Mn | 14.3 | 7.8 |
| 50 | 0.053C; 0.04Si; 0.04Mn | 15.2 | 23.4 |
| 100 | 0.046C; 0.04Si; 0.05Mn | 19.9 | – |

*Note.* Composition of vapour-gas bubble, %: $O_2 < 0.52$; $H_2 = 85–92$; $CO + CO_2 = 8–15$.

10 $cm^3/100$ g, while for low-alloy steel 17G1S they are equal to 4 $cm^3/100$ g. This shows that the risk of formation of hydrogen-induced cracks is very high in this case.

Samples (15×10×25 mm in size, GOST 23338–91) for evaluation of diffusible hydrogen by the chromatographic method [9] were used as model samples to perform the experimental part of the study. Welding was carried out under the above conditions in a hydraulic test chamber by simulating depths from 0.1 to 100 m. In addition to $H_{dif}$, also the content of residual hydrogen $H_{res}$ and chemical composition of deposited metal were determined on these samples. The results obtained for different depths are given in Table 2.

Experimental results show that the FZ metal oxidises very intensively. This leads to a low content of carbon, silicon and manganese. The base metal of a sample has an insignificant effect. The content of diffusible and residual hydrogen in deposited metal increases with increase in the depth of welding. Naturally, the content of hydrogen in the HAZ metal also grows, but it is very difficult to measure it by a standard method (given that the HAZ is small in size). The use of the local analysis procedure [5] would allow only the qualitative estimation, as the conditions of cooling of a welded joint (see Figure 1) and a model sample (Figure 2) markedly differ from each other, and it is difficult to conduct measurements on a full-scale sample having a large cross section.

The data on heating of a model sample and the results of measurement of the hydrogen content of the deposited metal make it possible to identify to a certain extent the boundary conditions for mathematical modelling.

**Modelling of a temperature field.** The software for 2D conditions developed by the E.O. Paton Electric Welding Institute was used to describe distribution of temperatures in section $z$ = const (see Figure 1). The distribution of temperature $T(x, y, t)$ is determined by a solution of the following boundary problem:

$$\frac{\partial}{\partial x}\left(\lambda \frac{\partial T}{\partial x}\right) + \frac{\partial}{\partial y}\left(\lambda \frac{\partial T}{\partial y}\right) + W(x, y, z) = c\gamma \frac{\partial T}{\partial t}, \quad (3)$$

$$\text{at } t = 0 \quad T = T_0(x, y, 0) =$$

$$= \begin{cases} T^{melt}_{mean} \approx 1700\ ^\circ C \text{ inside the FZ}, \\ 20\ ^\circ C \text{ outside the FZ}, \end{cases} \quad (4)$$

$$\text{at } y = 0 \quad \frac{\partial T}{\partial x} = 0. \quad (5)$$

At the rest of the boundary the heat exchange, according to the Newton's law, has the following form:

$$\lambda \frac{\partial T}{\partial n} = -\alpha (T - T_{med}) \quad (6)$$

at $\alpha = \alpha_{out}$ — outside the vapour-gas bubble, and $\alpha = \alpha_{v\text{-}g}$ — inside the vapour-gas bubble.

Conditions of existence of the vapour-gas bubble are determined by surface temperature $T_{surf}$ and welding depth $L$:

$$\begin{aligned} &T_{surf} > 100\ ^\circ C \text{ at } L = 0 \text{ m}; \\ &T_{surf} > 120\ ^\circ C \text{ at } L = 10 \text{ m}; \\ &T_{surf} > 160\ ^\circ C \text{ at } L = 50 \text{ m}; \\ &T_{surf} > 185\ ^\circ C \text{ at } L = 100 \text{ m}. \end{aligned} \quad (7)$$

In formula (3), $\lambda$ and $c\gamma$ are the thermal-physical properties of a material. In the temperature range of solidification of the FZ metal, the values of $c\gamma$ allow for the latent heat of solidification of a material, $q_{lat}$, and effective thermal conductivity coefficient $\lambda_e \cong \cong 5\lambda(T_S)$; $c\gamma_e = c\gamma(T_S) + q_{lat}/(T_L - T_S)$, where $T_S$ and $T_L$ are the solidus and liquidus temperatures in the FZ, respectively.

The distributed source $W$ within the FZ is calculated using the following formula:

$$W = \left[\frac{q_{surf}}{F_{FZ}} - c\gamma(T^{filler}_{mean} - T_0) - q_{lat}\right]\frac{1}{t_0},$$

where $q_{surf} = \dfrac{I_w U_w}{v_w}\eta_s$, $F_{FZ}$ is the cross section area of the FZ; $\eta_s$ is the net efficiency of the heat source; and $t_0$ is the time of heat input.

Values of $\eta_s$, $\alpha_{out}$ and $\alpha_{v\text{-}g}$ were determined experimentally on model samples. A good agreement with an experiment was achieved at $T_0 = 20\ ^\circ C$, $\alpha_{out} \approx \approx \alpha_{v\text{-}g} \approx 0.208\ W/(cm^2 \cdot ^\circ C)$, $\eta_s = 0.50$, 0.45 and 0.40, and $L$ = 0–10, 50 and 100 m, respectively.

**Mathematical model of hydrogen transport.** The software suggested by the authors of [6] was used. Basic principles of the calculation algorithm are as follows.

Transport of diffusible hydrogen in metal of a welded joint is studied on the basis of a diffusion

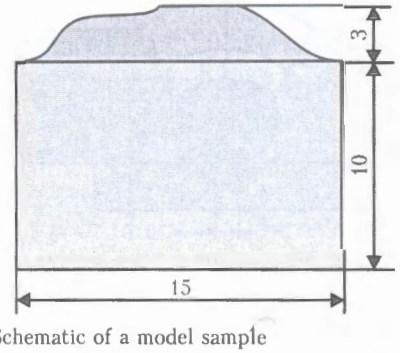


**Figure 2.** Schematic of a model sample

model [6–8] for heterogeneous medium, the transporting properties of which are characterised by diffusion coefficient $D$ and solubility coefficient $K$ (or by penetrability coefficient $KD$). The driving force for transport is the potential concentration gradient $\Pi$ (according to the Sieverts law $\Pi = \sqrt{P}$, where $P$ is the partial pressure of a certain concentration of hydrogen in unit volume at a temperature of 20 °C [6]). The initial condition at $t = 0$ is characterised by assigned mean values of the concentration of diffusible hydrogen in the base and FZ metals, based on the model experiment. Physics of a short-time process of ingress of hydrogen into the FZ metal was ignored in this case.

For the region under consideration, potential of the concentration, $\Pi(x, y, t)$, of diffusible hydrogen $H(x, y, t)$ is determined by solving the following boundary problem:

$$\frac{\partial}{\partial x}\left(KD\frac{\partial \Pi}{\partial x}\right)+\frac{\partial}{\partial y}\left(KD\frac{\partial \Pi}{\partial y}\right)-Q(x, y, t)=\frac{\partial}{\partial t}(K\Pi), \quad (8)$$

$$\text{at } t=0 \quad \Pi(x, y, 0)=\frac{H(x, y, 0)}{K(x, y, 0)}; \quad (9)$$

$$\text{at } x=0 \quad \frac{\partial \Pi}{\partial x}=0, \quad (10)$$

where $Q$ is the variation in the hydrogen content of the traps (reversible and irreversible) calculated at 20 °C and atmospheric pressure using the following formula:

$$Q=\mu\frac{\partial}{\partial t}\left(\beta\frac{100\text{ g}}{\gamma_m}\frac{\Pi^2}{1\text{ atm}}\frac{293}{(273+T)}\right), \quad (11)$$

where $\beta$ is the relative volume of the traps in unit volume, and $\gamma_m$ is the metal density.

Coefficient $\mu$ is determined as follows:

$$\mu = 0 \text{ at } T < T_r \text{ and}$$

$$\frac{\partial \beta}{\partial t}-\frac{2\beta}{\Pi}\frac{\partial \Pi}{\partial t}-\beta\frac{\partial T}{\partial t}\frac{1}{T+273}<0, \quad (12)$$

$$\mu = 1 \text{ in all the rest of the cases;} \quad (13)$$

$T_r$ is the temperature below which a trap becomes irreversible.

**Table 3.** Calculation results and experimental data on measurement of mean concentrations of $H_{dif}$ and $H_{res}$ for a model sample depending upon the welding depth

| $L$, m | $t$, s | $T_{max}$, °C | FZ | | HAZ |
|---|---|---|---|---|---|
| | | | $H_{dif}$, cm³/100 g | $H_{res}$, cm³/100 g | $H_{dif}$, cm³/100 g |
| 0.1 | 10 | 258 | 16.5 | 5.5 | 8.5 |
| | 20 | 78 | 13.5 | 7.9 | 6.8 |
| | 28 | 38 | 13.0 (14.3) | 8.2 (7.8) | 6.6 |
| 100 | 10 | – | 21.3 | 3.7 | 10.0 |
| | 20 | – | 19.03 | 5.6 | 8.5 |
| | 28 | – | 18.6 (19.9) | 5.9 | 8.2 |

*Note.* Experimental data are given in brackets.

$\Pi(x, y, t) \equiv 0$ at the boundary with water. $\Pi(x, y, t) = \sqrt{P_H}$, where $P_H$ is the partial pressure of hydrogen in the vapour-gas bubble, at the boundary in the vapour-gas bubble. Potential of the concentration of diffusible hydrogen $H(x, y, 0) = H_0$ in the FZ, and in the rest of material $H(x, y, 0) = 0.5$ cm³/100 g.

It is suggested in [6] that the values of $K(x, y, t)$, $D(x, y, t)$ and $\beta(x, y, t)$ should be estimated depending upon the microstructure at a given point of the FZ or HAZ metal in the following form:

$$J(x, y, t)=\sum_j J_j(T)V_j(x, y, t), \quad (14)$$

where $J = K, D, \beta$; $j = a, f, p, b, m$, respectively, for austenite, ferrite, pearlite, bainite and martensite; $V_j(x, y, t)$ is the mass fraction of the $j$-th microstructure at point $(x, y)$ at time moment $t$. The values of $K_j(T)$, $D_j(T)$ and $\beta_j(T)$ were estimated using dependencies suggested in [6].

$H_0$ and $\beta_j$, which were not determined in the given model, were estimated on model samples. Table 3 gives results of the calculations made by using the described algorithm for a model sample at $H_0 = 25$ cm³/100 g; $\beta_a = 0$; $\beta_{fp} = 0.005$ and $\beta_m = 0.05$, compared with the experimental data for the FZ metal.

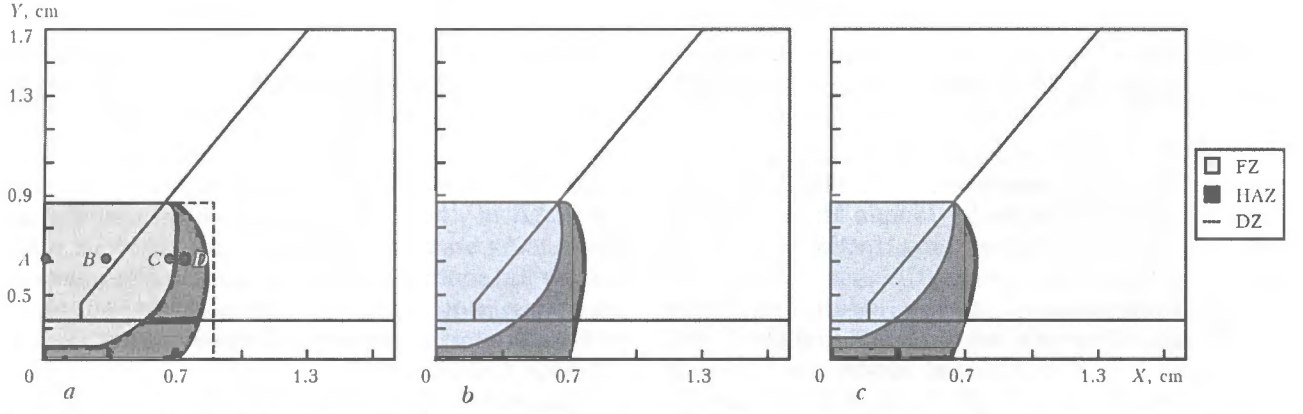


**Figure 3.** FZ, HAZ and diffusion zone (DZ) at a depth of 0.1 (*a*), 50 (*b*) and 100 (*c*) m (*A*, *B*, *C*, *D* — characteristic points)

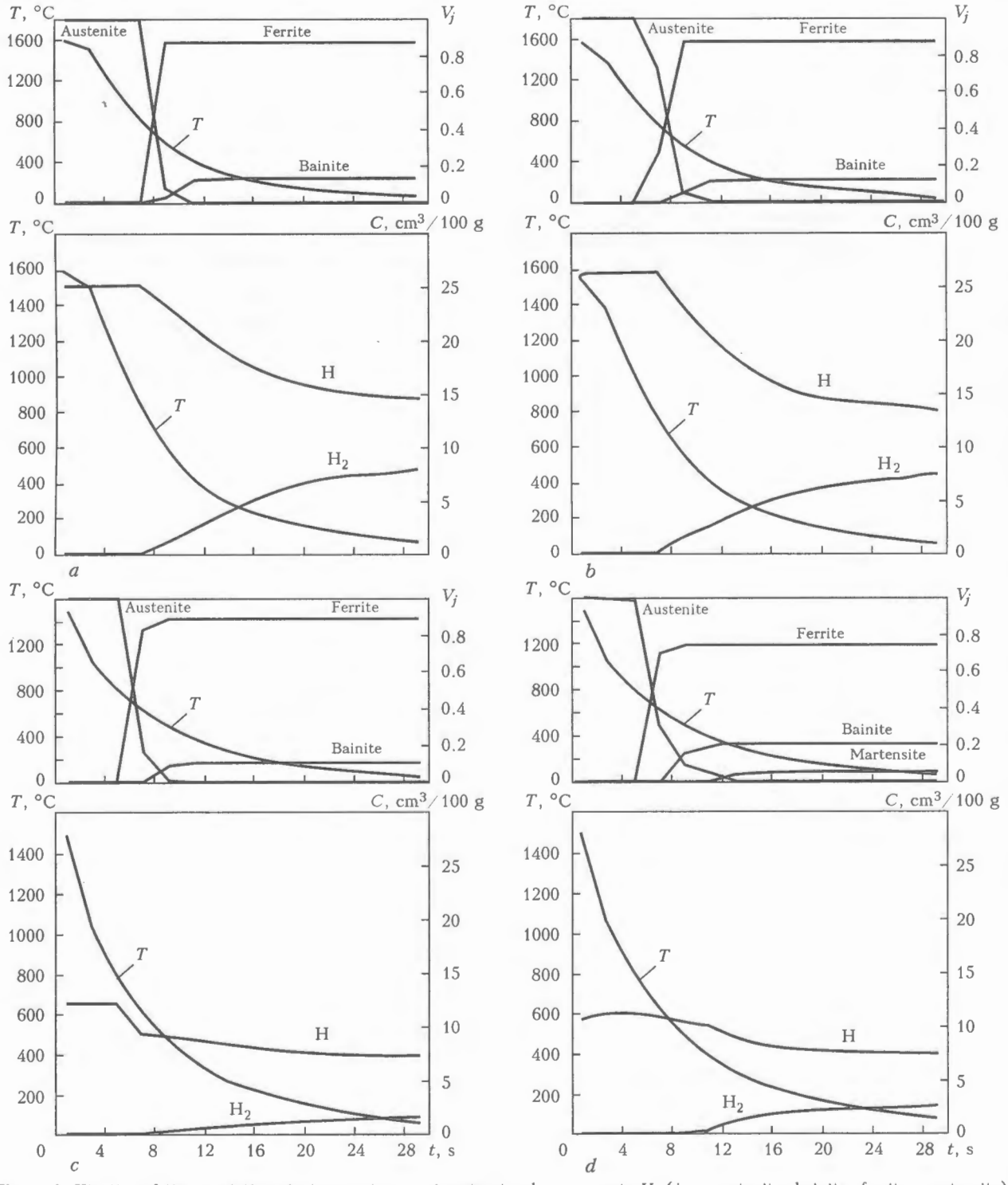


**Figure 4.** Kinetics of time variations in temperatures, microstructural components $V_j$ ($j$ — austenite, bainite, ferrite, martensite), diffusible hydrogen H, and hydrogen in traps, $H_2$, for a welded joint in steel St3 at characteristic points $A$ (*a*), $B$ (*b*), $C$ (*c*) and $D$ (*d*) at a depth of 0.1 m

Selected parameters $H_0$ and $\beta_j$ provide a satisfactory agreement of experiment with calculations. In the HAZ metal of a model sample the content of diffusible hydrogen is very close to the critical one according to Table 1.

**Results of numerical studies.** Figure 3 shows the data of calculation of sizes of the FZ and HAZ for a joint under consideration made under the following welding conditions: $I_w$ = 180 A, $U_w$ = 32 V and $v_w$ = 0.17 cm/s (thermal-physical properties of steels St3 and 17G1S are approximately the same, which determines the insignificant difference in size of the FZ and HAZ of these steels in welding at different depths). As seen, the FZ and HAZ decrease with increase in depth $L$, which is natural for constant conditions, as $\eta_s$ decreases, and energy expenditures for formation of a vapour-gas bubble around the arc increase.

Figures 4–7 show the calculated data on the kinetics of variations in temperatures, microstructures

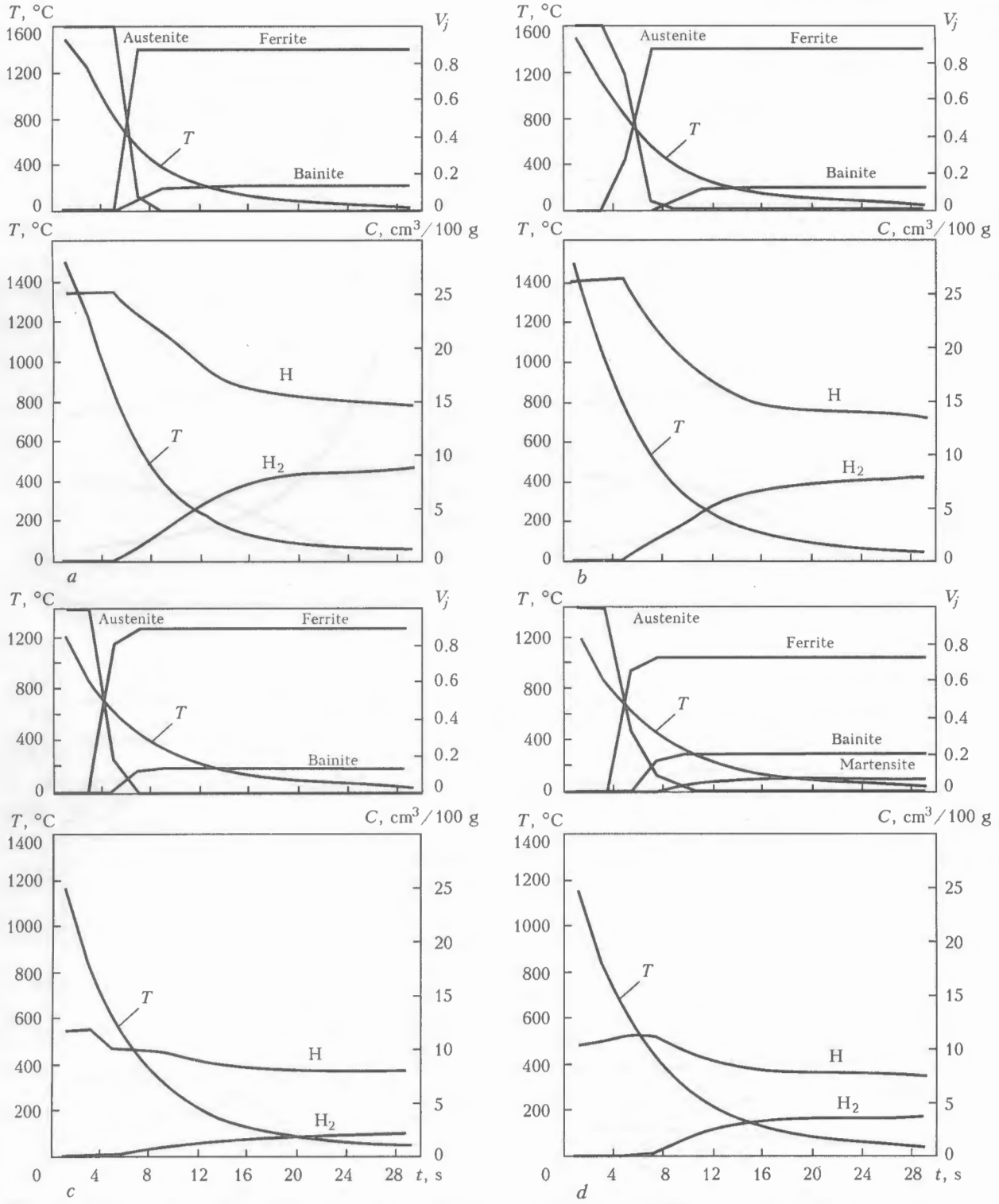


**Figure 5.** Kinetics of time variations in temperatures, microstructural components $V_j$, diffusible hydrogen H, and hydrogen in traps, $H_2$, for a welded joint in steel St3 at characteristic points *A* (*a*), *B* (*b*), *C* (*c*) and *D* (*d*) at a depth of 100 m

(procedure of study [6] was used), diffusible hydrogen H and hydrogen in traps, $H_2$, in welding at a depth of 0.1 to 100 m for characteristic points *A*, *B*, *C* in the FZ and *D* in the HAZ. The data in Figures 4 and 5 relate to steel St3, while those in Figures 6 and 7 – to steel 17G1S. Analysis of the data shows that variations in a microstructure (low content of carbon and alloying elements) with increase in depth *L* are insignificant for the fusion zone (points *A*–*C*). Accordingly, little changes are seen in the kinetics of variations in H and $H_2$ at points *A*–*C* for the steels considered. Point *D* in the HAZ is a bit different. For steel St3 this difference shows up as increase in H and $H_2$ within 10 %, as *L* increases from 0.1 to 100 m (Figures 4 and 5). For steel 17G1S this difference is more pronounced and shows up as increase in $H_2$ at point *D* from 7 to 9.5 $cm^3/100$ g (Figures 6 and 7) at approximately constant H equal to

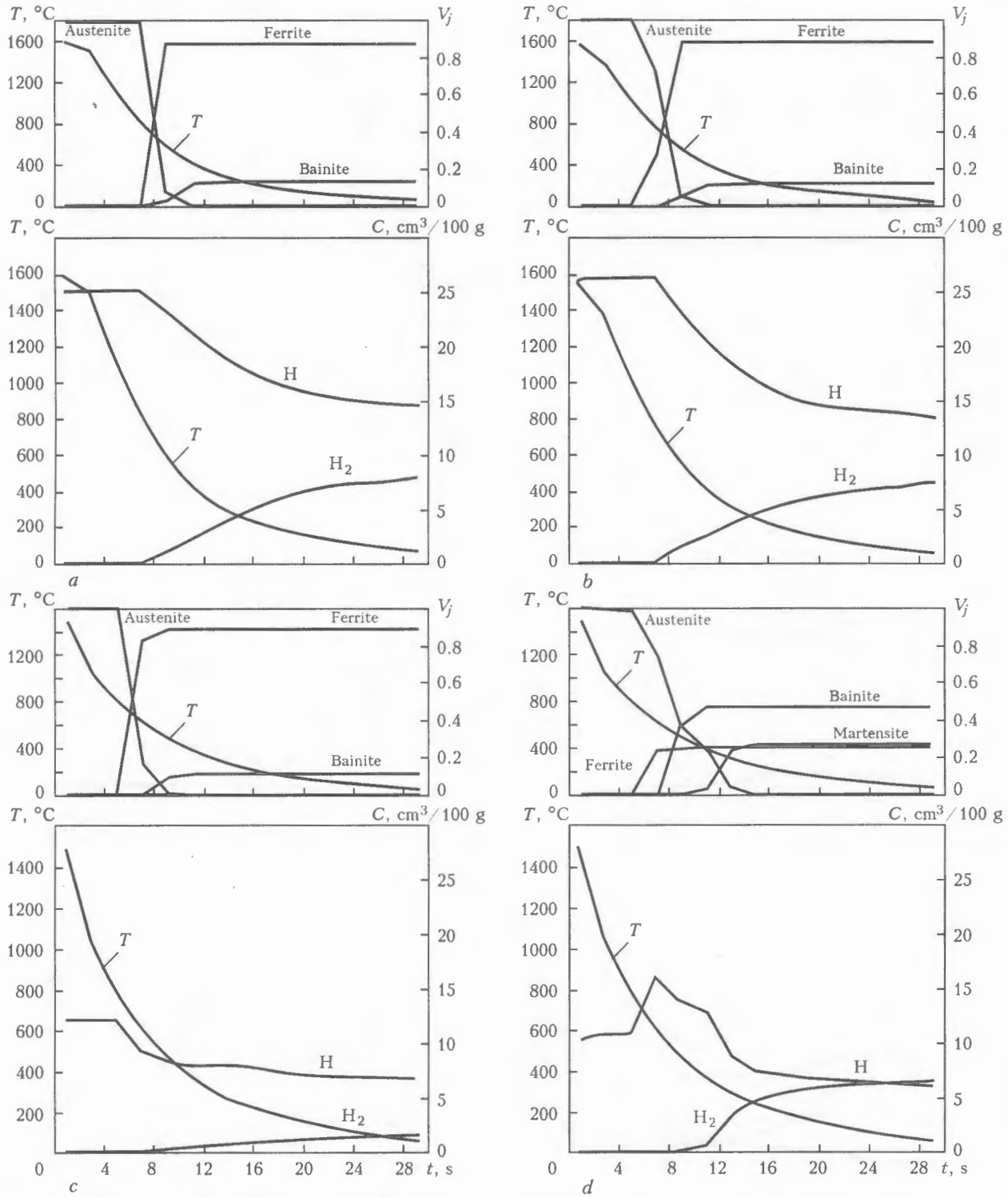


**Figure 6.** Kinetics of time variations in temperatures, microstructural components $V_j$, diffusible hydrogen H, and hydrogen in traps, $H_2$, for a welded joint in steel 17G1S at characteristic points *A* (*a*), *B* (*b*), *C* (*c*) and *D* (*d*) at a depth of 0.1 m

7 $cm^3/100$ g, which is attributable to a higher content of martensite (about 30 % compared with steel St3, where $V_m \approx 0.07 = 7$ %).

Mean values of the concentration of $H_{dif} = H$ and $H_{res} = H_2$ in the FZ and HAZ metal for steels under consideration at different moments of the cooling time in welding at different depths are given in Table 4. It can also be seen from these data that an increase in depth leads to growth of the mean values of H and $H_2$ in the FZ and HAZ metals in cooling of a welded joint. However, for the welding conditions under consideration it is not in excess of 10 %.

As in the scheme considered the increase in ingress of hydrogen is determined by the partial pressure of the latter in the vapour-gas bubble and time of existence of this bubble in a particular region of a welded joint, consideration was given to a variant of welding of the root pass in the joint shown in Figure 1 at a double heat input. As shown by the calculations, considerable differences in the concentration of hydrogen

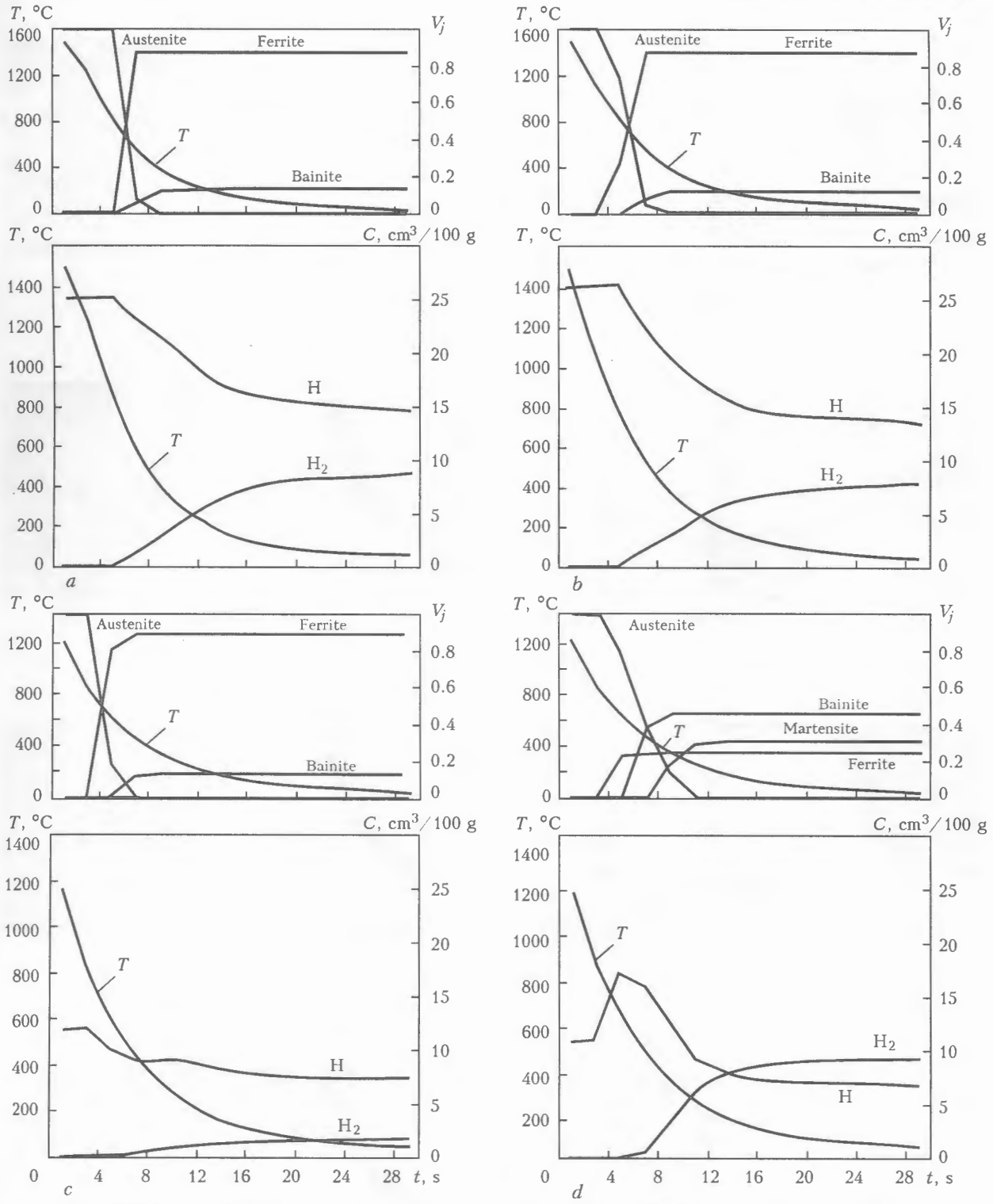


**Figure 7.** Kinetics of time variations in temperatures, microstructural components $V_j$, diffusible hydrogen H, and hydrogen in traps, $H_2$, for a welded joint in steel 17G1S at characteristic points *A* (*a*), *B* (*b*), *C* (*c*) and *D* (*d*) at a depth of 100 m

are seen only in a thin surface layer at the time moments of an active mass exchange with the vapour-gas bubble (Figures 8 and 9). The total hydrogen content is seen to increase as a result of growth of the FZ, the mean concentration of hydrogen in which changes but insignificantly, this being associated with a short time of an active mass exchange with the vapour-gas bubble.

It can be seen from the data of Table 4 that the mean content of diffusible hydrogen H in the HAZ metal on steel 17G1S is quite enough for formation of cold cracks. In this connection, the use was made of a well-known approach associated with the application of an austenitic filler metal to reduce the concentration of diffusible hydrogen in the HAZ metal. The data on chemical composition of the FZ metal required for the calculations were generated experimentally on a model sample. They are given in Table 5.

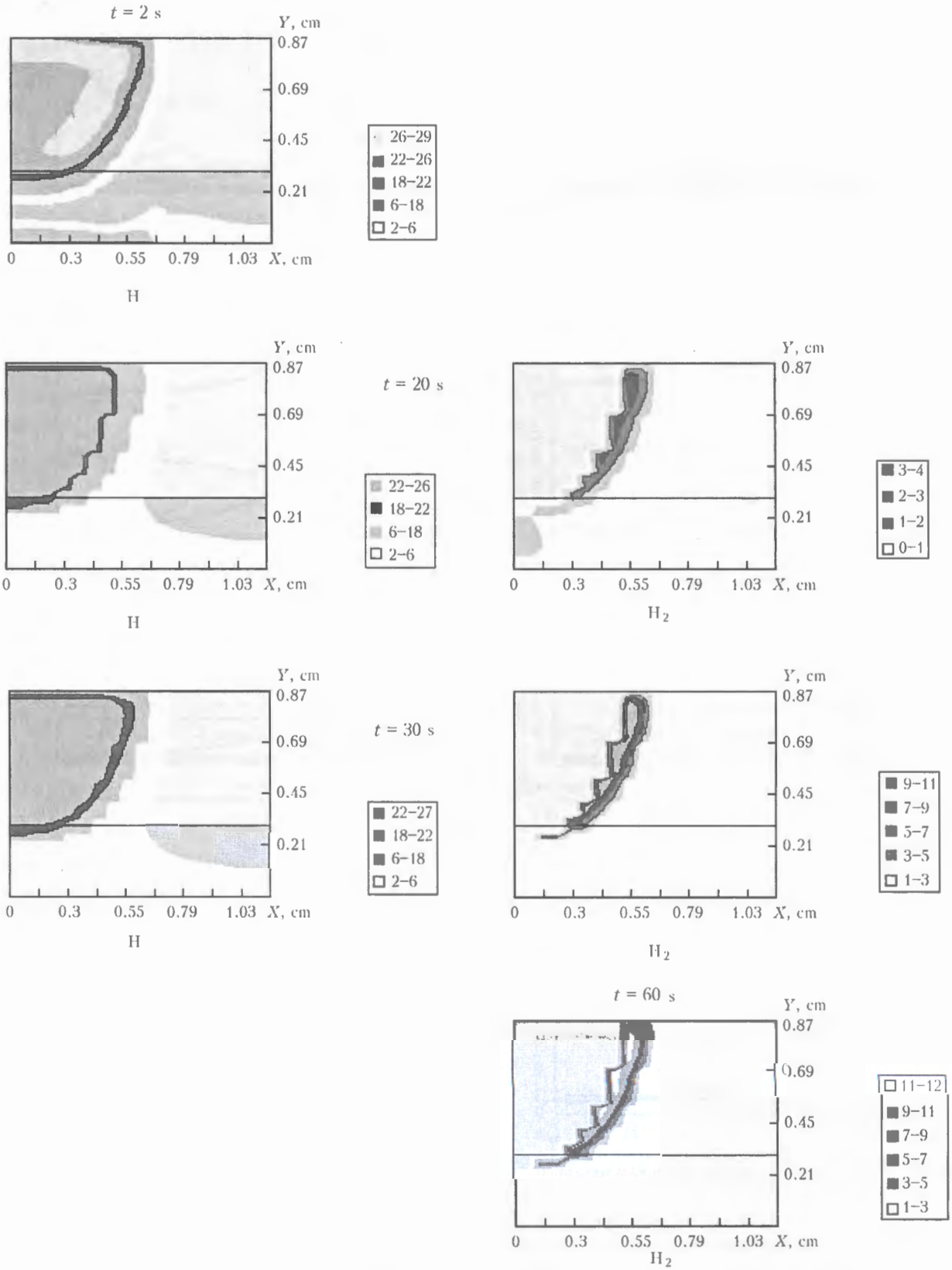


**Figure 8.** Distribution of H and $H_2$ across the section of a root weld at different time moments $t$ under standard conditions

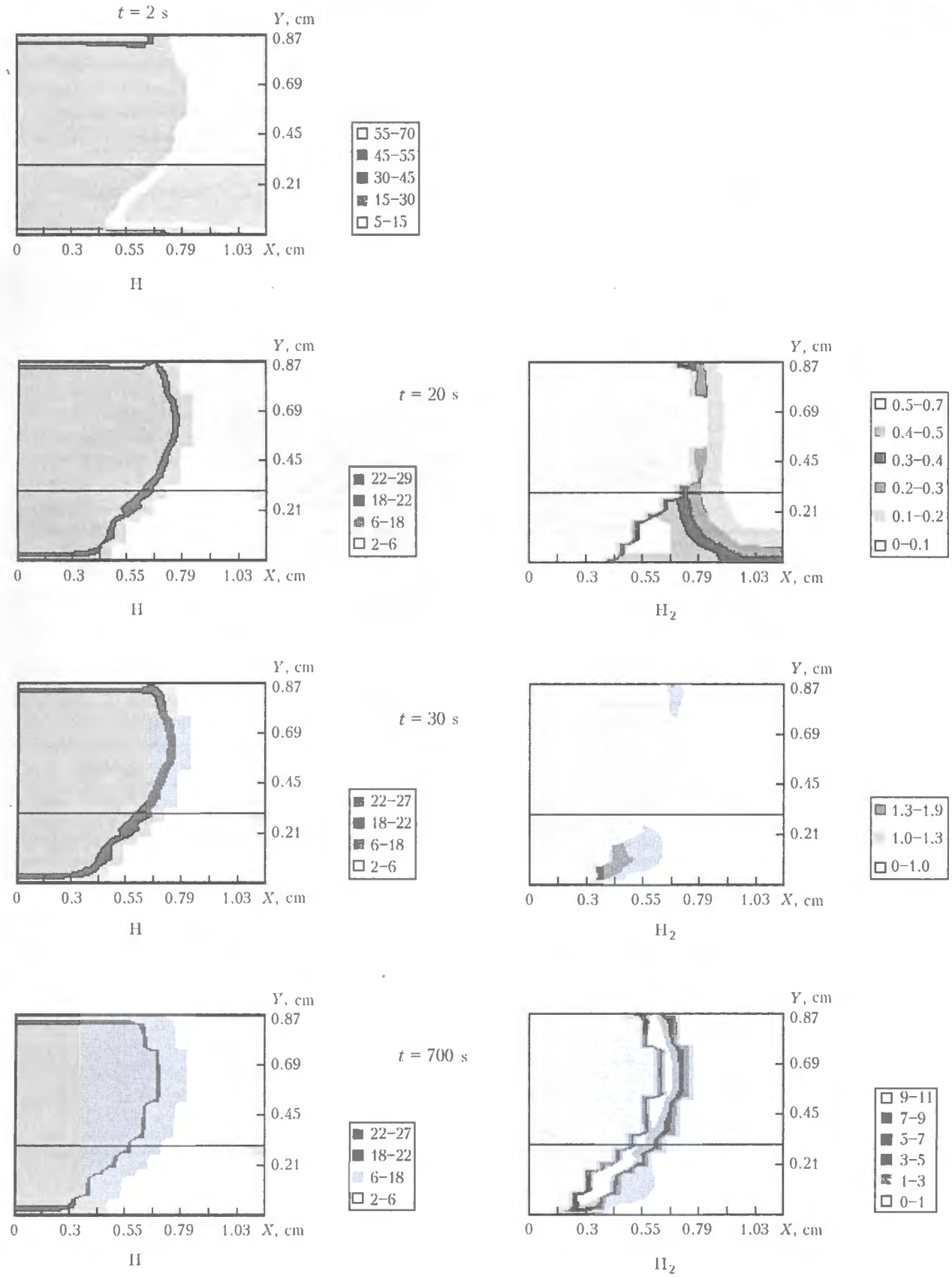


**Figure 9.** Distribution of H and $H_2$ across the section of a root weld at different time moments $t$ at a double heat input

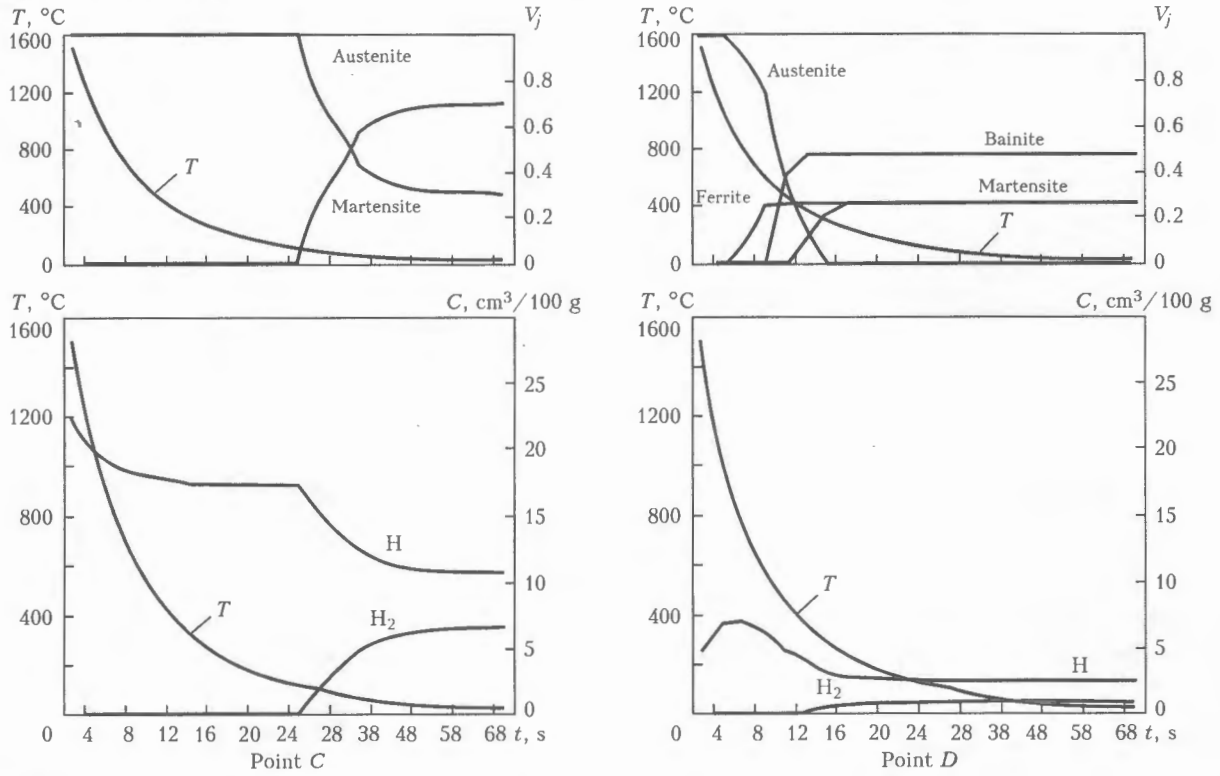


**Figure 10.** Kinetics of time variations in temperature, microstructural components $V_j$, diffusible hydrogen H, and hydrogen in traps, $H_2$, for a welded joint in steel 17G1S made using an austenitic filler metal at a depth of 0.1 m at characteristic points *C* and *D*

**Table 4.** Mean values of the concentration of H and $H_2$ in the FZ and HAZ metals depending upon the welding depth *L* at different moments of cooling time *t*

| *L, m* | *t, s* | *H, cm³/100 g* | | | | $H_2$, *cm³/100 g* | | | |
|---|---|---|---|---|---|---|---|---|---|
| | | *St3* | | *17G1S* | | *St3* | | *17G1S* | |
| | | *FZ* | *HAZ* | *FZ* | *HAZ* | *FZ* | *HAZ* | *FZ* | *HAZ* |
| 0.1 | 10 | 14.5 | 4.1 | 14.5 | 4.6 | 0.9 | 0.07 | 0.9 | 0.05 |
| | 20 | 9.6 | 3.9 | 9.5 | 3.5 | 3.5 | 0.8 | 3.5 | 1.9 |
| | 30 | 8.8 | 3.7 | 8.7 | 3.2 | 4.3 | 1.0 | 4.3 | 2.3 |
| 50 | 10 | 16.4 | 6.0 | 16.3 | 6.9 | 1.5 | 0.14 | 1.5 | 0.1 |
| | 20 | 11.4 | 5.1 | 11.2 | 4.4 | 4.6 | 1.3 | 4.5 | 3.0 |
| | 30 | 10.8 | 5.0 | 10.7 | 4.2 | 5.2 | 1.5 | 5.1 | 3.3 |
| 100 | 10 | 15.2 | 5.9 | 15.0 | 6.4 | 2.2 | 0.43 | 2.1 | 0.8 |
| | 20 | 11.4 | 5.2 | 11.3 | 4.3 | 4.9 | 1.48 | 4.8 | 3.2 |
| | 30 | 10.9 | 5.0 | 10.9 | 4.1 | 5.5 | 1.63 | 5.4 | 5.3 |

**Table 5.** Chemical composition of the FZ metal for a variant with austenitic filler metal

| *Region in FZ* | *Content of elements, wt.%* | | | | | | $Cr^{eq}$ | $Ni^{eq}$ |
|---|---|---|---|---|---|---|---|---|
| | *C* | *Ni* | *Mn* | *Cr* | *Mo* | *Si* | | |
| Major mass of the FZ metal | 0.066 | 14.70 | 5.00 | 14.20 | 2.80 | 0.50 | 17.7 | 19.2 |
| Layer near the base metal interface | 0.066 | 8.74 | 3.85 | 7.32 | 1.86 | 0.45 | 9.7 | 12.8 |

The FZ metal contains a small layer 0.1–0.2 mm thick, located near the interface with the base metal. Chemical composition of this layer is substantially different from the mean one for the FZ metal.

Table 5 gives values of $Cr^{eq}$ and $Ni^{eq}$ of the compositions for the Schaeffler diagram, allowing estimation of a microstructure after complete cooling (the major mass of the FZ metal has an austenitic microstructure, while the layer near the interface has a martensitic-austenitic microstructure). In this case the martensitic transformation begins at a temperature of +115 °C and ends at a temperature of −15 °C. At the end of the transformation the martensite content is ≈ 70 %, i.e. $V_m = 0.1$. Figure 10 shows the calculated data on the kinetics of variations in temperature, microstructure and concentration of hydrogen H and $H_2$ at characteristic points: $C$ — layer with the final martensitic-austenitic structure and $D$ — point of the HAZ metal (see Figure 3). By comparing data in Figures 8 and 9 with the corresponding ones in Figure 6, we can see that the concentration of hydrogen in the HAZ metal at point $D$ decreased from 7.0 to 1.0 $cm^3/100$ g, which is attributable to its accumulation in the austenitic weld metal, i.e. in wet underwater welding the use of an austenitic filler metal is an efficient method to decrease the content of hydrogen in the HAZ metal of carbon and low-alloy steels.

## CONCLUSIONS

1. Increase in depth of wet underwater welding of low-carbon and low-alloy steels from 0.1 to 100 m leads to increase in the content of diffusible hydrogen in the FZ metal. However, its mean content is not high (within a range of 10 %).

2. Increase in the welding heat input leads to an increase in the total content of hydrogen in a welded joint mostly due to growth of the FZ size. The mass exchange processes occurring in the vapour-gas bubble affect the concentration of hydrogen only in a thin surface layer.

3. The content of $H_{dif}$ in the HAZ metal of steel St3 is insufficient for formation of cold cracks even in welding under the restrained conditions.

4. The content of diffusible hydrogen in the HAZ metal of steel 17G1S is sufficient for formation of cold cracks in a joint welded under the restrained conditions.

5. The use of the austenitic filler metal is an efficient method for decreasing the concentration of diffusible hydrogen in the HAZ metal of low-alloy steels in wet underwater welding.


1. Suga, J., Hasui, A. (1986) On formation of porosity in underwater wet weld metal (Report 1). *Transact. of JWS*, 17(1), 58–64.
2. Ando, S., Asahami, T. (1983) A study on the metallurgical properties of steel welds with underwater gravity welding. In: *Proc. of Conf. on Underwater Welding*. Pergamon Press.
3. Rowe, M.D., Liu, S., Reynolds, T.J. (2002) The effect of ferroalloy additions and depth on the quality of underwater wet welds. *Welding J.*, August, 156–166.
4. (1998) *Welding Handbook. Materials and applications*. Miami: AWS.
5. Smith, R.D., Landis, G.P., Maroff, I. et al. (2001) The determination of hydrogen distribution in high-strength steel weldments. Part 1. Laser ablation methods. *Welding J.*, **5**, 115–122.
6. Makhnenko, V.I., Korolyova, T.V., Lavrinets, I.G. (2002) Effect of microstructural transformations on redistribution of hydrogen in fusion welding of structural steels. *The Paton Welding J.*, **2**, 6–13.
7. Mikhailov, V.G., Thomas, K., Vohlfahrt, H. (1996) Numerische Simulation der Wasserstoffverteilung in mehrlagigen Schweissverbindungen. *Schweissen und Schneiden*, **48**, 47–50.
8. Yurioka, N., Ohkita, S., Nakamura, H. et al. An analysis of effect of microstructure, strain and stress on the hydrogen accumulation in the weld heat affected zone. *IIW Doc. IX-1161–80*.
9. Pokhodnya, I.K., Paltsevich, A.P., Yavdoshchin, I.P. (1978) *Chromatographic method for determination of the diffusible hydrogen content of the welds*. Kiev: PWI.

# MATHEMATICAL MODELLING OF THE PROCESS OF PLASMA SPRAYING OF COMPOSITE POWDERS ALLOWING FOR THE EXOTHERMIC REACTION OF SYNTHESIS OF COATING MATERIAL

**Yu.S. BORISOV, A.S. ZATSERKOVNY** and **I.V. KRIVTSUN**
E.O. Paton Electric Welding Institute, NASU, Kiev, Ukraine

Mathematical model has been developed for calculation of dynamics of heating of composite powder particles in a plasma jet, allowing for the heat released as a result of chemical reaction between the initial components of powder materials. Software has been developed to implement the model on a computer. Numerical analysis has been conducted for peculiarities of heating and movement of composite particles Ni–Al in the plasma jet, allowing for the heat released in the bulk of the particles through the exothermic reaction of formation of an intermetallic compound.

***Keywords:*** *plasma spraying, composite powder, heating of particles, exothermic reaction, intermetallic, mathematical model, software*

Proper selection of a set of process parameters determining spraying conditions is very important for production of sound coatings. A detailed theoretical study of some physical-chemical phenomena occurring in plasma spraying of coatings, and development of appropriate mathematical models on the base of the above study allow prediction of the effect of different factors on the course of the process as a whole and avoidance, in many cases, of excessive financial costs for conducting direct experiments.

To find optimal conditions for heating and movement of spray particles, it is necessary to predict dynamics of interaction of a particle with the plasma jet, as well as processes occurring inside the particle. An important technological peculiarity of spraying with a possibility of the exothermic reaction to occur between fillers of composite powders consists in utilisation of internal energy resources of the powder particles resulting from the reaction of synthesis of the coating material. In this case development of a mathematical model for plasma heating of a composite powder particle allowing for thermal-chemical transformations inside it and their effect on the plasma spraying process can provide the possibility of prediction and control of resulting characteristics of the coatings. The fundamental difference of such a model from that developed earlier lies in the fact that it should describe heating of a particle under the effect of two heat sources, i.e. external (in the form of a heat flow from the plasma jet) and internal (in the form of the synthesis reaction heat). Moreover, composition and structure of the particle and, therefore, its thermal-physical characteristics may substantially change during heating, as the chemical reaction occurs.

Consider the model of heating of a spherical particle that consists of the exothermally reacting composite material moving in the plasma jet with known (preliminarily calculated) distributions of plasma temperature and velocity. To calculate the path and velocity of the particle in the jet, we will use the earlier developed model [1] based on solution of the equation of movement of a particle in the plasma flow under the aerodynamic drag effect. To find temperature field in the bulk of the particle, we will use a non-stationary heat conduction equation with a volume heat source [2, 3]:

$$\rho\bar{C}\frac{\partial T}{\partial t} = \frac{1}{r^2}\frac{\partial}{\partial r}\left(r^2\chi\frac{\partial T}{\partial r}\right) + \rho W_r\Phi(T, \eta). \qquad (1)$$

Here $\rho(T)$ is the mass density of the particle; $\bar{C}(T)$ is its effective specific heat; $T(r, t)$ is the time-space distribution of temperature in the particle (where $r$ is the co-ordinate and $t$ is the time); $\chi(T)$ is the coefficient of thermal conductivity of the composite material; $W_r$ is the specific heat of the exothermic reaction of synthesis of the coating material, and $\Phi(T, \eta)$ is the rate of heat release as a result of occurrence of the above reaction. To find it, we can use, for example, the law which is valid for homogeneous reactions [2]:

$$\Phi(T, \eta) = K_0 \exp\left(-\frac{E}{RT}\right)(1 - \eta)^n, \qquad (2)$$

$$\frac{\partial \eta}{\partial t} = \Phi(T, \eta), \qquad (3)$$

where $\eta$ is the degree of transformation of the initial components into an end product; $K_0$ is the pre-exponential factor; $E$ is the activation energy; $R$ is the universal gas constant; and $n$ is the reaction order.

Equation (3) is solved at an initial condition that $\eta\,|_{t = t_b} = 0$, where $t_b$ is the time of beginning of the chemical reaction determined as the time to reaching the temperature of beginning of the reaction, $T_r$, by the particle material (allowing for the retardation time [4]).

Equation (1) is solved at the following initial condition:

$$T(r)\big|_{t=0} = T_0 \qquad (4)$$

(here $T_0$ is the initial temperature of the particle), and at the following boundary conditions:

$$\frac{\partial T}{\partial r}\Big|_{r=0} = 0; \quad \left(\chi \frac{\partial T}{\partial r}\right)\Big|_{r=a} = q, \qquad (5)$$

where $q(t)$ is the density of the heat flow introduced by plasma through the particle surface [1], and $a(t)$ is its current radius. At an initial radius of $a_0 = d_0/2$, where $d_0$ is the initial diameter of the particle, which may change with time as a result of chemical transformation of a porous composite material into a dense end reaction product, as well as its melting or evaporation.

Assume that the initial particle of a composite powder is a mixture of finer particles of two different materials and has initial porosity $\nu_0$. Then the following expression can be used to determine density of such a composite material:

$$\rho = \frac{1 - \nu_0}{m_1/\rho_1 + m_2/\rho_2}, \qquad (6)$$

where $\rho_1$ and $\rho_2$ are the densities of the initial components of the composite powder, and $m_1$ and $m_2$ are their mass fractions.

Effective specific heat of the composite material calculated with allowance for the extent of its transformation can be written down as follows:

$$\bar{C}(T) = (1 - \eta)\bar{C}_n(T) + \eta\bar{C}_r(T). \qquad (7)$$

Effective specific heat of the reacted, $\bar{C}_r(T)$, and non-reacted, $\bar{C}_n(T)$, parts of the particle material can be calculated from the following formulae:

$$\bar{C}_r(T) = c_r(T) + W_r^m\delta(T - T_r^m) + m_1W_1^b\delta(T - T_1^b) + m_2W_2^b\delta(T - T_2^b), \qquad (8)$$

where $c_r(T)$ is the specific heat of the reacted material; $W_r^m$ is its latent melting heat; $W_1^b$ and $W_2^b$ are the latent boiling heats of each of the components; $T_r^m$ is the melting temperature of the reacted material; and $T_1^b$ and $T_2^b$ are the boiling temperatures of each of the mixture components;

$$\bar{C}_n(T) = [c_1(T) + W_1^m\delta(T - T_1^m)]m_1 + [c_2(T) + W_2^m\delta(T - T_2^m)]m_2, \qquad (9)$$

where $c_1(T)$ and $c_2(T)$ are the specific heats of the mixture components; $W_1^m$ and $W_2^m$ are their latent melting heats; and $T_1^m$ and $T_2^m$ are the respective melting temperatures. In all the cases $\delta(x)$ stands for the $\delta$-function.

The above mathematical model was used to calculate the path, velocity and temperature field of the composite particles Ni–Al with the following weight content of the initial components: $m_1 = 0.69$ (Ni) and $m_2 = 0.31$ (Al), having an initial porosity of $\nu_0 = 0.3$ and initial diameter of 40–70 μm. The calculations were made for the conditions of spraying in a plasma jet of the Ar + 20 % $H_2$ mixture generated by the plasmatron. Diameter of the anode nozzle of the plasmatron was $d = 6$ mm, arc current was $I = 450$ A, plasma gas mixture flow rate was $G = 55$ l/min (the arc voltage being $U_a = 64.2$ V, electric power of the plasmatron – $P = 28.9$ kW and efficiency – 62 %), and the spraying distance was 10 cm. Calculations of spatial distributions of temperature and velocity of the plasma in the jet considered were made using software CASPSP [1]. The method of Crank–Nicolson [5] involving time splitting of a step to allow for the latent heat of melting and evaporation of the material was used to find numerical solution to the heat conduction equation (1).

Values of the coefficients of drag and heat exchange between the particle and plasma required to solve the movement and heat conduction equations were calculated using the known criterial dependencies derived for the case of a flow around a spherical particle [6]. Values of thermal-physical parameters of aluminium and nickel used for the calculations are given in the Table.

Thermal conductivity $\chi$ of a porous composite material Ni–Al was assumed to be equal to $\chi_{Ni}(0.8 - \nu_0)$ [7], specific heat of the reaction of formation of intermetallic AlNi was $W_r = 1.66 \cdot 10^6$ J/kg, order of the reaction was $n = 1$, activation energy was $E =$

Thermal-physical properties of components

| *Composite material components* | *Specific heat c, J/(kg·K)* | *Density ρ, kg/m³* | *Thermal conductivity χ, W/(m·K)* | *Latent heat, J/kg* | | *Temperature, K* | |
|---|---|---|---|---|---|---|---|
| | | | | *melting* $W^m \cdot 10^{-6}$ | *evaporation* $W^b \cdot 10^{-7}$ | *melting* $T^m$ | *boiling* $T^b$ |
| Aluminium: | | | | | | | |
| solid | $766 + 0.459T$ | 2620 | $254.7 - 0.0412T$ | 0.397 | 1.089 | 934 | 2720 |
| liquid | 1178 | 2080 | 106.4 | | | | |
| Nickel: | | | | | | | |
| solid | $506.2 + 0.71T \to 1.59 \cdot 10^7/T^2$ | 8900 | $67.3 - 0.033T + 8.8 \cdot 10^{-6}T^2$ | 0.302 | 0.638 | 1726 | 3073 |
| liquid | 662.6 | 7910 | 69 | | | | |

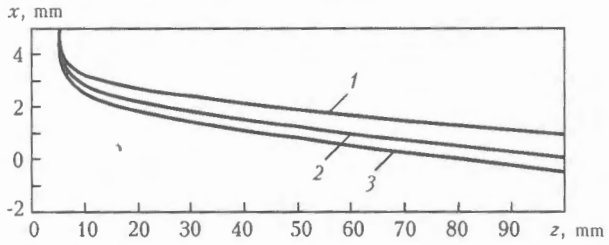


**Figure 1.** Paths of movement of the Ni–Al composite powder particles having different diameters in the plasma jet: *1* — $d_0$ = 40; *2* — 55; *3* — 70 μm

= $76 \cdot 10^3$ J/mol, and factor $K_0$ determining the rate of heat release during the reaction process varied from 0 to $1 \cdot 10^6$ $s^{-1}$ [2]. Density of the formed intermetallic AlNi was selected to be equal to 5945 kg/$m^3$, its thermal conductivity was 90 W/(m·K), and specific heat of the reacted material was $c_r(T) = 526.67 + 113.32 \cdot 10^{-3} T - 13.19 \cdot 10^5 T^2$ J/(kg·K) [2].

Conditions of introduction of particles into the jet were as follows: distance of the introduction point from the plasmatron axis was $x_0$ = 5 mm, and that from its exit section was $z_0$ = 0.5 cm, angle of introduction counted from the horizontal line was $\varphi = 0°$, diameter of the transportation channel was $d_c$ = 2 mm, transporting gas flow rate was $g_c$ = 2.2 l/min, and consumption of the powder was $M_p$ = 1–10 kg/h.

Figure 1 shows calculated paths of the Ni–Al composite powder particles having different diameters. They are indicative of a substantial effect of the initial diameter (mass) of a particle on its path. Conditions of introduction of particles into the jet were selected so that the deviation of a final position of a particle along the spraying distance from the jet axis was minimum (Figure 1, curve *2*) at a mean diameter of this particle ($d_0$ = 55 μm). Because of an increased inertia, particles with diameter $d_0$ = 70 μm get into hotter regions of the plasma jet, this ensuring their better heating. And vice versa, particles with a smaller diameter ($d_0$ = 40 μm) experience heat exchange with regions that are less hot, which allows overheating and loss of mass for evaporation to be avoided.

Calculations of the temperature field in a particle for different values of pre-exponential factor $K_0$ characterising the rate of release of the thermal energy due to occurrence of a chemical reaction were made at a fixed diameter of the particle ($d_0$ = 55 μm). It

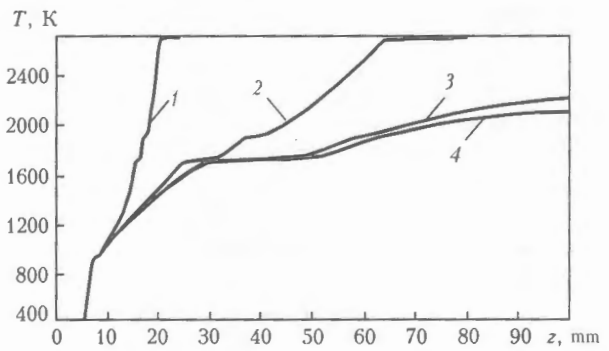


**Figure 2.** Effect of the rate of release of the reaction heat in the Ni–Al composite powder particle ($d_0$ = 55 μm) on dynamics of its heating in the plasma jet: *1* — $K_0 = 1 \cdot 10^6$; *2* — $1 \cdot 10^5$; *3* — $1 \cdot 10^4$ $s^{-1}$; *4* — with no allowance for release of the reaction heat

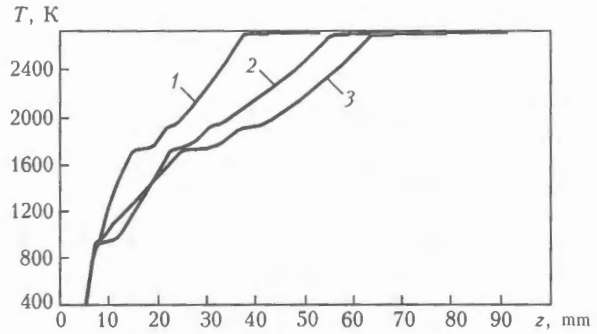


**Figure 3.** Effect of the initial diameter of the Ni–Al composite powder particles on dynamics of their heating in the plasma jet ($K_0 = 1 \cdot 10^5$ $s^{-1}$): *1* — $d_0$ = 40; *2* — 70; *3* — 55 μm

follows from Figure 2 that at $K_0 = 1 \cdot 10^6$ $s^{-1}$ the internal heat source makes a substantial contribution to the dynamics of heating of the particle as early as in the initial region of its movement (Figures 2–4 show the calculated curves for temperature at the centre and on the surface of particles along the spraying distance). Under the above conditions, the combined action of two thermal energy sources leads to an excessive overheating of a particle up to its boiling, i.e. to the inefficient utilisation of heat of the synthesis reaction.

Decrease in the $K_0$ values to $1 \cdot 10^5$ $s^{-1}$ shifts reaching the overheating zone to a point of 6.5 cm along the particle path, which means increase in the useful part of heat introduced by the internal source. At $K_0 = 1 \cdot 10^4$ $s^{-1}$ development of the process of exothermic synthesis is retarded to such an extent that the temperature curve for such a particle hardly differs from that for the Ni–Al particle, the release of heat due to the synthesis reaction being neglected. These results allow a conclusion that variations in the intensity of development of the process of exothermic synthesis in composite particles under the plasma spraying conditions may have a substantial effect on the dynamics of heating of a spray material.

Figure 3 show results of evaluation of the effect exerted by size of the composite powder particles on the dynamics of their heating. Although in this case the difference between the heating curves for particles with a diameter of 40, 55 and 70 μm is not as large as in the case of variations in $K_0$, it should be noted that increase in size of the particles leads to some retardation of development of the synthesis process. Under certain conditions this may lead to the fact that at the moment of reaching the surface of the substrate the particles of a different diameter will have not only a different temperature, but also a different degree of completion of the synthesis process.

The similar effect occurs with increase in consumption of a spray material powder (Figure 4). Increase in the powder consumption is accompanied by a delayed development of the synthesis process. As this causes the effect of cooling of the plasma jet, the similar result is likely to take place also in the case of decrease in the useful power of the plasmatron.

Therefore, the results of numerical experiments are indicative of a considerable effect exerted by heat of the chemical reaction of synthesis of a coating ma-

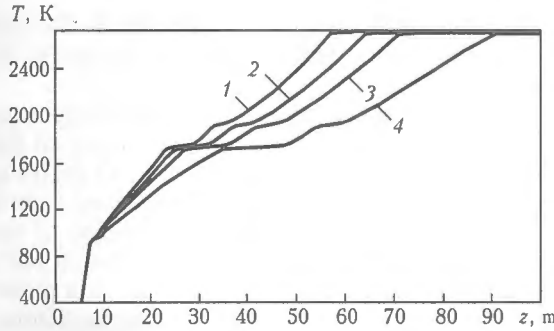


**Figure 4.** Dynamics of heating of the Ni–Al composite powder particles in the plasma jet at different loading of the jet with the powder ($d_0$ = 55 μm, $K_0$ = 1·10$^5$ s$^{-1}$): *1* — $M_p$ = 1; *2* — 3; *3* — 5; *4* — 10 kg/h

terial on the dynamics of plasma heating of the particles during the process of spraying of a composite powder. The mathematical model suggested in this study makes it possible to allow for the contribution by the thermal-chemical interaction of the powder particle components and predict the dynamics of heating, velocity and path of movement of the spray particles depending upon the different input parameters.

The software used to realise this model allows a computer-aided implementation of numerical experiments on plasma spraying of exothermally reacting composite powders, and can be used as a tool to solve engineering problems associated with selection of optimal parameters to provide coatings of this type of materials.


1. Borisov, Yu.S., Krivtsun, I.V., Muzhichenko, A.F. et al. (2000) Computer modelling of the plasma spraying process. *The Paton Welding J.*, **12**, 40–50.
2. Itin, V.I., Najborodenko, Yu.S. (1989) *High-temperature synthesis of intermetallic compounds*. Tomsk: TGU.
3. Shaw, K.G., McCoy, K.P., Trogolo, J.A. (1994) Fabrication of composite spray powders using reaction synthesis. In: *Proc. of 7th Int. Thermal Spray Conf.*, June 20–24, 1994. Boston.
4. Shorshorov, M.Kh (1981) Physical-chemical interaction of components in composite materials. In: *Composite materials*. Moscow: Nauka.
5. Anderson, D., Tannehill, J., Pletcher, R. (1990) *Computation hydromechanics and heat exchange*. Vol. 1. Moscow: Mir.
6. Tsvetkov, Yu.V., Panfilov, S.A. (1980) *Low-temperature plasma in reduction processes*. Moscow: Nauka.
7. Dulnev, G.N., Zarichnyak, Yu.P. (1974) *Thermal conductivity of mixtures and composite materials*. Leningrad: Energiya.


# EFFECT OF THE PROCESS FIXTURE MATERIAL ON STRENGTH CHARACTERISTICS OF TITANIUM AND ITS DIFFUSION BONDS


**L.S. KIREEV**[1], **V.V. SHURUPOV**[2], **V.V. PESHKOV**[2] and **G.P. BESPLOKHOTNY**[2]

[1]E.O. Paton Electric Welding Institute, NASU, Kiev, Ukraine

[2]Voronezh State Technical University, Voronezh, Russian Federation



Effect of material of a fixture used for diffusion bonding of thin-walled layered structures of titanium on its performance has been established. Fractography data and mechanical test results show that performance of the bonds in titanium is higher in the case of using the fixture of steel 20, compared with steel 12Kh18N10T.



***Keywords:*** *diffusion bonding, process fixture, titanium structures, adhesion, embrittled layer, mechanical tests*


As established before [1, 2], diffusion bonding results in contact and interaction of titanium billets with the process fixture. This leads to considerable changes in physical-chemical condition of the mating surfaces caused by development of the adhesion processes between titanium and steel, as well as diffusion saturation of the surface layers of titanium with the fixture material. Separation of the fixture from a part (steel from titanium) leads to fracture of the adhesion centres and formation of tears on the mating surfaces. Formation of the diffusion layers on titanium is accompanied by a change in their chemical composition, resulting in embrittlement.

In titanium structures with a honeycomb core, the load-carrying skins, which are in contact with the steel fixture during bonding, have a small thickness (up to 0.8 mm) and are not subjected to additional machining after diffusion bonding. This makes it necessary to quantitatively estimate the effect of the condition of the surface of titanium and its subsurface layers on performance of the titanium structures, i.e. mechanical properties and corrosion resistance.

Prior to mechanical tests, the plate samples of titanium alloy VT6 were annealed at a temperature of 900–950 °C in vacuum not worse than 1·10$^{-2}$ Pa to produce diffusion layers on their surfaces in contact with rectangular plate samples (fixtures) 2 mm thick with a size of 120×145 mm (or 180×60 mm) made from steel 20 or steel 12Kh18N10T. They were assembled into stacks, 5 plates in a stack, so that each titanium sample was placed between the steel samples. Development of the process of adhesion of titanium to steel during annealing led to a substantial defor-

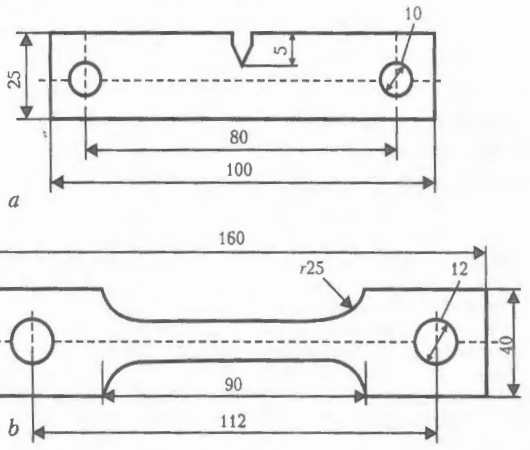


**Figure 1.** Schematics of specimens for the tests to cyclic fatigue by bending (*a*) and to repeated-static tension (*b*)

mation of the samples in their separation from the fixture. Therefore, the applied compressive pressure was decreased to 0.1 MPa.

Fractography of the surface of the titanium samples after annealing in contact with the steel samples revealed that the slightly developed adhesion regions were formed only after interaction of titanium with steel 12Kh18N10T. In this case almost no tears were found on the surface of titanium.

Thickness of the diffusion layers on titanium was quantitatively characterised by the depth of the embrittled zone, which was determined by the procedure described in [3]. Thickness of the embrittled layers on the surface of titanium was not in excess of 15–17 μm.

Testing the samples to uniaxial tension revealed no effect of the embrittled layers present on the surface of titanium on its performance. In all the cases the level of their properties remained not lower than the permissible one for alloy VT6.

Cyclic fatigue tests were conducted in compliance with the Drozdovsky's procedure by bending a flat specimen with a cantilever securing. Titanium specimens with a notch were used for the tests (Figure 1, *a*).

The time of loading of the specimens to the moment of initiation of crack up to 3 mm long was measured during the tests. Machine equipped with a vibration device and special clamps was manufactured to test the plate specimens to cyclic fatigue (Figure 2). One end of a specimen tested was secured in fixed clamp *1*, and the other end of the specimen was secured in mobile clamp *2* with eccentric *3* (disk with weights) located inside it. The eccentric was set to rotation through flexible shaft *4* from electric motor *5*. Distance from the notch point of the specimen to the axis of rotation of the eccentric was kept unchanged in all the experiments.

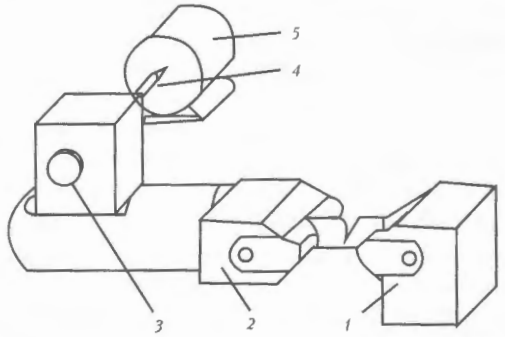


**Figure 2.** Schematic of machine to induce cracks in plate samples (see designations in the text)

Initiation of crack occurred as a result of constant vibration of the mobile clamp hanging freely on the specimen, the vibration frequency being 47 cycle/s. The moment of initiation of crack was fixed from a sudden growth of the amplitude of vibration of the mobile clamp. The machine was automatically switched off using a limit switch located at a preset distance from the axis of the vibration device. Knowing the time of operation of the specimen to initiation of crack and vibration frequency, it is possible to determine the number of cycles of loading of the specimen, $N_c$, to initiation of crack.

Results of the fatigue tests to cyclic bending showed that the presence on the VT6 specimens of the embrittled layers with thickness $\delta_{emb}$ = 0.1–0.5 μm, formed in contact with steel 20, led to an insignificant decrease in their cyclic fatigue life, compared with the material in the as-received condition.

Increase in thickness of an embrittled layer leads to decrease in the number of the loading cycles, $N_c$, to initiation of crack. The values of fatigue life of the specimens are in this case in a low-cycle region ($N_c < 50,000$) and decrease with increase in thickness of the embrittled layer (Figure 3).

As fatigue cracks are formed in surface layers of the specimens, their condition is very important. Therefore, providing high fatigue characteristics of titanium specimens at thickness of an embrittled layer equal to 0.5 μm is associated with the fact that its thickness is comparable with or smaller than the critical size of the formed crack. At the same time, it can be supposed that formation of the embrittled layer of

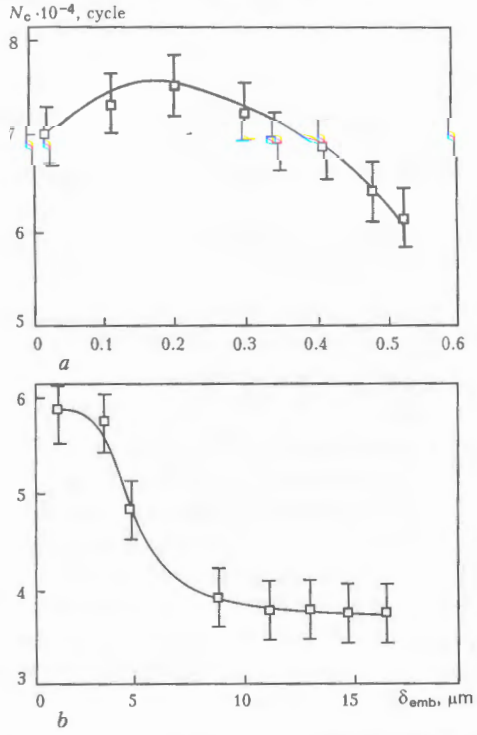


**Figure 3.** Dependence of the number of loading cycles, $N_c$, to initiation of crack upon the thickness of an embrittled layer, $\delta_{emb}$, in cyclic bend tests of specimens of alloy VT6 after annealing in contact with steel 20 (*a*) and steel 12Kh18N10T (*b*)

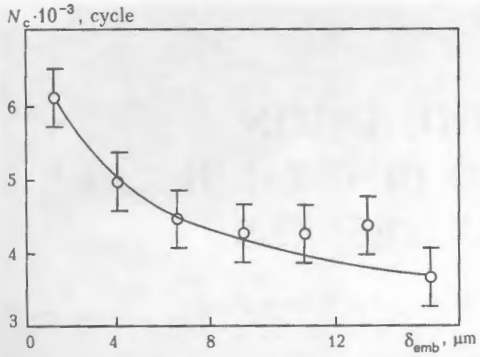


**Figure 4.** Dependence of the number of loading cycles, $N_c$, to initiation of crack upon the thickness of an embrittled layer in repeated-static tension tests of specimens of alloy VT6 after annealing in contact with steel 12Kh18N10T

a small thickness on the surface of titanium favours its hardening and formation of additional compressive stresses inhibiting the propagation of fatigue cracks.

In addition to the fatigue bend tests, the above specimens were subjected also to the repeated-static tension tests performed by the standard procedure (Figure 1, *b*). The tests were conducted using the UMM-10 machine (at frequency $f = 0.7–0.8$ Hz and cycle asymmetry coefficient $R = +0.1$).

The results of testing the specimens to repeated-static tension (Figure 4) are indicative of a similar character of the dependence of the fatigue life of titanium specimens upon the thickness of an embrittled layer to that established above.

It should be noted that under conditions of diffusion bonding of titanium structures with a honeycomb core, a compressive specific pressure in the zone of contact of the load-carrying skins with the process fixture is higher by a factor of 20 than that used in annealing of the mechanical test specimens. Therefore, the process of adhesion of titanium to the fixture occurs more intensively under actual condition than in experiments. Separation of the fixture from a part bonded may result in formation of defects of the type of tears on the surface of titanium. Under cyclic loads, they will act as stress raisers and centres of initiation of fatigue cracks.

Based on the above-said, part of the specimens for the repeated-static tension tests (see Figure 1, *b*) was made directly from the load-carrying skins (0.8 mm thick) of the panels with a honeycomb core, 20×150×500 mm in size. Bonding of these panels was performed in low vacuum. During the subsequent bend tests the fracture occurred in the zone of a diffusion bond between the skin and the honeycomb core, the skin in this case separated from the core.

The external surface of the load-carrying skins, which were in contact with the steel fixture during bonding, exhibited very clear traces of a direct interaction of the fixture with the part, i.e. contact regions. Fractography of these regions revealed a substantial effect exerted by the process fixture material on their topography on the surface of the titanium load-carrying skins.

In the case of using the fixture from steel 12Kh18N10T, the traces of tears and brittle fracture, which occurred not only in titanium but also in steel, were seen in the contact regions. Films (probably

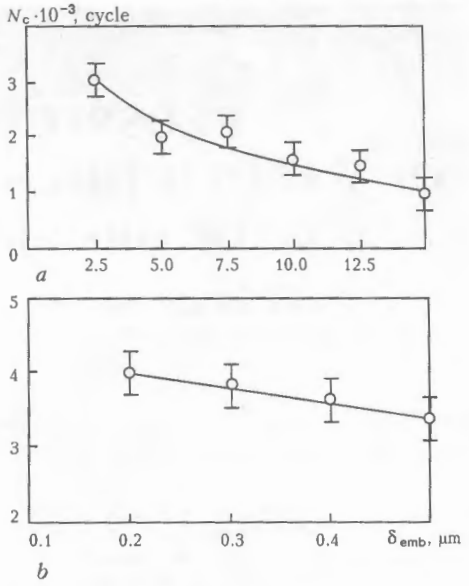


**Figure 5.** Dependence of the number of loading cycles, $N_c$, to initiation of crack upon the thickness of an embrittled layer in repeated-static tension tests of specimens of alloy VT6 after bonding at 950 °C in contact with steel 12Kh18N10T (*a*) and steel 20 (*b*)

containing titanium carbides) with slight traces of interaction of the fixture with a part were revealed in process plates of steel 20 in the regions which were in contact with titanium.

It should be noted that in the case of a repeated use of the process plates of both steel 12Kh18N10T and steel 20 for diffusion bonding, the number and size of defects in the contact regions increased. This also led to increase in the force required to separate the fixture from the part.

In the case of the fixture of steel 12Kh18N10T, this is attributable to saturation of its surface with titanium, and in the case of the fixture of steel 20 – to its depletion in carbon and suppression of the reaction of formation of titanium carbides.

The results of the repeated-static tension tests of the specimens are shown in Figure 5. It follows from them that, firstly, the earlier established dependence $N_c = f(\delta_{emb})$ holds and remains valid: at $\delta_{emb} \leq 0.5$ μm the number of loading cycles, $N_c$, varies but insignificantly, and further increase in $\delta_{emb}$ is accompanied by a substantial decrease in $N_c$. Secondly, the fatigue life of the specimens made from the load-carrying skins of the honeycomb panels subjected to a thermal-deformation cycle of bonding is much lower than that of the specimens of a plate material subjected to annealing (in fact, without deformation) in contact with steels: after interaction of titanium with steel 20 the values of $N_c$ decrease approximately 2 times, and with steel 12Kh18N10T – by a factor of 7–9. This decrease in the $N_c$ values is caused by microgeometry of the surface (formation of tears, undercuts etc.).

1. Fyodorov, S.N., Bondar, A.V., Peshkov, V.V. et al. (2000) Adhesion of titanium parts to steel fixture during diffusion bonding. *The Paton Welding J.*, **1**, 23–26.
2. Shurupov, V.V., Peshkov, V.V., Shushpanov, M.N. et al. (1999) Formation of embrittled layers on titanium in its interaction with steel fixture during diffusion bonding. *Avtomatich. Svarka*, **2**, 17–20.
3. Peshkov, V.V., Del, G.D., Orlova, L.M. et al. (1986) Determination of the depth of embrittled part of an oxidized layer on surface of titanium. *Zavod. Laboratoriya*, **9**, 75–77.

# PROSPECTS IN PRODUCTION OF WELDED THICK-WALLED BIMETAL BODIES OF HIGH-PRESSURE VESSELS

B.E. PATON[1], A.D. CHEPURNOJ[2], V.Ya. SAENKO[1] and L.B. MEDOVAR[1]
[1]E.O. Paton Electric Welding Institute, Kiev, Ukraine
[2]Mariupol Heavy Machine-Building Works, Mariupol, Ukraine

Main stages in creation of technology of manufacturing thick-walled bimetal high-pressure vessels are described and prospects in development of production of bimetal vessels at the present stage are outlined.

***Keywords:*** *bimetal bodies, high-pressure vessels, stamped-welded vessels, bimetal billets, bimetal plates, reactors for recycling the petroleum products, expanded multilayer shells, drums of steam boilers, electroslag welding, cladding in stamping, explosion cladding*

At the middle of the XX century, the science and industry faced the complicated problems, connected with the demand for the development of an effective technology of manufacture of thick-walled bimetal high-pressure vessels, capable to operate under the conditions of increased temperatures and pressures, periodical heat changes, long-term action of highly-aggressive medium, radiation, etc., in the process of the creation of the new engineering, first of all, nuclear power engineering, submarine, aerospace and petrochemical industries.

In most cases there is no need to manufacture a thick-walled vessel or high-pressure unit completely from the stainless high-alloy steel or alloy. It is enough to protect its internal surface from an aggressive effect of operating medium by a comparatively thin (3–8 mm) corrosion-resistant layer from this steel or alloy. Only in separate cases, for example, in manufacture of tube plates for heat exchange chemical units, it is necessary to deposit a protective layer on the internal and external surfaces. Here, the interest to the bimetal vessels is stipulated not only by the need in saving of highly-deficit materials. Application of bimetal with a basic layer from low- or medium-alloy steel of the increased or high strength makes it possible to decrease greatly the thickness of the vessel wall. As a result, the mass of this bimetal body, and also the labour-intensity in its manufacture become much lower than those of a single-layer body, for example, made completely from stainless steel 08Kh18N10T (wt.%: 0.08C, 19.5Cr, 11.3Ni, 0.5Ti).

Production of thick-walled bimetal vessels by forging in a press and subsequent cladding of corrosion-resistant steel on the inner surface was, at the beginning of the 1960s, the only method of producing, for example, bodies of nuclear power reactors. At the same time, the used technological process of manufacture of all-forged and forged-welded bimetal bodies was characterized by a low coefficient of utilization of materials (0.3 on average), high labour-intensity and long-time cycle of manufacture, that limited the production of the above-mentioned products.

It should be noted that as far back as 1952, the thick-walled drums of steam boilers of heat electric stations were manufactured first in the world practice from a plate rolled metal using the method of electroslag welding (ESW) at Taganrog Works «Krasny Kotelshchik» (TBW) in a close collaboration with the E.O. Paton Electric Welding Institute. Firstly, only welding of longitudinal welds was mastered, and then also that of circumferential welds. In 1954 the manufacture of stamped-welded drums of boilers using ESW was started at Barnaul Boiler Works (BBW). When the new technology of manufacture of drum of the boilers was mastering at TBW, the shells of 90 mm thick plate steel of 22K grade were expanded by rolling, while at BBW they were manufactured from two semi-shells (half-cylinders) which were stamped in a special press [1].

To realize the stamped-welded variant of manufacture of thick-walled bimetal bodies in industry, the large-sized bimetal plates of 80–300 mm thickness, up to 2500 mm width and up to 6000 mm length, having a guaranteed adhesion strength between the cladding and base layers over the entire area of the plate, which were not produced by our industry at that time, were required.

As a result of joint experiments, carried out by the E.O. Paton Electric Welding Institute, Kuznetsk Metallurgical Works and BBW under the experimental-industrial conditions, a method of producing bimetal plates using ESW was suggested [2]. The principle of this method is as follows: a cladding plate of stainless high-alloy steel or alloy was welded by ESW to one or two wide planes of ingot or forging from carbon, low- or medium-alloy steel, and then this welded billet was heated and rolled in the mill to produce two-, three-layer plate of the required sizes (Figure 1).

In 1961 the works om improvement of method of producing the two-, three-layer plate rolled metal using ESW were continued at Zhdanov Heavy Ma-

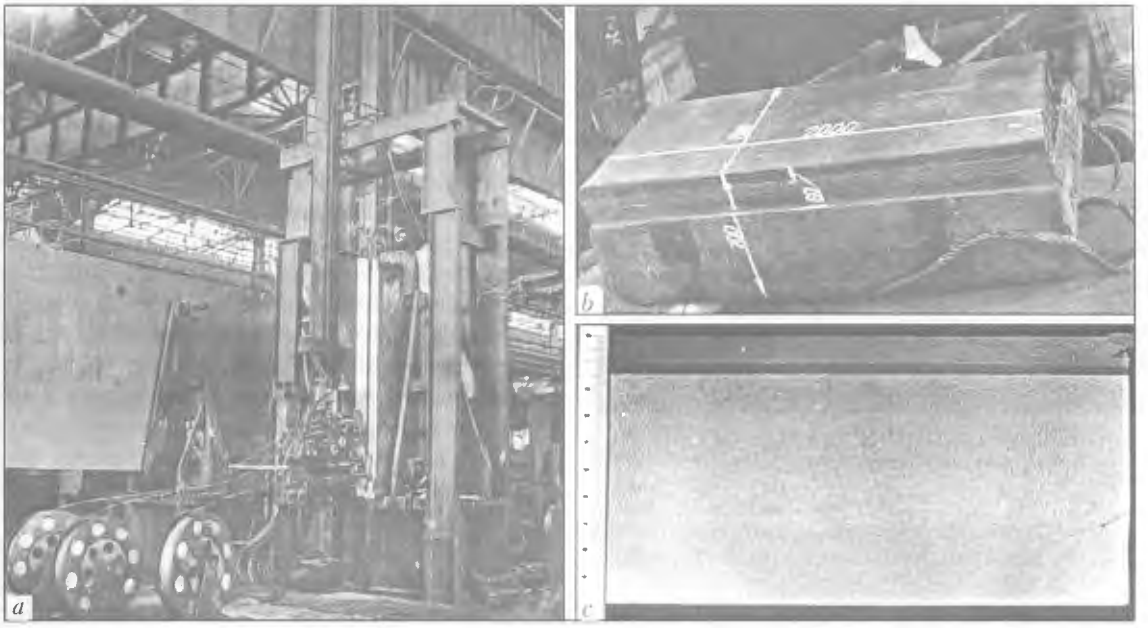

**Figure 1.** Two-layer billet, prepared for ESW using electrodes (6 pcs), by two machines A-535 simultaneously into a common weld pool (*a*), two-layer billet after ESW (*b*) and macrosection of bimetal 09G2DT + 1Kh18N10T (δ = 100 mm), rolled from mentioned two-layer billet (*c*)

chine-Building Works — ZhHMBW (now Mariupol Heavy Machine-Building Works — MHMBW), Iljich Metallurgical Works and Kommunarsk Metallurgical Works (now Alchevsk Metallurgical Works — AMW) in collaboration with PWI. As a result, the production of plates from 100–170 mm thick bimetal 09G2S + 0Kh18N10T using the ESW method was mastered at ZhHMBW and Iljich Metallurgical Works in collaboration with PWI. Here, the bimetal billets of up to 15 t mass were welded at ZhHMBW, and then they were subjected to rolling in mill 4500 at the Iljich Metallurgical Works [3, 4]. The important advantage of the mentioned method is that the anti-corrosion and other properties of the cladding layer, defined by a chemical composition of metal of the cladding plate, can be preset even before the manufacture of a bimetal welded billet. In addition, the ESW application for producing the bimetal ensures a reliable adhesion of the layers, not depending on the degree of reduction during rolling and attainable as a result of penetration of edges welded in ESW.

In the former USSR the bimetal thick-walled high-pressure vessels in a stamped-welded version were manufactured in 1962 at ZhHMBW using the technological process developed in collaboration with PWI. These were spherical cylinders [5] of 100 mm wall thickness and 1000 mm diameter made from 09G2S + 0Kh18N10T bimetal designed for operation under 35 MPa pressure and temperature from –70 up to 100 °C (Figure 2). In 1963 at the same plant the manufacture of cylindrical vessels [6] (with half-spherical bottoms) of 170 mm wall thickness and 1500 mm diameter made from bimetal 09G2S (wt.%: 0.1C, 1.5Mn, 0.6Si) + 0Kh18N10T, was mastered for operation at 32 MPa pressure and temperature from –40 up to 100 °C (Figure 3).

In 1967 at ZhHMBW a stamped-welded body of a transport nuclear power reactor OK-350 from bimetal rolled metal 18Kh2MA (wt.%: 0.17C, 1.8Cr, 0.25Mo) + 00Kh18N10T (wt.%: 0.03C, 18.5Cr, 10.0Ni, 0.45Ti) (Figure 4) was manufactured for the first time in the domestic practice. Many organizations, in parallel with PWI, ZhHNBW and Iljich Metallurgical Works, were participated in the creation of bimetal stamped-welded body OK-350, namely NIKIET, I.V. Kurchatov IAE, TsNII KM «Prometej» and others.

A great contribution to the creation of the new method and technology of producing stamped-welded version on the basis of welding processes for manu-

**Figure 2.** Stamped-welded spherical cylinder ($P_{op}$ = 35 MPa; $T_{op}$ = = –70–100 °C; $d_o$ = 1000 mm) from bimetal 09G2S + 0Kh18N10T (δ = 100 mm)

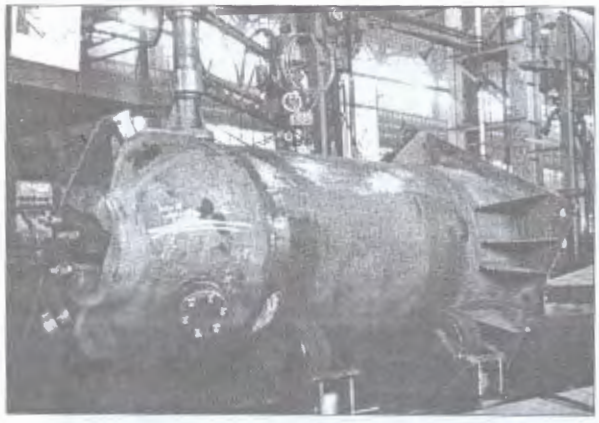

**Figure 3.** Stamped-welded cylindrical vessel ($P_{op}$ = 32 MPa; $T_{op}$ = = −40–100 °C; $d_o$ = 1500 mm) from bimetal 09G2S + 0Kh1810T (δ = 170 mm)

facture of thick-walled bimetal high-pressure vessels was made by Prof. B.I. Medovar, who supervised directly these works over many years.

The method of producing thick-plate bimetal using ESW was recognized both in our country and also abroad. Several special-purpose high-pressure vessels were manufactured from bimetal produced by this method. At the same time the wide application of the ESW method in production of bimetal at ZhHMBW was limited by a comparatively high labour intensity

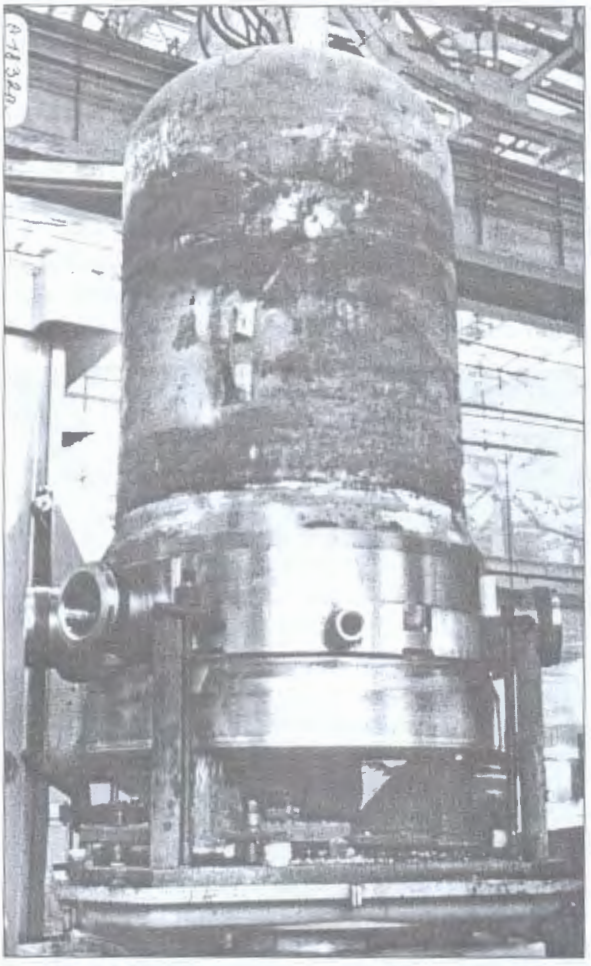

**Figure 4.** Stamped-welded body of transport nuclear power reactor of bimetal rolled metal 18Kh2MA + 00Kh18N10T in stand after final mechanical treatment

and complexity of the technology used at that time for ESW of bimetal billets of 800–1000 mm thickness and up to 2500 mm height. To provide a uniform and minimum penetration of edges being welded, the ESW was made by six electrodes of 3 mm diameter using two welding machines A-535. Here, all six electrodes were fed simultaneously through the nozzles into a common pool (by three from each side of the welding gap) (see Figure 1, *a*). During welding the reciprocal displacement of nozzles along the welding gap in butt thickness, i.e. from a lateral edge to the middle and back for each machine A-535, was realized.

At the end of the 1960s the production of thick-plate bimetal by the method of ESW for high-pressure vessels was interrupted because of the development and implementation at the above-mentioned plants of a new technology of bimetal producing using the method of autovacuum pressure welding (APW) by rolling of non-symmetrical packets. The new technology, as compared with the previous one on the basis of ESW, was characterized by higher technical-economical characteristics [7–9].

The application of thick-walled bimetal high-pressure vessels in petrochemical industry was very effective. The manufacture of stamped-welded reactors for hydrorefining and reforming from bimetal, produced by APW, with 08Kh18N10T steel corrosion-resistant layer and base layer from heat-resistant steel of 12KhM, 20Kh2M and other grades, was mastered since 1965 at PO «Zhdanovtyazhmash» [10], that could reduce the terms of their manufacture, assembly and putting into service, and increase also the reliability and safety in operation. It should be noted that bimetal reactors for products of petroleum refining do not require the obligatory periodic interruptions in the process of service for repair and lining replacement, as compared with single-layer reactors with a air-placed concrete inner lining.

Reactors for reforming and hydrorefining represent vertical cylindrical stamped-welded high-pressure vessels with half-spherical or elliptic bottoms. Bimetal bodies are freely mounted on conical supports fastened by anchor bolts to the concrete pedestals. Their sizes in diameter reach up to 4000 mm, length — up to 16 m, mass — up to 160 t, wall thickness — up to 150 mm.

Reactors for reforming (Figure 5) are designed for making reactions of reforming of petroleum products in the medium of hydrogen-containing gas in a catalyst layer. Operating pressure during reaction is 2.3–4.9 MPa depending on the design of reactor and catalyst, and the temperature is 480–540 °C. Reactors for hydrorefining (Figure 6) are designed for conductance of the process of hydrorefining of diesel fuels during interaction of hydrogen with olefines, which are transformed in the layer of an alumino-platinum catalyst into saturated hydrocarbons. Operating pressure during reaction is 2.6–6.0 MPa depending on the design of reactor, and temperature is 350–500 °C. In regeneration these parameters are equal, respectively, to

0.3–3.0 MPa and 480–550 °C. Working out of the designing technical documentation for manufacture of reactors for petroleum refining products was carried out in collaboration with VNIIINeftemash, Lengiproneftemash and others.

In the process of development of the stamped-welded variant of manufacture of thick-walled bimetal bodies at ZhHMBW the solution of some technical problems was required on stamping, welding, heat and mechanical treatment of separate components (shells, bottoms, branch pipes, etc.), made from bimetal, and on as-assembled bimetal vessels. Many technological problems had to be solved for the first time in the domestic practice. Let us dwell on one of them as an example.

The largest difficulties in manufacture of thick-walled semi-spherical bottoms (not only bimetal) are encountered in that case if they cannot be manufactured all-stamped due to limitation of a stamping space of presses or a limited capacity of the press. Usually, these bottoms are welded from pre-stamped lobes of length $1/3\pi R$ (where $R$ is the sphere radius) and a spherical disc. An essential drawback of the above method consists in the difficulty to manufacture bottoms of a preset geometric shape due to non-uniform shrinkage after stamping and also non-uniform deformation in welding. However, it is difficult to calculate these factors and they cannot be almost taken into account in the process of manufacture of thick-walled bottoms, in particular, bottoms made from thick-plate bimetal whose thermal shrinkage reaches large sizes due to difference in coefficients of expansion of the layers.

To facilitate the producing of a preset spherical shape, a method of manufacture of welded large-sized thick-walled semi-spherical lobe-type bottoms [11] has been developed, which consists of assembly of a symmetrical spherical girth, composed of lobes, in length of not less than $2/3\pi R$. Then the welding of lobes of the spherical girth is performed, for example, by ESW. Then two spherical discs are welded to the spherical girth and the sphere is subjected to heat treatment. The sphere manufactured is cut into two equal semi-spherical bottoms in equatorial plane, normal to the axis of symmetry passing through the centers of the spherical discs. An important advantage of this method is the feasibility of stamping the lobes and spherical disc in a single die. There is no need here to use a special sizing die. The mentioned method [11] was used successfully at ZhHMBW in manufacture of large-sized bottoms of bimetal bodies of reactors for products of petroleum refining.

Simultaneously with the development of the technology of manufacture of stamped-welded bottoms and shells from thick-plate bimetal, the problems of welding of vessels were solved. Application of ESW for welding thick-walled bimetal bodies is most rational.

The drawback of this method is the obligatory normalizing of the product after welding. In heat

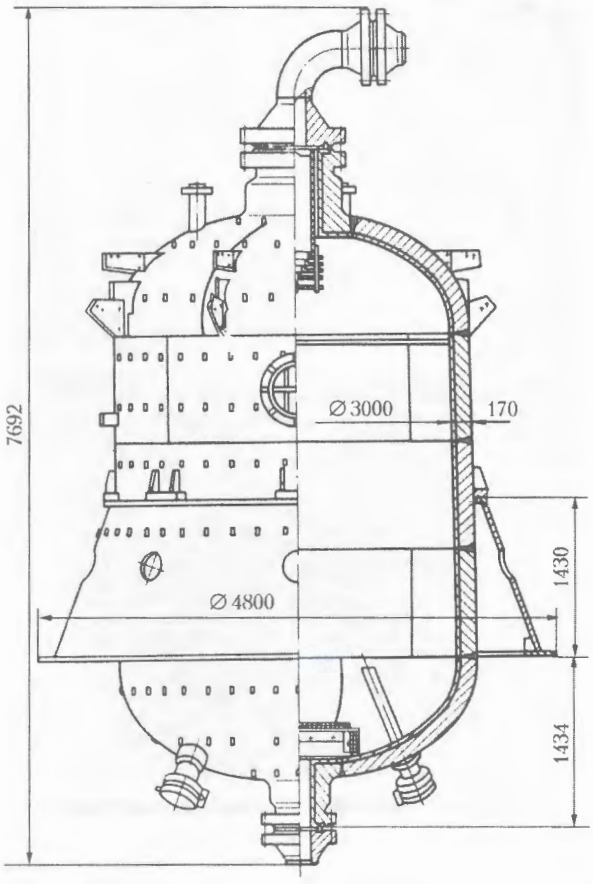


**Figure 5.** Schematic diagram of stamped-welded reactor for reforming ($P_{op}$ = 4.7 MPa; $T_{op}$ = 525 °C; $d_{in}$ = 3000 mm) from bimetal 12KhM + 08Kh18N10T ($\delta$ = 170 mm). Mass of unit in a working condition is 83.7 t

treatment of large-sized vessels this high-temperature heating can lead to the deterioration of the product shape. By this reason, the normalization of small vessels or separate units (of up to 4 m length) is performed, if possible, in a vertical position. Then separate as-welded normalized components are welded by the automatic multilayer submerged arc welding with a subsequent tempering of the ready product.

It should be noted that the high-temperature heating with excessive internal pressure was used at BBW for stamped-welded pressurized vessels after ESW. For this, the vessel was filled with a wood before heating for normalization, and then the vessel was

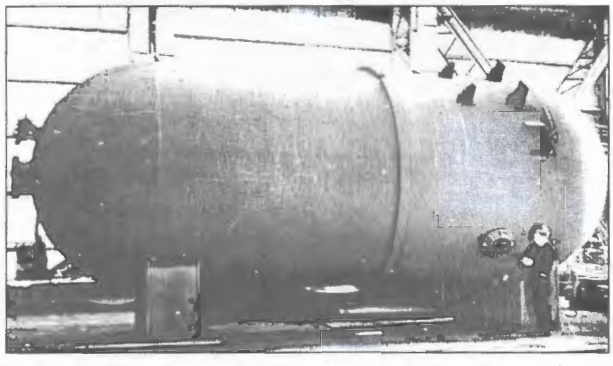

**Figure 6.** Stamped-welded reactor for hydrorefining ($P_{op}$ = = 6.0 MPa; $T_{op}$ = 425–500 °C; $d_{in}$ = 3560 mm) from bimetal 12KhM + 08Kh18N10T ($\delta_{body}$ = 135 mm; $\delta_{bottom}$ = 80 mm). Mass of unit in a working condition is 138.7 t

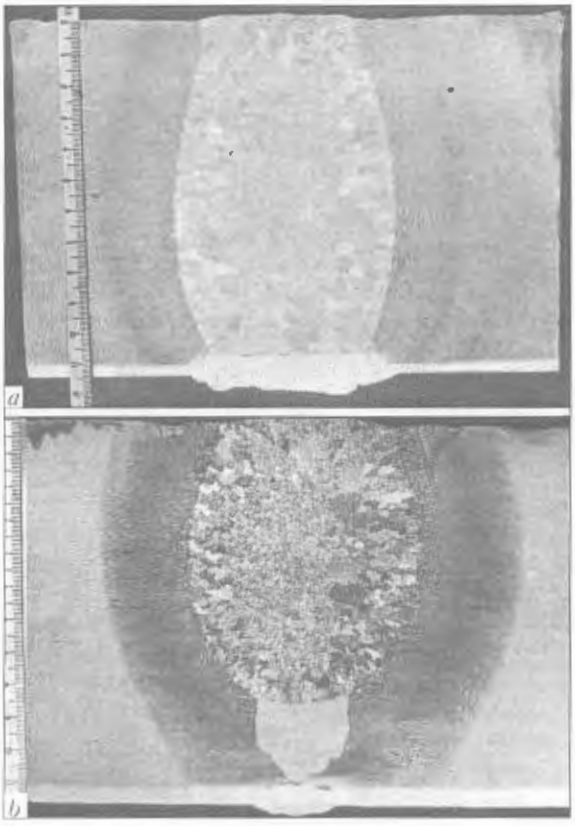

**Figure 7.** Macrostructure of longitudinal weld of stamped-welded vessel of bimetal 09G2S + 0Kh18N10T (δ = 170 mm) with a complete removal of cladding layer in the zone of welding (*a*) and with a combined edge grooving, providing a preliminary welding of a base layer (*b*). Mass of unit in a working condition is 138 t

pressurized. As a result of a dry distillation of wood during heating a pressure is created inside the vessel, which is sufficient to prevent its buckling and distortion [1].

Grooving (Figure 7, *a*) with a complete removal of a cladding layer by gouging (20–40 mm per each edge) is recommended for ESW of longitudinal and circumferential welds of the bimetal body. In addition, a combined grooving (Figure 7, *b*) with a preliminary welding of a base layer inside the vessel was tested for longitudinal welds, which can easily provide the required geometric shape of shells and decreases significantly the volume of cladding works inside the body. This technology was implemented in welding of a cylindrical vessel of 170 mm wall thickness, made from two-layer steel 09G2S + 0Kh18N10T.

**Figure 8.** Macrostructure of circumferential diametric weld of spherical cylinder from bimetal 20Kh2MA + 0Kh18N10T (δ = = 120 mm) made by the automatic welding at a single-sided access to edges being welded (only outside) from the side of the base metal

However, this type of grooving relative to welding of bodies from bimetal 18Kh2MA + 0Kh18N10T was not acceptable, because preheating and also the subsequent tempering are required for arc prewelding of the base layer, thus complicating the technological process.

The shape of edge preparation with a complete removal of a cladding layer in the zone of welding (Figure 7, *a*) is most adaptable as it produces a welded joint of equal strength without prefusion of austenitic cladding with non-alloyed welds that prevents the formation of brittle quenched structures in the zone of fusion of dissimilar steels. Welding of the base layer is performed according to conventional ESW technology accepted for the parent metal, and then hardfacing of a corrosion-resistant layer is made in places of removal of a cladding layer (in grooves) by two or more passes, for example, by a strip electrode using an automatic submerged arc welding.

The variant of a single-sided welding of a diametric weld was also developed and implemented in 1963 at ZhHMBW for manufacture of spherical bimetal cylinders from 120 mm thick steels 09G2S + 0Kh18N10T and 20Kh2MA + 0Kh18N10T (Figure 8). Its development was due to the fact that access inside the spherical cylinder was impossible because of a small hole in a neck. In this case a root weld, located in austenitic cladding layer, is made by a mechanized $CO_2$ welding with wire of Kh20N9S2BTYu type, providing a high weld metal resistance against the crystalline corrosion. Welding of the root weld is performed in a vertical position with a through penetration and reverse weld formation without backings owing to the surface tension forces. Then that part, which was made in a cladding layer, is filled with austenitic electrodes, and then the surface of the austenitic deposited metal is deposited by a separating layer (two passes) using the armco-iron electrode wire. The multipass submerged arc welding is performed by a conventional technology over the separating layer. Ferritic separating layer provides the minimum reduction in ductile properties of the deposited metal alloyed with chromium and nickel as a result of inevitable penetration of the austenitic metal, and prevents also the formation of cracks in metal of the weld transition zone (Figure 8).

As a result of a large complex of investigations on full-scale and experimental samples at ZhHMBW, an optimum process was developed for manufacture of bimetal bodies in a stamped-welded version and the technologies of bending, stamping, welding and heat treatment were mastered, providing the required ge-

ometry of the body (maximum misalignment of body shells and bottoms being assembled is not more than 2.5 mm).

As is known, it is more rational from the technical and economical point of view to use low- and medium-alloy steels of increased and high strength for manufacture of a wide group of high-pressure welded vessels. Actually, the application of steels with a high strength, ductility and toughness can not only decrease significantly the dimensions of welded products, but also promotes the creation of new design and technological solutions, whose realization without use of these steels could be impossible. Integrated experimental-research works carried out with our participation in the middle of the 1960s to increase the quality of the base layer metal of bimetal bodies of high-pressure vessels showed that the thick-plate rolled metal of steels 09G2S, 16GNM (wt.%: 0.15C, 0.6Ni, 1.1Mn), 18Kh2M ($\delta$ = 80–115 mm) after electroslag remelting (ESR) is characterized by improved (as compared with initial open-hearth metal) properties: it contains a much lower amount of sulphur, non-metallic inclusions, gases, there is no anisotropy of ductile properties, the impact strength of transverse samples is increased by 40–80 %, and across the plate thickness (in axis $Z$) — by 300–400 % as compared with the initial metal. Cold shortness threshold of samples of ESR metal, cut in axis $Z$, is shifted by 30° towards the negative temperatures for a normalized metal and by 50° — for the quenched metal. Welded joints of steel 09G2S after ESW can be subjected only to high tempering, which provides the required impact strength in HAZ metal [12].

As the investigations showed [13], the application of electron beam welding (EBW), for the realization of which the normalization is not obligatory, can occur to be rather promising in manufacture of bimetal bodies of high-pressure vessels from thick-plate low- and medium-alloy ESR steel. Thus, in EBW of 80 mm thick steel 18Kh3MASh the only tempering after welding is enough to produce almost equal-strength joint with a high level of impact strength of weld and HAZ metal at −70 °C. Besides, the width of a path of the cladding layer, removed before welding, does not exceed 5 mm per a side in EBW of bimetal bodies, that gives an opportunity to decrease the volume of hardfacing works inside the vessel after EBW of the base layer.

During mastering the industrial manufacture of bimetal stamped-welded vessels at ZhHMBW, the search works were also conducted simultaneously for the development of radically new less expensive and effective methods of their manufacture, not requiring bimetal rolled metal for their realization. We shall dwell on some of these developments, which were not completed until their industrial implementation by different reasons, but are still important now after many years.

In the method offered [14] the process of cladding of billet (product) surface is combined in one technological operation with a process of its hot stamping, i.e. two operations; namely formation of a strong adhesion between layers and manufacture of the required billet or product from bimetal are combined into a single operation. Figure 9, *a* shows an appearance of a bimetal (18Kh2MA + 08Kh18N10T) semi-shell of 120 mm thickness, 1800 mm diameter, manufactured under the industrial conditions of ZhHMBW directly in the process of hot stamping using a method of a press braze welding (PBW) developed at the E.O. Paton Electric Welding Institute [9]. At stamping preheating ($T_{st}$ = 1150–1170 °C), the powder of 60Mn–40Ni alloy with $T_{melt}$ = = 1018 °C, placed in a gap between base and cladding layers of a two-layer billet, sealed around the perimeter by welding, is melted, thus dissolving the surface oxide film and providing a reliable contact between planes being welded. During stamping, the interlayer is extruded to the periphery into special receivers and its thickness in a ready bimetal billet does not exceed 0.25 mm that provides a guaranteed adhesion between layers ($\sigma_{sh}$ > 300 MPa). Macro- and microinvestigations of the fusion zone in bimetal showed its high quality over the entire surface of cladding (Figure 9, *b*).

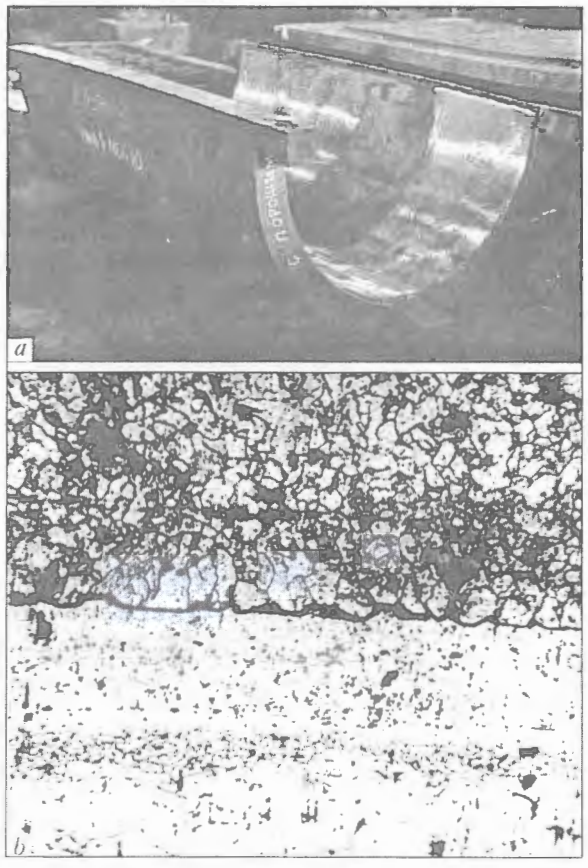


**Figure 9.** Appearance (*a*) of bimetal semi-shell ($d_o$ = 1800 mm; $\delta$ = 120 mm) produced in the process of hot stamping using a Ni–Mn interlayer, and microstructure of zone of layers joining in bimetal 18Kh2MA + 08Kh18N10T after stamping (*b*) (×100)

At the beginning of the 1980s a radically new technology of producing cylindrical billets was suggested at PWI for the high-pressure vessels made from expanded multilayer billets [15]. The principle of this technological diagram consists in that the multilayer

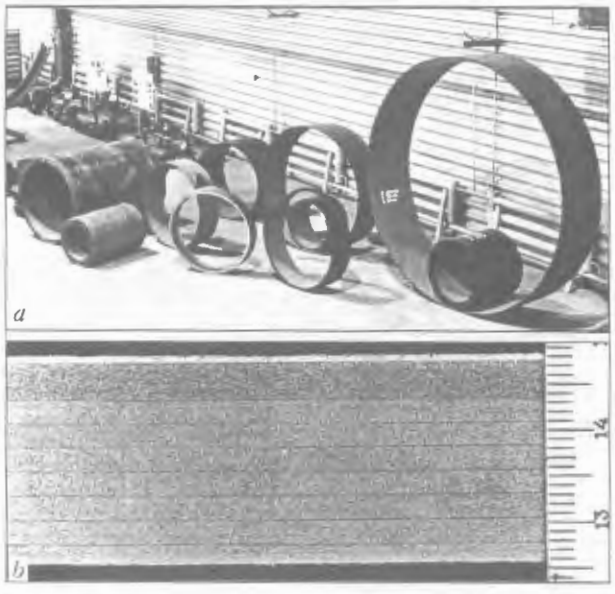

**Figure 10.** Appearance of ring-type QLMM shells (thinner and larger-diameter) produced by the method of hot expansion by rolling in a ring rolling mill, multilayer billets (thicker and lower-diameter) manufactured by a canonical winding of a coiled strip of steel 09G2SF (*a*), macrostructure of metal of QLMM shells with a corrosion-resistant layer (*b*)

billet, produced by a canonical winding at straight angle of a 3–6 mm thick coiled strip, is heated in a furnace, and then this multilayer billet is expanded by rolling in a ring-rolling mill until adhesion between layers using APW. As the diameter of multilayer billet is increased in the process of hot deformation, so the billets are taken for rolling with a smaller diameter than the required final diameter of the cylindrical shell, and with a larger total thickness.

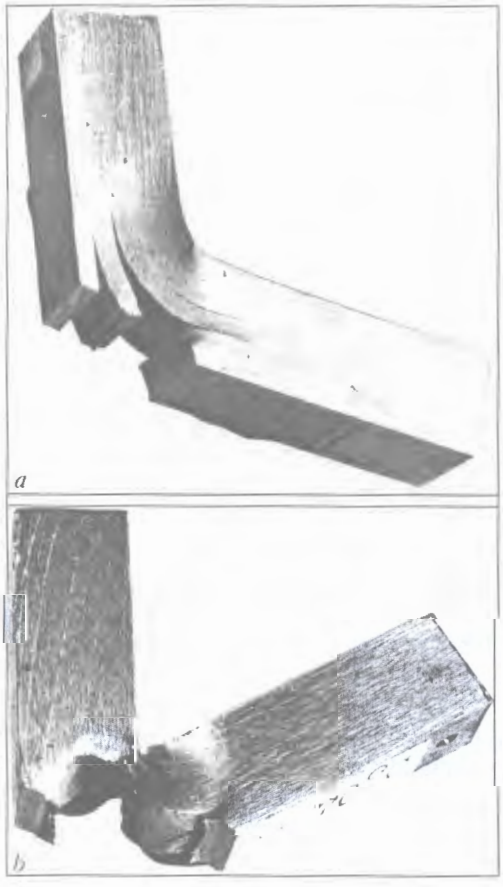

**Figure 11.** Nature of fracture of Charpy samples made from steel 09G2SF QLMM (*a*) and 09G2SF (*b*) at impact bending

The use of the coiled steel not requiring a special preparation of the surface before winding of multilayer billet, and also the combination of processes of joining layers and formation of the shell of preset sizes make it possible to produce comparatively inexpensive seamless ring billets. Experimental-industrial trials [16, 17] showed that a special design of multilayer billet and optimum technology of its expansion by rolling guarantee a reliable adhesion between layers and producing of a monolithic metallic material with a special macrostructure, named a quasi-laminar metallic material (QLMM) (Figure 10). The specifics of QLMM consists in an organized laminar internal structure. This material is characterized by properties of multilayer metallic materials at dynamic loads and low temperatures, and also conventional monolithic metallic materials at static load. At impact bend tests, if the notch is made on the QLMM surface, the sample metal cannot be fractured (Figure 11). Material resistance to crack propagation is provided by splitting of the QLMM metal into number of layers at its apex. The advantage of the technology of hot expansion by rolling of QLMM shells is the feasibility of producing the quasi-laminar structure with a corrosion-resistant cladding layer (internal or external or simultaneously with both).

Metal QLMM can be subjected to all types and methods of welding, the same as a conventional monolithic metal. On the basis of hot rolling of multilayer billets it is possible to produce different ring billets of high-pressure vessels, pipes for power plants, including bimetal pipes with a corrosion-resistant internal layer, and also for other critical products, whose material should possess the high resistance against brittle fractures, at negative temperature in particular. However, to organize the industrial production of these shells, the creation of mills for rolling billets of 2000 mm height and more will be required, as the existing mills can expand the shells by rolling up to the height of 750 mm [18].

In this connection, the work [19] deserves attention, as it suggests technology of rolling ring billets for manufacture of NPS equipment. Using the ring-rolling mill (radial or vertical type), the large-sized billets of high-precision reactors (with minimum tolerances) of up to 8 m diameter and up to 4 m height are manufactured, that can decrease abruptly (almost by 30 %) the metal consumption. Alongside, the labour-intensity of forging is decreased by 20–25 % and that of mechanical treatment — by 1.5–2 times, the consumption of cutting tools is reduced, the cycle of manufacture of large-sized ring products is decreased, production capacities of steel melting, forge-pressing and machining are partially released. Simultaneously, as was shown in [17], the problem of producing bimetal shells is solved in the process of hot rolling of ring billets in the ring-rolling mill.

The results obtained give grounds for the conductance of a complex of works for the creation of the equipment for expansion by rolling and industrial technology of production of different ring billets of high-pressure vessels, bodies of nuclear reactors, bimetal pipes for power plants and other special-purpose products whose material should have improved characteristics of toughness and brittle fracture resistance under conditions of operation at low temperatures, aggressive medium and neutron radiation.

The problem of cladding of internal surface of thick-walled vessels, including those manufactured from expanded shells, can be also solved by using the explosion welding. According to the method, developed at ZhHMBW in collaboration with PWI [20], a cladding material, for example, corrosion-resistant steel of 12Kh18N10T grade in the form of a strip of 0.5–1.5 mm thickness, preliminary coiled into a coil, is placed inside the vessel and fastened in a yoke (Figure 12). Vessel is mounted on a roller stand to set the rotation. The coil is gradually uncoiled and placed in a flat position on the internal surface of the vessel and fastened by clamps in two places over the entire length of the vessel. Between clamps a linear charge of explosive ($E$), which is initiated, is located over the entire length of the vessel. Thus, a local explosion welding takes place. Then the clamps are removed and the roller stand is rotated per one pitch equal to 50–200 mm. The coil is gradually uncoiled now and the above operations are repeated. Periodically, at the moment of rotation interruption, a local explosion welding of the first cladding layer with a vessel surface, and also all subsequent layers in a chessboard order are made. The number of layers, and also the total thickness of the cladding layer is determined by the conditions of the vessel operation.

At closing each cladding layer, equal to the length of an appropriate circumference, a sealing weld is deposited over the entire length of the vessel generatrix, which prevents the possibility of aggressive medium penetration into a gap between the cladding layers in case of damage of one of the upper layers. The cladding layer can be produced both by a spiral layout of turns, and also concentric turns of the metallic strip.

Owing to the multilayer design of the cladding layer and application of a local explosion welding of the lining strip with a body and separate layers with each other, the conditions are provided for compensation of temperature stresses in the zone of joining of dissimilar materials, occurring usually due to a difference in coefficients of a linear expansion of metal of base and cladding layers of the bimetal body. At the same time, when realizing the above-mentioned method of cladding in production of bimetal vessels, it is necessary to develop a reliable system of control, which could signal the violation in sealing of the interlayer spacing (both at the stage of product manufacture and also in the process of its service) because

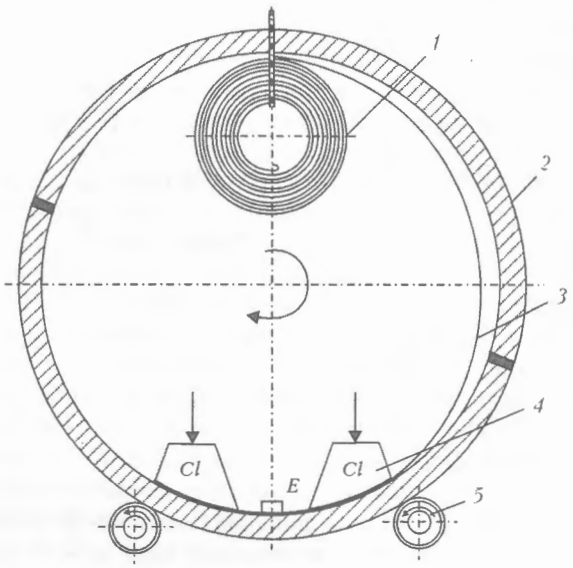


**Figure 12.** Schematic diagram of cladding of inner surface of cylindrical vessels using explosion welding: *1* — coil of cladding metal; *2* — vessel body; *3* — cladding metal; *4* — clamps; *5* — roller stand

of a possible damage of sealing welded joints or one of the cladding layers.

At the middle of the 1990s numerous publications appeared [21–24] devoted to different aspects of application and producing thick-plate bimetal using methods based on using the electroslag cladding (ESC) of a layer from corrosion-resistant steel on the base made from a structural steel. It is noted in these works that in production of corrosion-resistant bimetal billets by ESC method the highest strength of joint of cladding and base layers is provided as compared with other methods of bimetal producing (packet method or explosion welding). Thus, the shear resistance, determined in place of contact of layers, is 400–450 MPa, that is comparable with a yield strength of the base layer [23]. There is information about the development of the technology of vertical ESC of bimetal billets of rectangular and square section in operating ESR furnaces, which, from the data of [24], are used for this purpose almost without modification of main elements and units. It is also noted here that the production of bimetal billets of mass up to 15 t in specially-designed installations of an inclined type for ESC occurred to be rather labour- and power-consuming due to the presence of three consumable electrodes and a movable mould, which require special slags and sensors of movement.

In addition, in the opinion of authors [24], the non-parallel mutual arrangement of consumable electrodes and a slab of the base layer does not ensure a similar depth of penetration in the zone under and between the electrodes, as a spray metal transfer in slag influences the heat distribution.

It should be outlined that the specifics of a single-pass ESC both at inclined and vertical arrangement of the billet being clad is the use of a common heat source for two different technological processes (melting of electrode metal and penetration of base

metal), i.e. there is a rigid relation between them. It creates definite difficulties in providing minimum and uniform penetration of the base layer in ESC, that is necessary for producing the deposited layer of a stable chemical composition over the entire area.

The new opportunities for production of bimetal billets for welded high-pressure bodies are opened up owing to the application of the ESC using a liquid filler metal (ESC LFM) [25–27]. The investigations showed that the application of the ESC LFM as compared with a canonical ESC process makes it possible to deposit the cladding layer with a minimum depth of penetration of the base layer both in section and also in billet height. When necessary, the cladding can be performed also by the diagram of braze welding, i.e. almost without penetration of the base layer [25, 26]. As a result, it is managed to provide the higher quality in this bimetal as compared with bimetal produced by other methods. It is also important that ESC LFM does not require the use of a consumable electrode, whose manufacture, in particular from high-alloy steels and alloys, composes a significant estimate of expenses for industrial realization of the ESC.

Unfortunately, over the recent years the MHMBW does not produce the bimetal stamped high-pressure vessels due to lack of orders for them.

At the same time, in spite of objective difficulties the MHMBW could preserve the basic equipment, personnel and production-technical potential. All this inspires confidence that at certain capital investments and the presence of orders for the production of thick-walled high-pressure vessels can be not only recovered to the previous volumes but also widened taking into account the new achievements appeared during recent years in the world in the field of metallurgy, pressure treatment and welding. Moreover, the production-technical base of MHMBW allows mastering in short periods of time the production of single-layer high-pressure bodies, such as thick-walled drums of steam boilers in a set with other equipment, which were not serially manufactured in Ukraine until now.


1. (1959) *Electroslag welding*. Ed. by B.E. Paton. Moscow-Kiev: Mashgiz.
2. Paton, B.E., Medovar, B.I., Makara, A.M. et al. *Process of production of multilayer rolled metal*. USSR author's cert. 129473. Publ. 03.04.60.
3. Paton, B.E., Medovar, B.I., Lutsyuk-Khudin, V.A. (1962) Manufacturing of two-layer sheets using the electroslag welding. In: *Bull. TsNIIChM*.
4. Medovar, B.I., Lutsyuk-Khudin, V.A., Saenko, V.Ya. et al. (1963) Manufacturing of thick-walled vessels from two-layer steel with corrosion-resistant austenitic lining. In: *Manufacturing, welding and application of two-layer steel*. Moscow: GOSINTI.
5. Kumysh, I.I., Lutsyuk-Khudin, V.A., Saenko, V.Ya. et al. (1964) Automatic circumferential welding of two-layer steel vessels. *Svarochn. Proizvodstvo*, **2**, 8–10.
6. Lutsyuk-Khudin, V.A., Kumysh, I.I., Saenko, V.Ya. (1967) Mechanized welding of thick-walled vessels from two-layer steel. *Khim. i Neft. Mashinostroenie*, **6**, 14–19.
7. Lutsyuk-Khudin, V.A., Saenko, V.Ya., Kumysh, I.I. et al. (1968) *New technology of manufacturing thick-walled bimetal pressure vessels*. Moscow: NIIInformtyazhmash.
8. Medovar, B.I., Saenko, V.Ya., Nagaevsky, I.D. et al. (1984) *Electroslag technology in mechanical engineering*. Ed. by B.E. Paton. Kiev: Tekhnika.
9. (1984) *Multilayer steel in welded structures*. Ed. by B.E. Paton, B.I. Medovar. Kiev: Naukova Dumka.
10. Amelchakov, S.I., Buraya, L.E., Matyash, M.F. et al. (1980) *Reactors for petroleum refining*. Kiev: Reklama.
11. Karpov, V.F., Dovzhenko, A.F., Kononov, V.G. et al. *Process of manufacturing large-sized hemispherical bottoms*. USSR author's cert. 339088. Publ. 09.10.71.
12. Paton, B.E., Medovar, B.I., Saenko, V.Ya. et al. (1974) About expediency of manufacturing critical welded structures from thick-plate metal improved by ESR method. In: *Refining remeltings*. Kiev: Naukova Dumka.
13. Medovar, B.I., Saenko, V.Ya. (1981) Problems of welding of low- and medium-alloy thick-plate electroslag steel. In: *Problems of special electrometallurgy*. Issue 14.
14. Lutsyuk-Khudin, V.A., Saenko, V.Ya., Andrianov, G.G. et al. *Process of manufacturing bimetal stamped-welded products*. USSR author's cert. 218640. Publ. 17.05.68.
15. Paton, B.E., Medovar, B.I., Saenko, V.Ya. et al. (1980) New technology of manufacturing pressure vessels from expanded multilayer shells. In: *Abstr. of pap. of All-Union Conf. on Multilayer Welded Structures and Tubes*. Kiev: PWI.
16. Paton, B.E., Medovar, B.I., Saenko, V.Ya. et al. (1981) New approach to manufacturing and development of multilayer materials from low- and medium-alloy steels. In: *Problems of special electrometallurgy*. Issue 15.
17. Paton, B.E., Medovar, B.I., Saenko, V.Ya. et al. (1984) Seamless quasi-layer tubes manufactured by hot expansion of multilayer billets. *Ibid*. Issue 21.
18. (1993) *Hot expansion of steel rings and shells*. Ed. by B.E. Paton, B.I. Medovar. Kiev: Naukova Dumka.
19. Eletsky, S.A., Reshetnikov, V.A., Telesh, V.V. et al. (1987) Implementation of technology expansion of circumferential billets for manufacturing nuclear power plant equipment. *Kuzn.-Shtamp. Proizvodstvo*, **10**, 16–17.
20. Nagaevsky, I.D., Aleksandrov, V.A., Saenko, V.Ya. et al. *Method of cladding of internal surface of cylindrical vessels*. USSR author's cert. 607707. Publ. 09.10.78.
21. Popov, A.V., Shejko, V.I., Kudinov, E.D. et al. (1994) Development of electroslag cladding technology in manufacturing of bimetal sheets. *Tyazh. Mashinostroenie*, **1**, 29–30.
22. Tishkov, V.A., Rodionova, I.G., Puzachyov, V.I. et al. (1995) Manufacturing of bimetal rolled products by electroslag cladding method. *Metallurgiya*, **8**, 30–31.
23. Sharapov, A.A., Rodionova, I.G., Shalimov, A.G. et al. (1996) Manufacturing of billets for corrosion-resistant bimetal in electroslag furnaces by cladding method. In: *Proc. of 3rd Congress of Steelmakers*. Moscow.
24. Sharapov, A.A., Rodionova, I.G., Puzachyov, V.I. et al. (1996) Experience of development of technology for bimetal billet manufacturing using the electroslag remelting. *Stal*, **12**, 27–29.
25. Medovar, B.I., Saenko, V.Ja., Medovar, L.B. (1999) Electroslag processes used in production of clad steel. *The Paton Welding J.*, Pilot Issue, July, 71–75.
26. Medovar, B.I., Saenko, V.Ya., Medovar, L.B. (2000) Manufacturing of billets from corrosion-resistant bimetal by electroslag cladding method. *Problemy Spets. Elektrometallurgii*, **2**, 3–11.
27. Paton, B.E., Medovar, L.B., Saenko, V.Ya. (2003) New opportunities of electroslag technologies in mechanical engineering, *Metallurgiya Mashinostroeniya*, **1**, 2–5.

# TENDENCIES IN DEVELOPMENT OF POWER SOURCES AND CONTROL SYSTEMS (based on materials of US patents)

V.K. LEBEDEV
E.O. Paton Electric Welding Institute, NASU, Kiev, Ukraine

The paper presents US patent information over the last two years outlining modern trends in the field of development of power units and control systems for arc and resistance welding processes.

***Keywords:*** *arc welding, resistance welding, power sources, control systems, drop transfer, gas mixtures, US patents*

US Patent Office has an extensive fund of more than 6.5 mln registered patents. Their authors are citizens of not only the USA, but also many other countries. Patent fund is being continuously increased through Internet and is accessible to a wide circle of specialists. Studying US patents can provide information on the avenues of developments of a particular engineering field.

This work presents a brief review of patents on power sources and control systems for the most widely accepted processes of arc and resistance welding. The review only covers patents published over the last two years and characterizing the state-of-the-art of the engineering field of interest to us.

Illustrations are shown in the form, in which they are given in the original descriptions. Numbers of all the positions are unchanged. And even though these numbers are almost not used in the review, they may be useful for the reader in case of a more detailed study of the contents of the patents proper.

The second half of the previous century was characterized by tremendous achievements in the field of semi-conductor devices that promoted development of many fields of engineering, including welding equipment. It can be definitely stated that the most significant progress in welding is related to the introduction of new semi-conductors. Initially these were power diodes, which ousted electromechanical converters. Later on thyristors were introduced, which are partially controlled semi-conductor devices, which began to be used as power devices, as well as in the control system circuits. Still another area should be mentioned, where the focus is on improvement of welding process stability through power sources and control systems.

The next stage of development of welding engineering associated with transistors has partly been covered, however, the possibilities of their application in welding are far from having been exhausted. The method of pulsed-arc welding [1] developed even before the introduction of powerful controlled devices into the market, can be included into this category. These devices enabled pulsed-arc welding going beyond the laboratory testing stage and becoming a widely accepted manufacturing process. Experiments on short-circuiting welding were conducted in parallel. One of the main goals of these experiments was reducing liquid metal spatter, arising at metal transfer with short-circuiting of the arc gap. In this area, studies of the following PWI scientists are known: I.I. Zaruba, A.G. Potapievsky, N.M. Voropaj and many others, as well as of staff members of various educational establishments and research organizations, such as G.M. Kasprazhak, N.M. Dyurgerov, A.F. Knyazkov, Yu.N. Saraev, etc. Later on positive results were obtained on the use of an improved method of controlling metal transfer at short-circuiting of the arc gap [2]. However, further development of this process and batch-production of new equipment turned out to be not very promising in connection with introduction of a comparatively inexpensive shielding gas such as argon in the market. Therefore, investigations were interrupted, although they are still being pursued abroad now, as will be shown further on. The cause for that are the known advantages of «short» arc welding. Application of transistors permitted reducing the mass and dimensions of the power sources, increasing their efficiency and power, and giving the power source the properties of easily controllable and low-inertia devices.

Further improvement of arc welding equipment will, probably, be related to a considerable extent, to use of transistors and microprocessor control systems and primarily aimed at improvement of adaptability of arc welding to fabrication.

A similar tendency will be observed also in the field of resistance welding, particularly, in microwelding. To get an idea of the avenues of development in the welding engineering field, which is of interest to us, it is worthwhile to study the appropriate patent sources, recently published in the USA.

Patent 6476354 «Method for Controlling a Welding Apparatus and Corresponding Control Device» (Fronius Schweismaschinen) [3] gives a description of a method to control the welding process, characteristic for modern welding equipment (Figure 1).

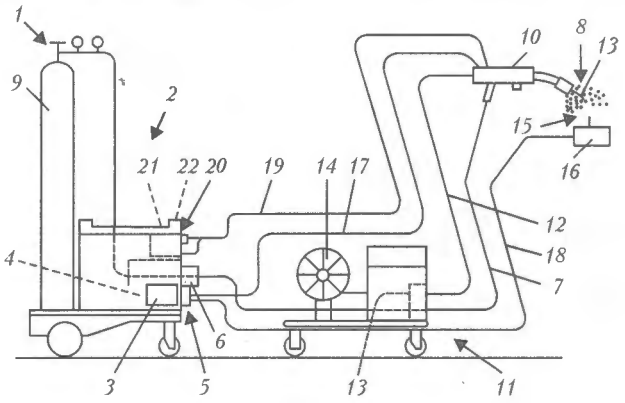


Figure 1

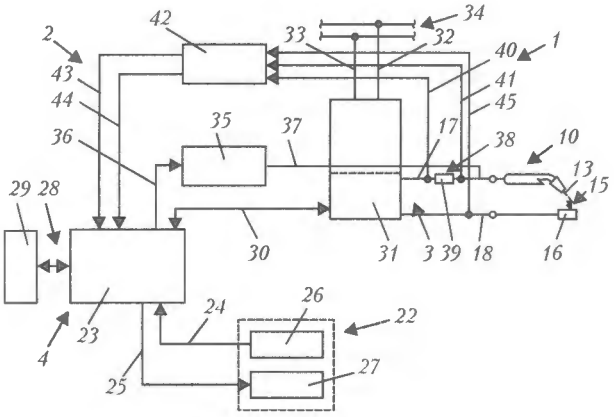


Figure 2

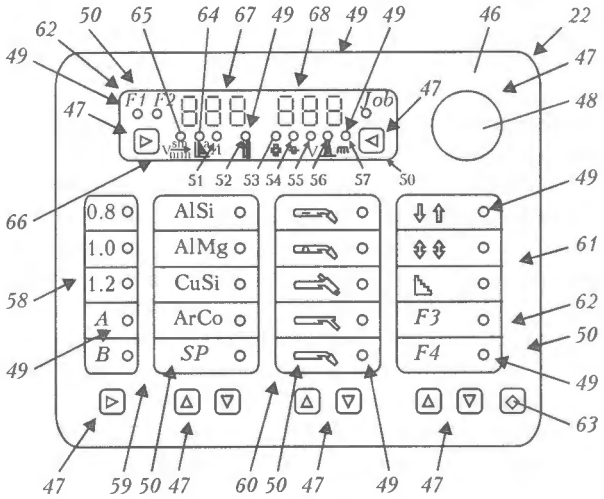


Figure 3

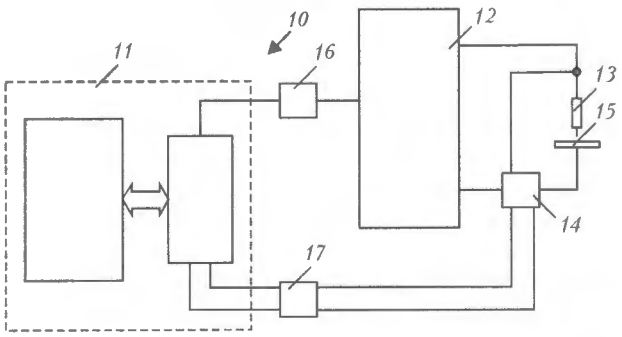


Figure 4

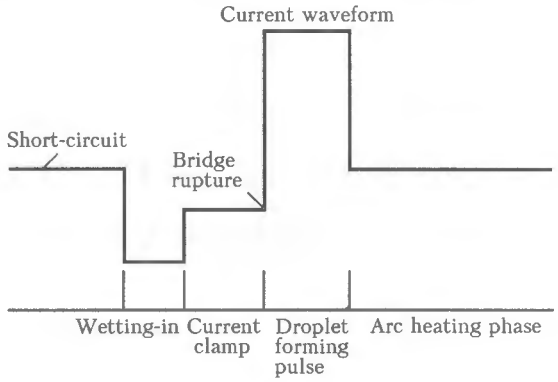


Figure 5

Control is performed, using a microprocessor device, into which the data on the material being welded, electrode diameter, its feed rate, shielding gas, welding process, etc. are entered before the start of welding. Connections diagram is shown in Figure 2. In addition to inverter-type power source, the unit further incorporates high-frequency generator *35*, connected in series into the arc power circuit, and closed-loop water cooling system (not shown in the Figure). Microprocessor *23* receives information on arc current and voltage from the sensors and performs control in keeping with the data entered into memory *29*. Microprocessor is connected to inverter *31* through a fiber-optic cable. Schematic of the unit panel is shown in Figure 3.

A welding control system of similar design was patented by CRC for Welding Structures Company [4]. Block diagram of the power source with the control system has a standard structure (Figure 4). Control is performed by a microprocessor, operating at the frequency above 200 MHz. It supports voltage feedback (also current feedback, if required), and also controls electrode wire feed. It may be assumed that the control system is chiefly designed for welding with short-circuiting of the arc gap at transfer of molten metal drops. The control system ensures a small amount of liquid metal spatter during welding (Figure 5). A high speed of the system reaction allows quickly varying the current, for instance reducing it to 10–20 A, so that closing of the arc gap proceeded without the drop bouncing off the weld pool under the impact of electrodynamic forces. This prevents the growth of the drop and its spontaneous motion,

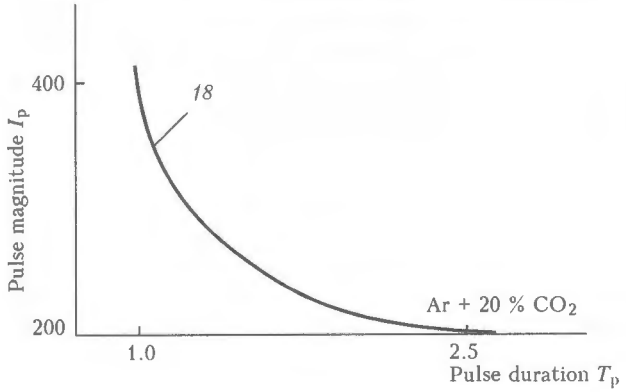


Figure 6

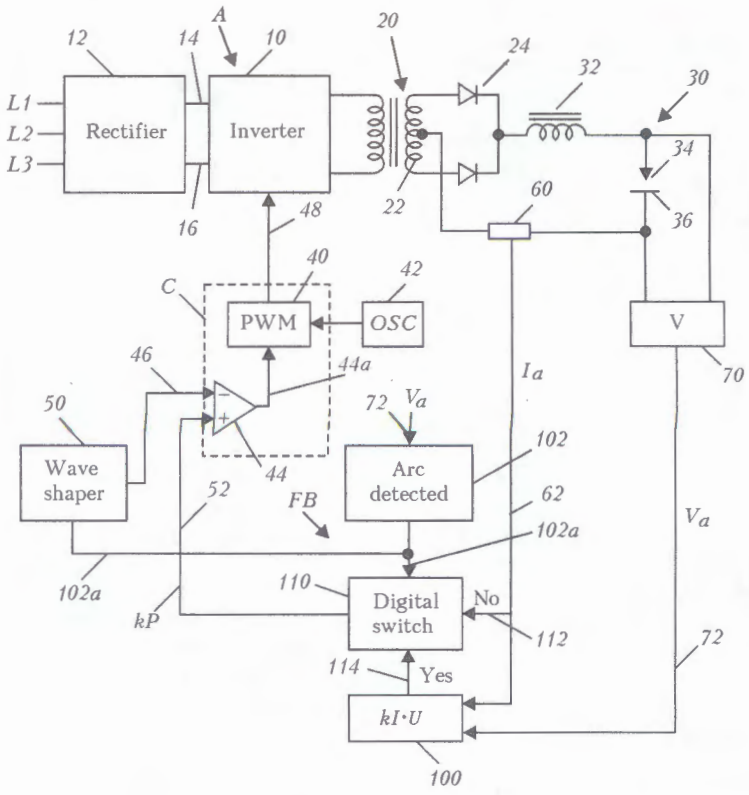


**Figure 7**

which otherwise leads to spatter. After that the current is slightly increased, which kind of «facilitates» the drop transfer into the pool without causing any noticeable spatter. A «soft» transfer of the drop into the pool occurs (which is characteristic for the above invention). Then a pulse is applied, which completes the drop transfer into the pool, and this cycle is repeated many times. Value of current pulse is set, depending on electrode diameter, and carbon dioxide gas content in the gas mixture. The range of values of the current pulses is between 200 and 400 A with process duration from 0.5 to 3.0 ms, electrode wire diameter being from 1.2 to 2.5 mm (Figure 6). Short-circuiting time is equal to 2.0 to 4.8 ms. Current mode and welding time can be adjusted separately in stages, if values of these parameters exceed the above limits.

The system can operate in three modes. Maximum and minimum current values are assigned in the normal mode, and are maintained during welding. In the correction mode, if current value goes beyond the established limits, welding time changes, and current limitations are eliminated. During operation in the third mode, called adaptive, the system independently selects minimum values of current and time intervals. However, the search algorithm is not quite clear from the description, given in the patent.

Lincoln Global, Inc. took Patent 6498321 called «System and Method for Controlling an Electric Arc Welding» [5]. From the viewpoint of the power component design this control system is a welding inverter (Figure 7). It incorporates several power feedbacks. Control system is based on computer *C*. *Arc detector* device has two outputs. Output *72* identifies a short-circuit, and *102a* identifies arcing. Device *50* assigns the shape of the power curve. The latter is calculated by multiplying current by voltage (device *100*); calculation result in the digital form is compared with the current set power value. The device incorporates short-circuit indicator *102*. Curves of time variation of current and power are shown in Figure 8. Electrode wire feed motor also is an actuator, providing welding

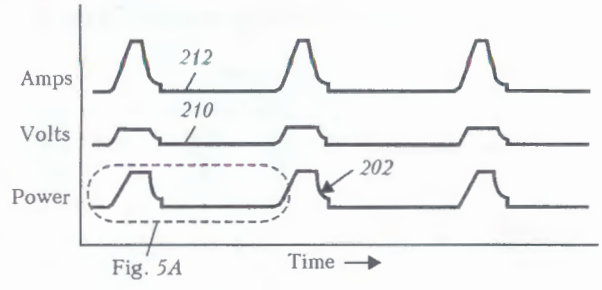


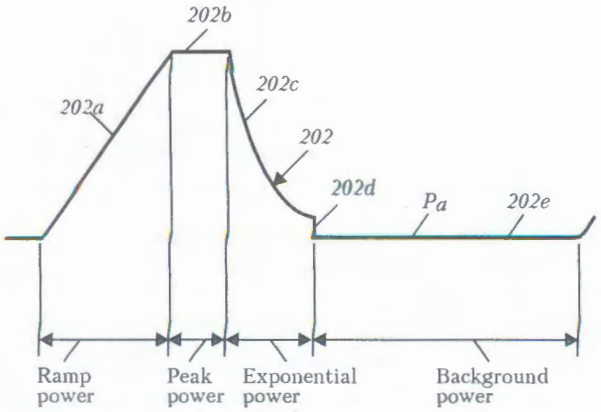


**Figure 8**

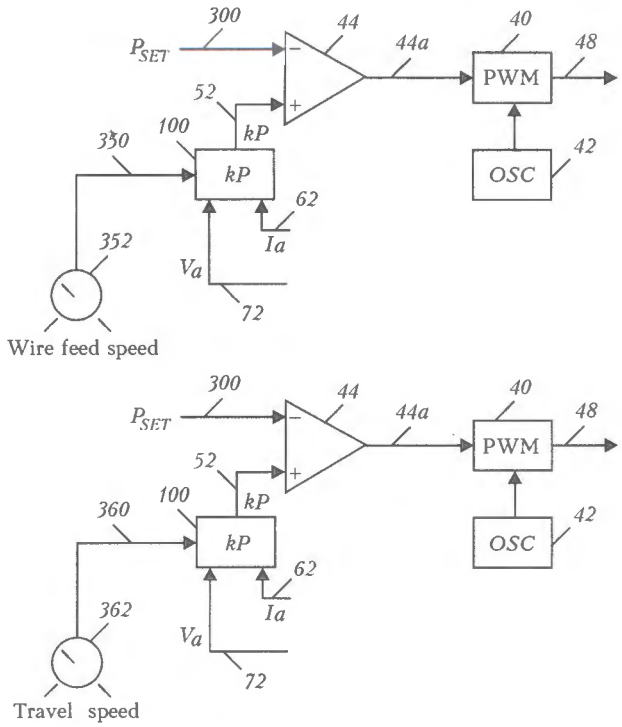


Figure 9

arc power feedback (Figure 9). Values of highest current and current of metal transfer into the weld pool are set in the first mode. The second mode is used in the case, if the short-circuit time exceeds the set limit. In this case the highest current values are determined. When the third mode is used, the minimum current value can be lowered to the admissible limit in the case of increasing the pulse energy in the earlier established range. In $CO_2$ welding the arcing time is up to 20 ms, and current before the short-circuit is from 10 up to 20 A.

French inventors were granted Patent 6518545 «Welding Arc Penetrating Power Realtime Detection

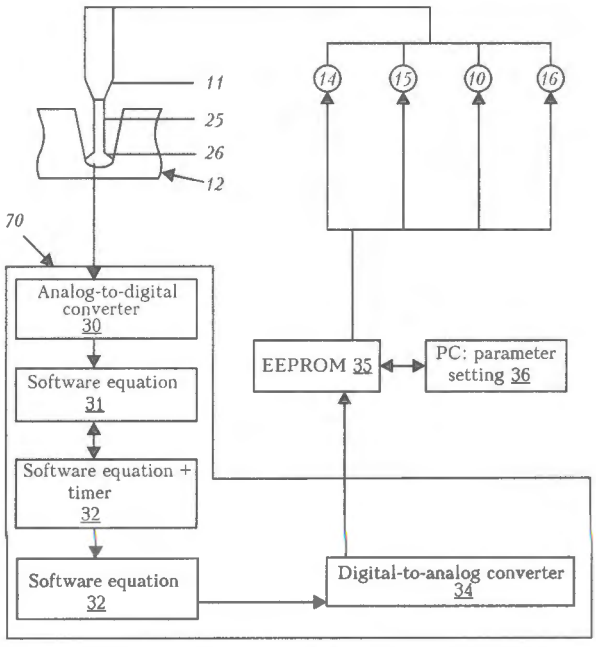


Figure 10

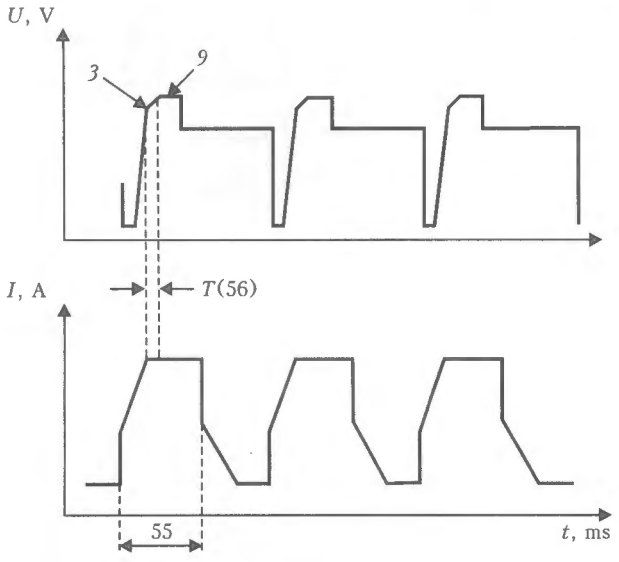


Figure 11

System» [6], which offers a system for control of pipe welding. The arc is powered from inverter *14*. Welding program is loaded into PC36 and stored in EEPROM 35 for use with microprocessor *70* (Figure 10). At normal penetration the voltage and current vary as shown in Figure 11. Current value is lowered to the minimum one before short-circuiting of the arc gap, in order to reduce spattering. Immediately after the drop transfer from the electrode to the weld pool, the current rises up to the earlier established maximum value. Then a new drop forms, and the cycle is repeated. Impedance $Z$ of the circuit including the arc and cycle time $T$ are used to control the process. Positions *A*, *C* and *B* (Figure 12) are characteristic for various situations, arising in welding with short-circuiting of the arc gap. With through penetration of the pipe walls the arc is elongated, which affects the current and voltage. The patent defines the conditions, under which the process runs with through penetration or without it, depending on the nature of impedance variation. These conditions were the basis for controlling the welding process.

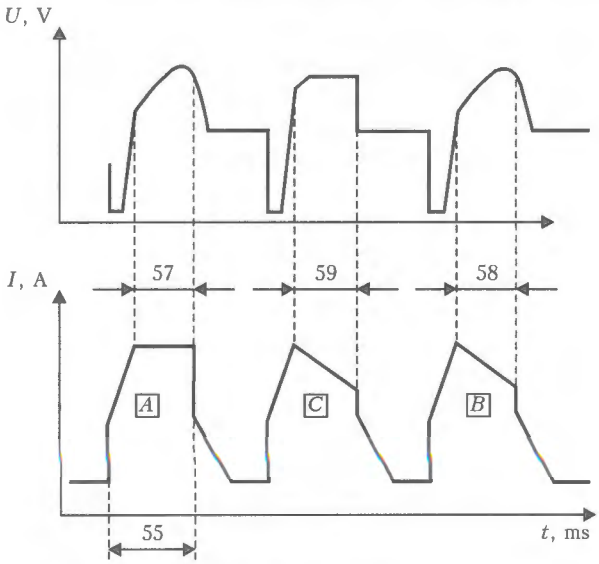


Figure 12

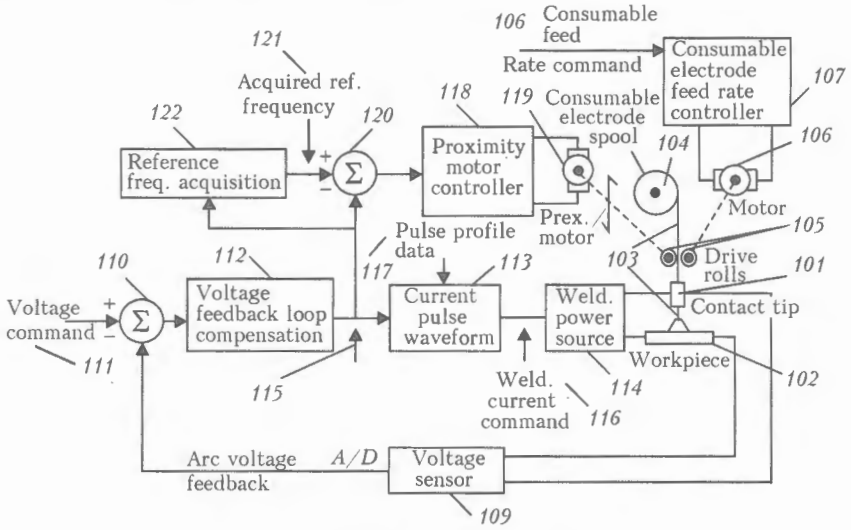


**Figure 13**

Computer is also used for controlling the feed mechanism and device for applying transverse oscillations to the electrode.

An automatic control system was developed earlier, where radiation from the reverse side of the weld was used in the circuit of welding current feedback. Additional equipment with the temperature sensor was to be introduced inside the pipe, which is not always possible. On the other hand, the system and traditional power source did not have the operation speed, required in this case. The system described in the patent did not have this drawback.

Patent 6335514 «Control Method and Apparatus for an Arc Welding System» [7] gives a description of a system for consumable-electrode pulsed-arc welding (Figure 13), which has a closed-loop feedback system for voltage stabilization. This circuit has a link, converting voltage deviation into a signal, controlling the power source, taking into account the set shape and frequency of the current pulse. The system also has another feedback, acting slower. The actuator is motor *119*, which moves the welding head along the vertical and provides frequency stabilization. In addition to the power source, the system also controls

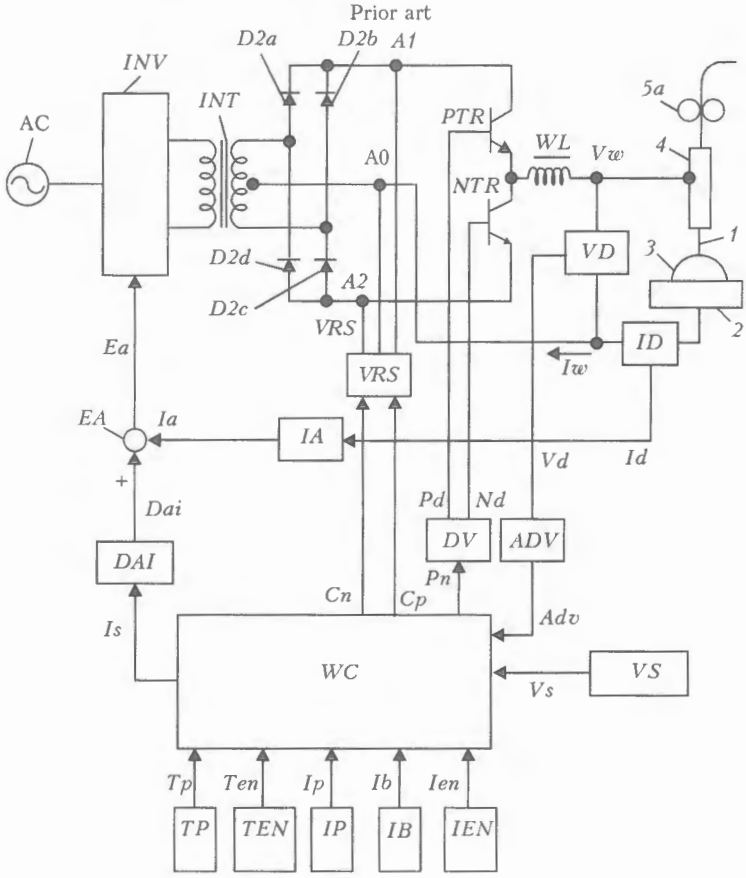


**Figure 14**

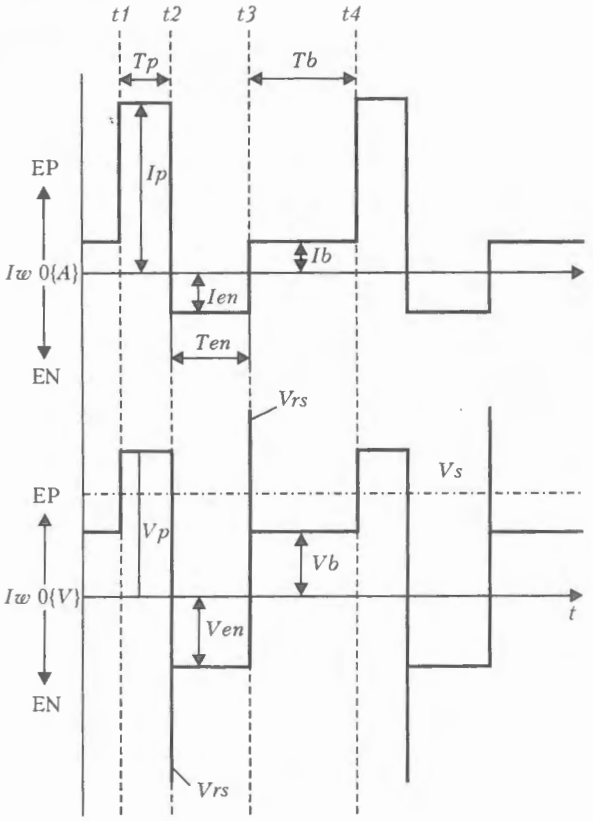


Figure 15

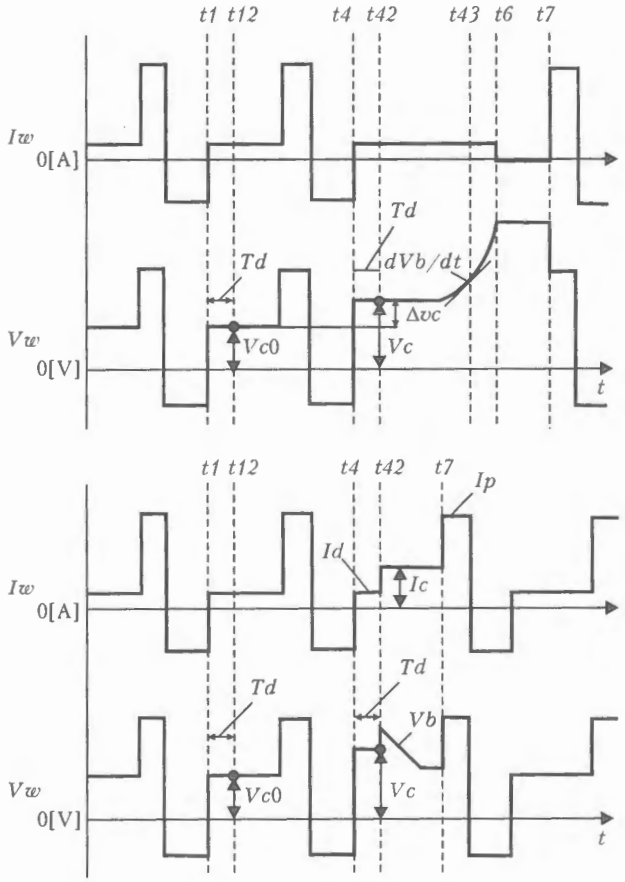


Figure 16

two motors: one of them feeds the electrode wire, and the second is the actuator ensuring the electrode position relative to the joint line of the parts being welded.

Patent 6531684 «Method and Apparatus for Welding and Control» deals with arc welding and mainly differs from the traditional patents in this field in that it incorporates data on provision of the system stability by variation of feedback parameters. This operation is performed by the system without operator participation.

Original engineering solution in terms of control is suggested in Patent 6376802 «Method of Controlling the AC Pulsed-Arc Welding and Welding Power Supply Apparatus Therefor» [8]. Power source circuit (Figure 14) includes blocks, consisting of four high-frequency power valves and two power transistors, as well as a reactor. Control is performed using a computer. Essentially, one of the possible variants of series connection of two inverters operating at different frequencies is proposed. The first of them is designed for high (ultrasonic) frequency, and the second for a much lower one. Transfer of metal drops from the electrode into the weld pool proceeds at a pulse of straight polarity current. Current frequency is selected so that one drop corresponds to each period of current. First the data on current and duration of welding at straight and reverse polarity current and electrode wire feed are entered into the computer. The computer corrects the mode so that the process runs steadily. As an illustration, Figure 15 shows a system without disturbances, and Figure 16 — a system at arc elongation. For setting up, the welder uses a screen, which displays information on task performance.

The system described in Patent 2003/0071026 «Electric Arc Welder and Controller to Duplicate a Known Waveform Therefor» is designed for setting up the power source [9] (Figure 17). The system may be used for manual setting up or transferring the

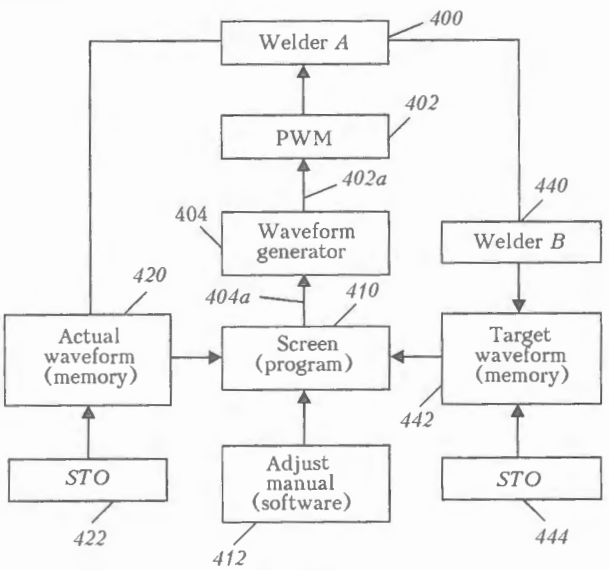


Figure 17

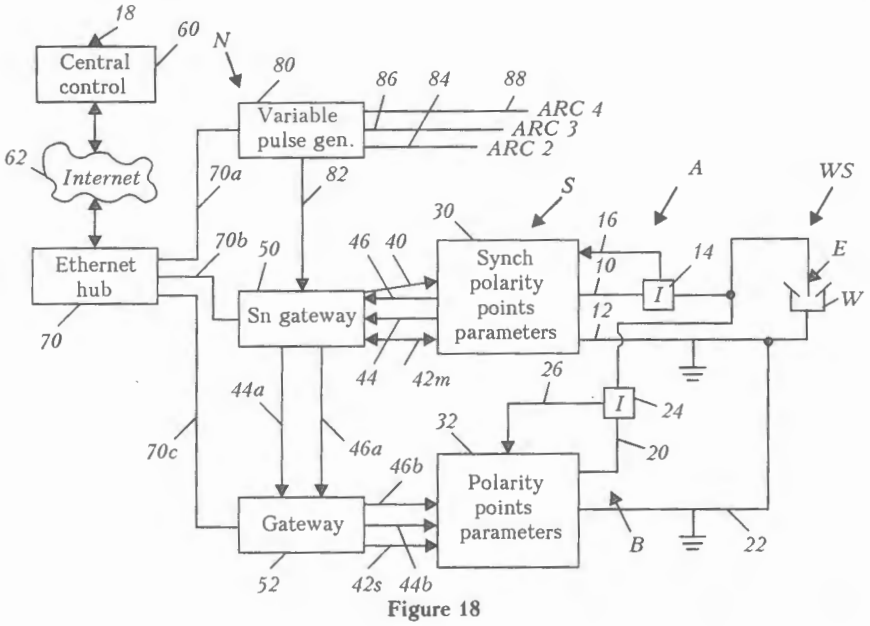


**Figure 18**

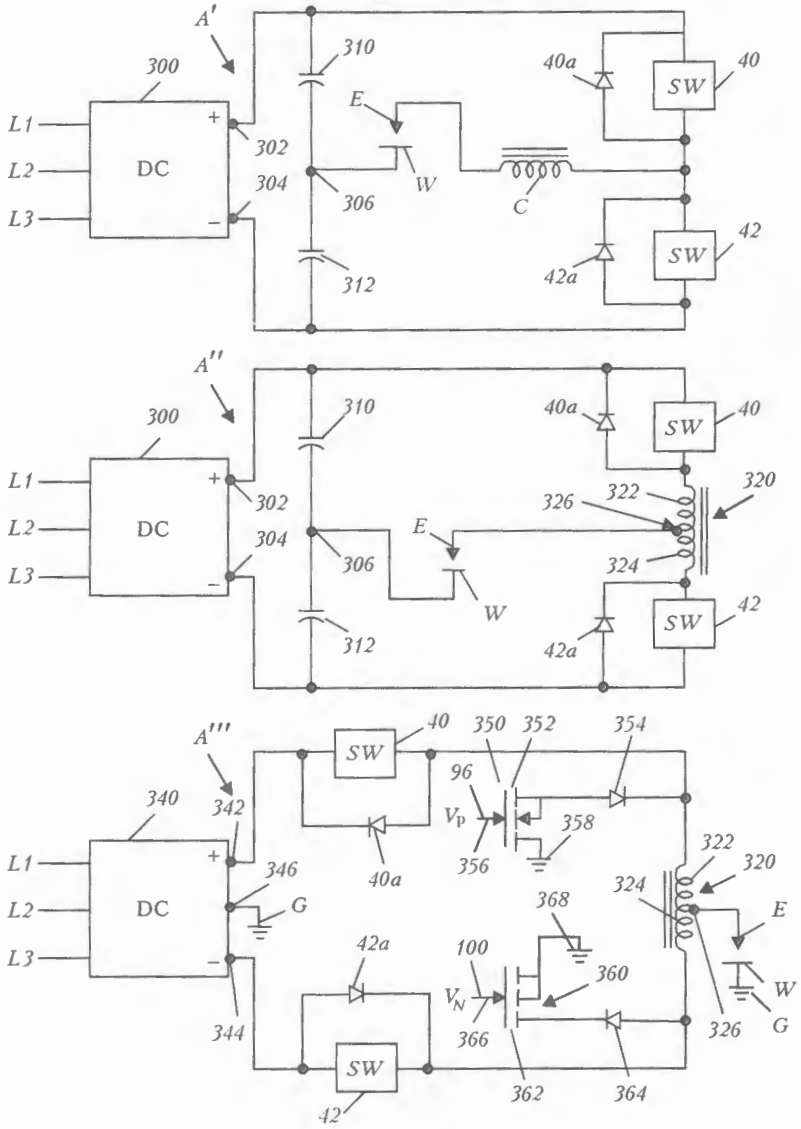


**Figure 19**

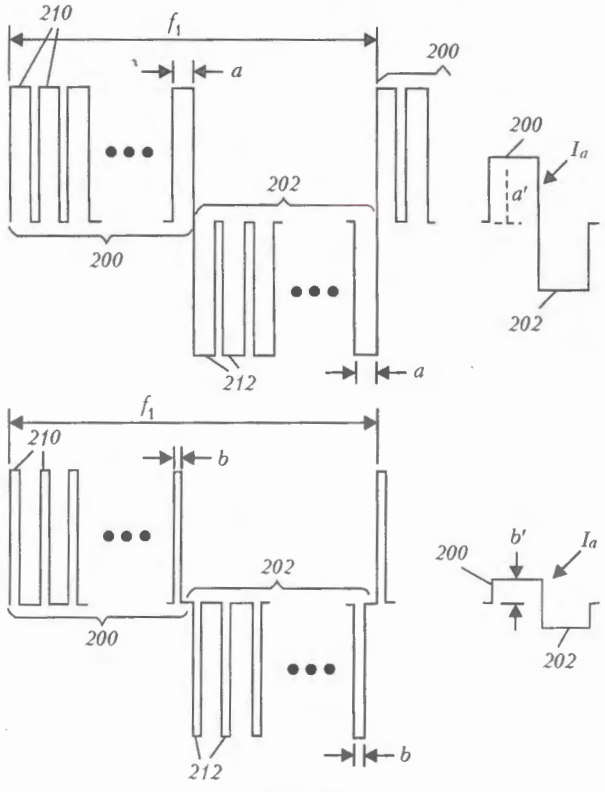


Figure 20

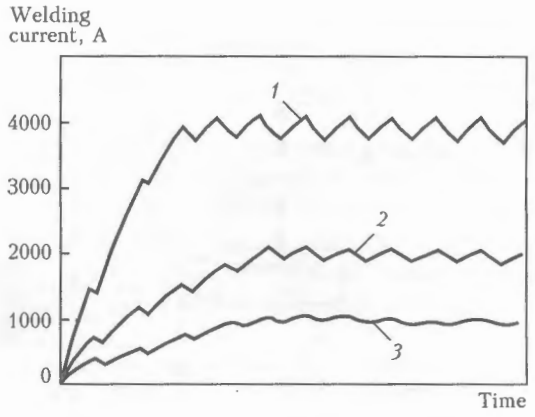


Figure 21

power mode preset in some other power source into another computer.

Patent 2003/0006222 «Electric Arc Welding System» [10] describes a system, consisting of several AC current stations (Figure 18). Data on the modes and task fulfillment are transferred to both sides of the central control station via Internet.

Patent 2002/0070205 «Power Supply for Electric Arc Welding» gives several designs of a power source for AC welding (Figure 19) [11]. The source is connected to AC mains via a commercial frequency transformer and rectifier. Control system generates pulse bursts of different polarity, controlling two groups of transistors, alternatively powering the welding arc (Figure 20). Pulse number determines the current. At different pulse numbers the current will contain a direct component, which is required, for instance, in welding aluminium and alloys on its base. Power of the AC source can be increased by parallel connection of lower power sources, combining them into the control system.

The invention of a Japanese expert, described in Patent 2003/0052107 «Arc Welding Quality Evaluation Apparatus» [12] must be one of the first in the field of diagnostics of the quality of spot welds directly during welding. The system is based on acquisition and processing data on each joint separately. It is anticipated that this invention will be developed further.

Power sources and systems of control of the processes of resistance welding are suggested just in several patents. One of them attracts particular attention in connection with the absence of the traditional welding transformer in this power system. The author of Patent 2001/0047982 «Resistance Welding Power Supply Apparatus» [13] is a Japanese inventor. Patent content is disclosed by Figures 21 and 22. Development of such a power system was made possible by appearance of power transistors, designed for high currents and electrolytic capacitors, acting as pulsed devices at the frequency of about 1 kHz. As a example, the patent author gives some data, shown in the Table.

The system is easily controlled during short time intervals and can be used in microwelding equipment.

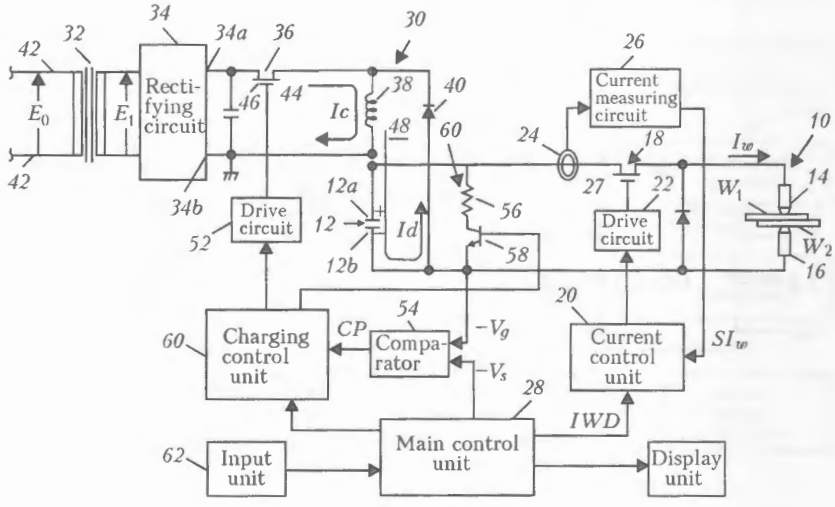


Figure 22

In conclusion the following should be noted.

• Content of most of the patents is related to varying degrees to control of transfer of liquid metal drops, both with short-circuiting of the arc gap and without it. This area of arc welding equipment is still being actively developed. Devices for metal transfer with short-circuiting of the arc gap should be noted.

• Established procedures of control of «short» arc welding consist in lowering the current before the short-circuits to a minimum level, which ensures metal drop transfer into the weld pool without its bouncing off, or uncontrollable growth of drop volume, leading to spatter. In this respect, the control procedure has been simplified, compared to that known earlier.

• It is anticipated that metal transfer with short-circuiting of the arc should also be effective in welding in Ar-based mixtures.

• Penetration stabilization in making welds from one side should be noted, which is based on automatic analysis of variations of welding mode at transition to through penetration and vice versa.

• New arc welding power sources are developed mostly on the basis of computer-controlled power transistors.

• New power sources are based on frequency and phase converters, which not only provide certain advantages in terms of energy, but also ensure fast operation of the control systems.

• New AC power sources are developed as cascades of inverters connected in series. The first inverter is connected to a three-phase mains and converts the rectified mains voltage into single-phase high-frequency voltage, which is then lowered to the required value by the high-frequency transformer. Second inverter converts the single-phase high-frequency voltage into the low-frequency voltage, the value of which is selected automatically and is equal to the frequency of drop transfer from the electrode into the weld pool.

• Resistance welding is also developed due to advances in semi-conductor engineering, but just one or two patents were filed in the considered period. Familiarization with one of the above-mentioned patents allows anticipating the greatest changes in the field of resistance microwelding.

| *Curve number in Figure 21* | *Welding current, A* | *Capacitor voltage, V* |
|---|---|---|
| 1 | 4000 | 30 |
| 2 | 2000 | 28 |
| 3 | 1000 | 24 |

• It is quite possible that automatic control of the welding process will turn out to be an effective means of detecting defective areas of welds.


1. Paton, B.E., Potapievsky, A.G., Podola, N.V. (1964) Consumable-electrode pulsed-arc welding with programmable control of process. *Avtomatich. Svarka*, **1**, 1–6.
2. Paton, B.E., Lebedev, A.V. (1988) Control of fusion and metal transfer in $CO_2$ welding. *Ibid.*, **11**, 1–5.
3. Jank, V., Ruehrhoesse, M., Fnouenschuh, R. et al. *Method for controlling a welding apparatus and corresponding control device*. Pat. 6476354 USA. Int. Cl. B 23 K 9/10. Publ. 05.11.02.
4. Norrish, J. et al. *Welding control system*. Pat. 6512200 USA. Int. Cl. B 23 K 9/10. Publ. 28.01.03.
5. Fulmer, B.E., Peters, S.R. *System and method for controlling an electric arc welding*. Pat. 6498321 USA. Int. Cl. 23 K 9/10. Publ. 05.11.02.
6. Richard, C. et al. *Welding arc penetrating power realtime detection system*. Pat. 6518545 USA. Int. Cl. B 23 K 9/10. Publ. 11.02.03.
7. Rothermel, R. *Control method and apparatus for an arc welding system*. Pat. 6335514 USA. Int. Cl. B 23 K 9/10. Publ. 01.01.02.
8. Tong, H. et al. *Method of controlling the AC pulsed-arc welding and welding power supply apparatus therefor*. Pat. 6376802 USA. Int. Cl. B 23 K 9/10. Publ. 23.04.02.
9. Hsu, C. et al. *Electric arc welder and controller to duplicate a known waveform therefor*. Pat. 2003/0071026 USA. Int. Cl. B 23 K 9/10. Publ. 17.04.03.
10. Houston, W.S., Myers, R.K., Stava, E.K. *Electric arc welding system*. Pat. 2003/0006222 USA. Int. Cl. B 23 K 9/10. Publ. 09.01.03.
11. Stava, E. *Power supply for electric arc welding*. Pat. 2002/0070205 USA. Int. Cl. B 23 K 9/10. Publ. 13.06.02.
12. Suzuki, Y. *Arc welding quality evaluation apparatus*. Pat. 2003/0052107 USA. Int. Cl. B 23 K 9/10. Publ. 20.03.03.
13. Watanabe, M. *Resistance welding power supply apparatus*. Pat. 2001/0047982 USA. Int. Cl. B 23 K 9/10. Publ. 06.12.01.

# RESISTANCE WELDING OF SILVER-COPPER CURRENT-CARRYING BUSBARS

V.S. KUCHUK-YATSENKO, A.G. SAKHATSKY and A.A. NAKONECHNY
E.O. Paton Electric Welding Institute, NASU, Kiev, Ukraine

Technology of resistance welding in air and shielding gas atmosphere has been developed for joining flexible copper busbars to silver plates welded to contact pads for manufacturing flexible connections for high-voltage vacuum switches. It has been established that the use of a certain thermal-deformation cycle can provide a sound welded joint on the copper-silver foil pack. The mechanisms of deformation of the pack and formation of a welded joint have been studied. A pilot welding machine and control unit have been manufactured.

***Keywords:*** *resistance welding, autovacuum welding, foil pack, silver, copper, high-voltage vacuum switch*

Development of the technology of resistance welding of a flexible current-carrying bimetal busbar was made necessary by the need to apply in industry a cost-effective process of manufacture of copper and silver-copper flexible connections providing a high quality, in particular, for high-voltage vacuum switches. The main requirements made of the flexible busbars are provision of reliable contact, consistently low transient resistance during operation and high fatigue strength at alternating cyclic loading [1].

Various methods of joining the ends of flexible copper busbars are currently applied, namely mechanical clamping of the pack to the current-conduit, soldering with Sn–Pb solders and brazing with braze alloys of Ag–Cu and Cu–P system, welding copper coverplates to the pack by electric-arc or gas welding, resistance autovacuum welding, explosion welding, and diffusion welding in vacuum [2].

Mechanical clamping is usually performed with bolts, which become loose during operation, particularly in the units exposed to vibration loads, which leads to violation of the contact.

Brazing of the flexible busbar ends is usually performed by dipping into the weld pool of molten braze alloy or induction heating of the pack with inserts of braze alloy foil. The thus joined packs lose their flexibility as a result of braze alloy flowing over the joint boundary, this leading to foil separation from the contact pad during operation. Brazing does not provide a stable low transient resistance or geometry of the monolithic part. In addition, fluxing remnants accumulate inside the pack, which leads to oxidation and corrosion of flexible connections, inadmissible in operation of a flexible busbar in vacuum [3, 4].

Foil burn-through occurs, when copper coverplates are welded to the pack by arc or gas process, and it is not possible to produce a uniform joint over the entire section of the pack.

Explosion welding involves higher labour consumption and cost, and welding a pack of thin foil runs into certain difficulties, because of the upper layers burning out.

High quality of the joint and stability of operating parameters can be achieved by applying diffusion welding in vacuum. This welding process provides a mode, which ensures weldability of the silver-copper pack, where the welding temperature is 750 °C, and the compressive force is 3 MPa, while minimum welding time is approximately 15 min [5]. However, long-term annealing at a high temperature leads to grain coarsening in the transition zone of the flexible part–monolith material, which lowers the fatigue strength of the flexible busbar [6]. Moreover, vacuum welding involves high equipment and operating costs, as well as a low process efficiency.

The most cost-effective is the process of resistance welding of multi-layer packs of copper foil due to the effect of autovacuumizing and simultaneous plastic deformation [7]. The process envisages welding of flexible busbars of different type, features simplicity and availability of the equipment and capability of a high level of process automation. The main disadvantages of resistance welding are overheating of the layers, adjacent to the monolithic part, and lowering of fatigue strength values.

The main problem in resistance welding of a pack of silver and copper foil is contact melting of copper and silver with formation of 72 % Ag and 28 % Cu eutectic at 780 °C. However, as was experimentally established, welding of copper foil is possible at the temperature higher than 830 °C. Therefore, in resistance welding of a copper pack in the currently used modes, the silver plates are melted and the liquid phase comes to the pack surface.

The purpose of this work was to study the features of resistance welding of a pack of silver and copper foil, investigate the processes of silver–copper and copper–copper interaction in various welding modes.

Optimizing the modes and studying the features of welded joint formation were performed on samples of 90×40×10 mm size, which were a pack of copper foil of M1 grade 50 μm thick, to which 20×40×0.3 mm silver coverplates were welded in monolithized regions. Therefore, the area of monolithized regions was

1600 mm$^2$. Such a sample is a blank for a flexible busbar, used in high-voltage vacuum switches.

In order to conduct the experiments, resistance welding machine K602 was upgraded, taking into account the following technology features: both ends of the flexible connection were welded simultaneously to avoid current shunting; for uniform heat evolution in each monolithized region uniform pressure application to each pair of electrodes and uniform current density distribution both between the electrode pairs and over the welded area were provided. Test welds were made in air and in shielding gases.

At compression in air, the air remains in the microvolumes formed by the abutted surfaces, which cannot be removed from the butt even in vacuum and affects the process of solid-phase welding of the surfaces in contact. During heating, processes of surface self-cleaning from oxide films and vacuum formation proceed in these microvolumes [7]. At heating and plastic deformation the pressure of the gas medium should reach values, commensurate with the yield point of copper at the welding temperature.

Copper surface consists of grains, covered with a layer of copper oxides $Cu_2O$ and CuO with gases and moisture adsorbed on their surface [8]. At heating of the contacting surfaces, self-sealing of closed microvolumes by the oxide layer occurs. Oxygen in them burns out completely with formation of copper oxide $Cu_2O$, which, forming an eutectic with copper along the grain boundaries, penetrates inside the metal [9]. Nitrogen, not dissolving in the copper, is removed from the microvoids during high-temperature plastic deformation.

It is established that plastic deformation in copper at high temperatures runs by the diffusion creep mode. In this case, intensive formation of micropores entrapping the nitrogen atoms, proceeds along the grain boundaries. Micropores are chaotically located along the transverse boundaries. Methods of optical metallography do not allow revealing the zones of micropore formation. There is a certain dependence of micropore formation on relative orientation of the grains: the pores never form on twinning boundaries [10].

As follows from [10], copper is characterized by an unsteady state of diffusion creep, at which the deformation rate is by an order of magnitude higher than in the case of a steady-state diffusion creep. Research performed by the authors revealed that unsteady creep state at premelting temperatures is due to non-equilibrium condition of the samples. Sample annealing before testing led to disappearance of the unsteady creep state.

Therefore, a mandatory condition for producing a sound welded joint of a copper foil pack is activation of the diffusion creep of copper, in particular, its primary unsteady state, where active mass transfer occurs in the HAZ. Energy required for process activation is by an order of magnitude lower for a material deformed above the critical degree of deformation [11, 12]. This is in agreement with the conducted experiments, in which activation of the creep process proceeds at 800–810 °C for cold-rolled foil, while for foil after annealing it occurs at 900 °C.

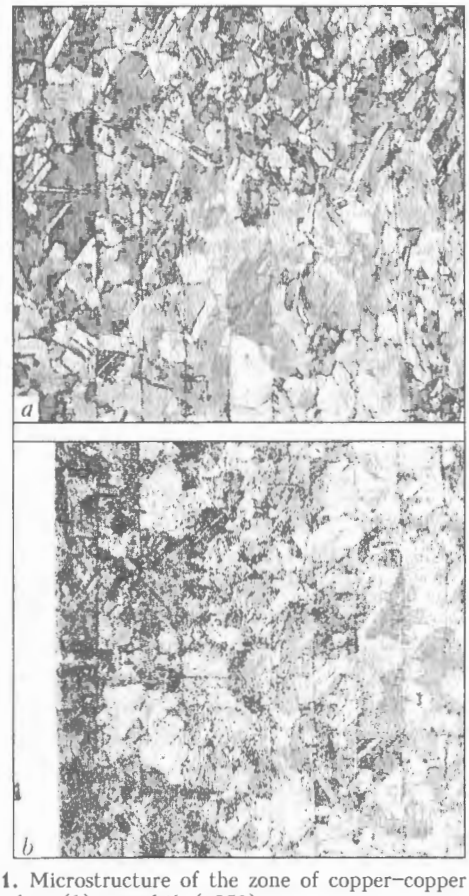


**Figure 1.** Microstructure of the zone of copper–copper (*a*) and copper–silver (*b*) monolith (×250)

Such a thermal-deformation cycle of resistance welding of a silver-copper foil pack has been developed, which ensures sound welding of both the copper pack and the silver coverplates. The most complex part was to develop the welding current cyclogram, providing heating in the welding zone above the point of eutectic melting, but not longer that the dwell time for Cu–Ag eutectic formation.

Conducted experimental series demonstrated the high consistency of the results, absence of lacks-of-

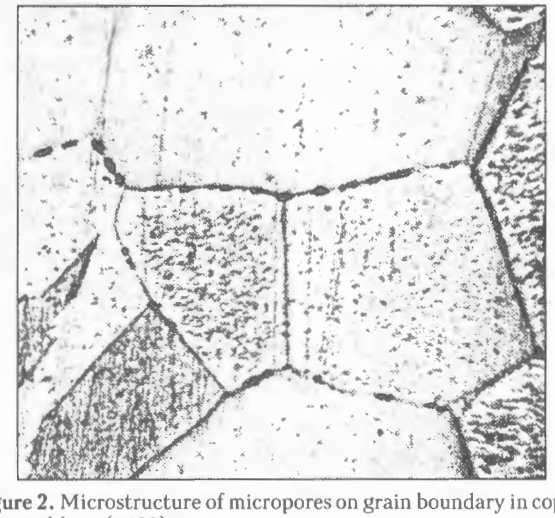

**Figure 2.** Microstructure of micropores on grain boundary in copper after welding (×400)

penetration or partial melting of the silver coverplates. Compared to earlier known modes of copper pack welding, the welding time was shortened from 2 min to 14 s, thus preventing overheating of the layers adjacent to the monolithic part. Therefore, the developed thermal-deformation cycle can be recommended for welding not only the silver-copper flexible busbars, but also purely copper current-carrying ones.

In order to determine the quality of the welded joint, flexible copper connections were subjected to metallographic examination and mechanical testing.

Formation of silver–copper and copper–copper welded joints was studied on microsections, using optical microscope MIM-7. The copper–silver pair forms on the joint boundary a layer of copper solution in silver about 20 μm thick. Thickness of diffusion zone of silver penetration is 150 μm on average, which is indicative of active mass transfer in welding. Measurement of microhardness in the welding zone did not indicate formation of any brittle phases. Results of studying the joint on the boundary of the copper sheets revealed presence of common grains, which is indicative of recrystallization proceeding during welding. Micropores were detected along the grain boundaries, which points to plastic deformation developing by the diffusion creep mode.

Strength properties of welded joints were determined by full-scale testing on a mock-up of a high-voltage switch. Samples stood 250 ths cycles without change of geometry, mechanical or electric properties. According to operation standards a flexible connection in a high-voltage switch should stand 100 ths cycles. Flexible connections were subjected to one more method of control, namely measurement of electric resistance, which showed that flexible connection resistance is equal to ≈ 15 μOhm, which is almost 2–2.5 times smaller than the resistance of brazed flexible connections.

## CONCLUSIONS

1. It is established that sound autovacuum resistance welding of a copper pack requires initiation of the process of diffusion creep, where the activation energy depends on the degree of copper foil work-hardening.

2. Use of cold-rolled copper foil in combination with dosed energy input allows significantly improving the quality of this type of joints, particularly fatigue strength values, and making joints with a high electric conductivity. The problem of applying silver coatings on copper packs is solved simultaneously.


1. Chmyryov, I.A., Yavorskỳ, Yu.D. (1968) Resistance welding of copper foil packs. *Avtomatich. Svarka*, **6**, 55–57.
2. Masterov, V.A., Saksonov, Yu.V. ((1979) *Silver, alloys and bimetal on its base*. Refer. Book. Moscow: Metallurgiya.
3. Mikhajlova, E.M. (1972) Vacuum resistance welding of copper flexible connections. *Svarochn. Proizvodstvo*, **10**, 42–43.
4. Kvasnitsky, V.F. (1973) Investigation of the process and development of the technology of copper bonding without melting. In: *Technology of shipbuilding and welding production in shipbuilding*. Nikolaev.
5. Kozakov, N.F., Bojchenko, A.N. (1971) Investigations of vacuum diffusion welding process of some precious metals and alloys to non-precious metals and alloys. In: *Vacuum diffusion bonds*. Moscow: MTIMMP.
6. Abramov, V.V., Akhundanova, L.A. (1986) Ductility and microhardness of copper near-contact layers in pressure welding with preheating. *Svarochn. Proizvodstvo*, **11**, 23–24.
7. Kuchuk-Yatsenko, S.I., Kharchenko, G.K., Falchenko, Yu.V. et al. (1998) Self-cleaning from oxides of abutted surfaces in solid-phase welding with heating. *Avtomatich. Svarka*, **2**, 16–24.
8. Suchkov, D.I. (1967) *Copper and its alloys*. Moscow: Metallurgiya.
9. Geguzin, Ya.E. (1967) *Physics of sintering*. Moscow: Nauka.
10. Rozenberg, V.M. (1967) *Creep of metals*. Moscow: Metallurgiya.
11. Malevsky, Yu.B., Markashova, L.I. (1968) Formation of active zones in welding without melting. *Avtomatich. Svarka*, **5**, 71.
12. Malevsky, Yu.B., Markashova, L.I., Nesmikh, V.S. (1971) Role of recrystallization in bond formation in solid-phase welding. In: *Vacuum diffusion bonds*. Moscow: MTIMMP.

# APPLICATION OF FLAME BRAZING FOR MANUFACTURE OF BEER COOLER UNITS

V.F. KHORUNOV[1], S.V. MAKSIMOVA[1], B.V. STEFANIV[1], G.G. KARACHENTSEV[2] and V.Yu. ZADIRAKA[2]
[1]E.O. Paton Electric Welding Institute, NASU, Kiev, Ukraine
[2]Closed Joint-Stock Company «UKsnab», Krasnoperekopsk, Ukraine

Defects which may be formed in production of tubular brazed joints in beer cooler units are analysed. Examples of the tubular brazed joints in similar (copper–copper) and dissimilar (brass–stainless steel, copper–stainless steel) materials are given.

***Keywords:*** *brazing, brazing alloys, fluxes, bear coolers, defects, flame heating, oxidation, brass, copper, stainless steel*

Production of beer in Ukraine is a rapidly growing industry. New plants are built and the old ones are reconstructed. The demand is met mostly due to local products. Every year the import of beer decreases and export increases.

No production line for bottling of beer, one of the elements of which is a beer cooler, has been manufactured or assembled in Ukraine until now. This drawback has been eliminated by the «Ukrainian Beer Company» that arranged the factory for manufacture of beer coolers and ceramic beer columns in the town of Krasnoperekopsk (Autonomous Republic of Crimea), which is now the Closed Joint-Stock Company «UKsnab». The factory has the most advanced English, German and Danish equipment for the manufacture of coolers. 4–6 new coolers are developed every year, out of them 2–3 models are commercialised. Then they are delivered throughout Ukraine, to Russia and Kazakhstan.

The disadvantage in the activity of the Company lay in the absence of a sufficient experience in assembly brazing, which caused failure of the equipment after its transportation and during operation. This problem was resolved by the joint efforts of the «UKsnab» and the E.O. Paton Electric Welding Institute.

The following problems had to be addressed:

- analysis of the brazing process, revealing of its drawbacks and determination of the cause of reject;
- development of the brazing technology at a level of the world standards for different materials used in production;
- training of the Company's brazing operators.

Beer coolers consist of propulsion and processing modules housed in a metal casing (Figure 1). The cooling machine located in the propulsion module consists of tubes containing overlap tubular joints from 6 to 10 mm in diameter, as well as a throttle (a capillary tube with an outside diameter of 2 mm, that enters into the evaporator with an inside diameter of 7–9 mm). All the butt joints in tubes of the cooling machine are made by brazing.

It is a well-known fact that brazing is a sophisticated technological process that depends upon many inter-related parameters. The latter should be selected so that they provide capillary brazing, i.e. spreading of a brazing alloy and its flowing into the gap under the effect of capillary forces.

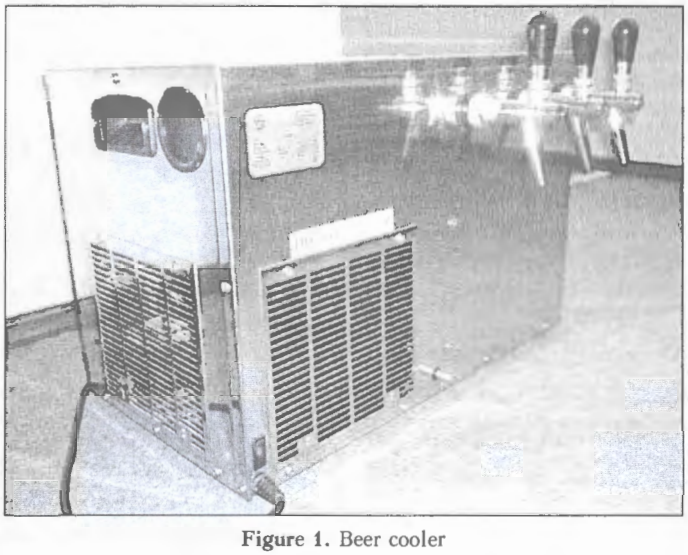

**Figure 1.** Beer cooler

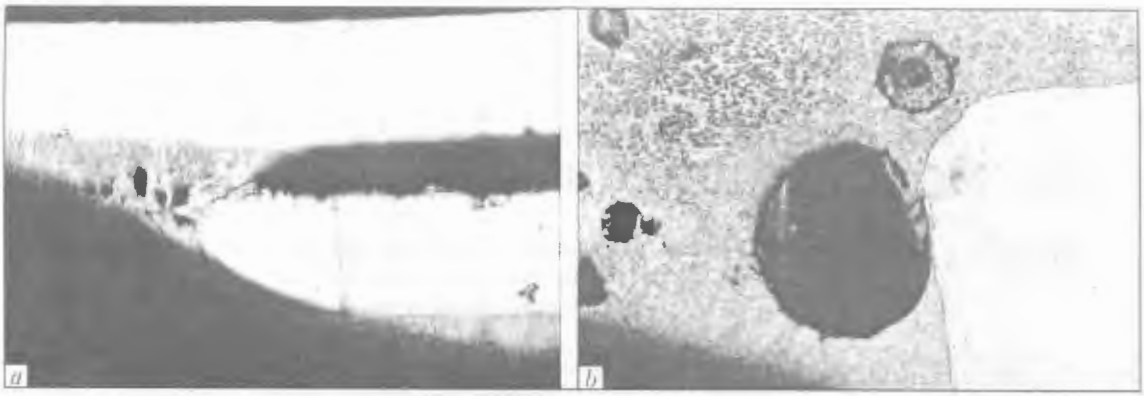

**Figure 2.** Defects in brazed joints: *a* — lack of penetration (×25); *b* — porosity (×100)

**Figure 3.** Brazed beer cooler unit

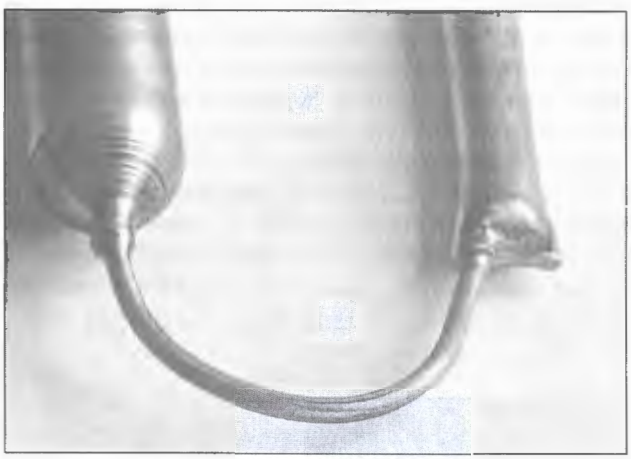

**Figure 4.** Brazed joint between a capillary 2 mm in diameter and tubes 5.4 and 10 mm in diameter

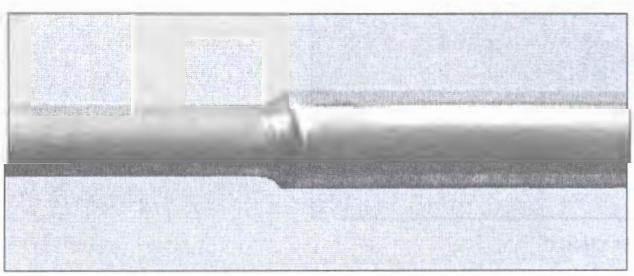

**Figure 5.** Tubular copper brazed joint

Technical analysis of the brazing process was conducted by assessing the quality of mass-produced copper brazed joints. This was done by visual examinations and metallography using optical and scanning electron microscopes. Visual examinations of overlap tubular joints showed an excessive amount of the brazing alloy above the overlap region, while metallography of the same joints revealed more serious defects which might lead to the loss of performance of a joint (Figure 2). The presence of such defects is caused by violation of the technological process used to produce the brazed joints.

The technology for flame brazing of tubular joints in different materials (including preparation of mating surfaces for brazing) was optimised on the basis of the studies conducted by the E.O. Paton Electric Welding Institute.

Flame brazing of the copper tubular joints was performed by using silver and phosphorus-copper brazing alloys. These alloys provided sound brazed joints with good formation of external and internal fillets (Figures 3–5). Microstructure of the brazed seal comprises copper- and eutectic-base solid solution grains (Figure 6).

Brazing of dissimilar joints between copper and stainless steel performed in air presents a more complicated problem, as it has specific features caused by formation of oxides on the surfaces being brazed. For

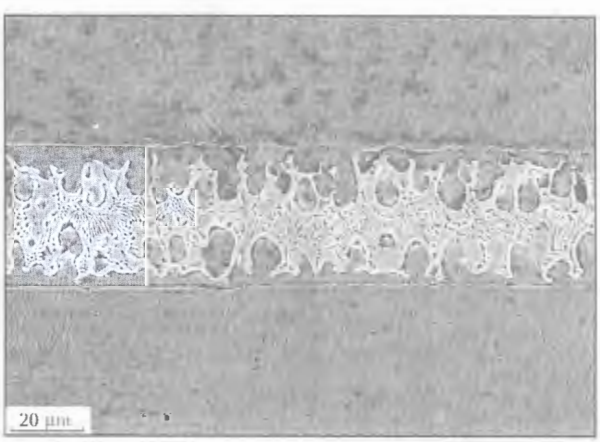


**Figure 6.** Microstructure of the brazed seal in a tubular copper joint (×1000)

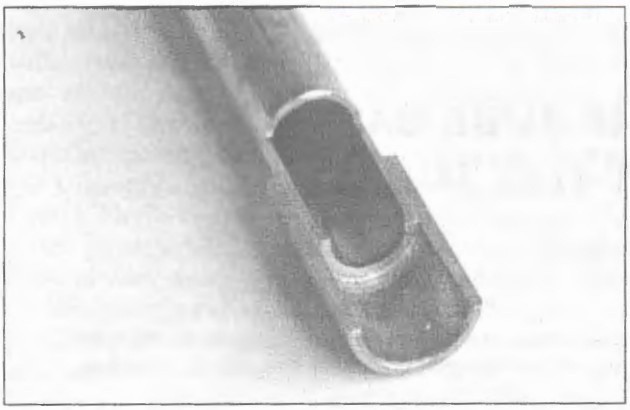

**Figure 7.** Copper–stainless steel brazed joint

brazing of stainless steel, it is necessary to use active fluxes and brazing alloys with a lower melting point.

All the fluxes recommended for brazing these materials rapidly lose their activity in flame of the torch, this making the heating technique very important. In addition, it is necessary to provide a simultaneous wetting of both materials and satisfactory strength of the brazed joints. In this case the suitable brazing alloys are the silver ones. They have the required temperature range and a high fluidity, only negligibly dissolve corrosion-resistant steels during brazing, have no penetrating (along the grain boundaries) ability and form no brittle intermetallic interlayers (provided that the brazing technology is strictly kept to). The resulting brazed joints are characterised by dense defect-free seals, as well as the presence of the internal and external fillets (Figure 7).

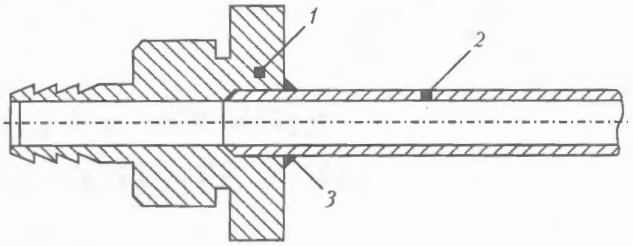


**Figure 8.** Schematic of the brazed joint in dissimilar materials: *1* — fitting (brass); *2* — tube (stainless steel); *3* — brazing filler metal

Dissimilar joints between brass and stainless steel (Figure 8) present a special case. On the one hand, these materials must not be overheated, as stainless steel rapidly oxidises, and brass is characterised by a low melting point because of the presence of a readily evaporating element, i.e. zinc. On the other hand, production of a sound joint requires slow and complete heating through both stainless steel tube and massive brass fitting. These peculiarities create extra limitations in selection of a brazing alloy and conditions of flame heating.

Such undesirable phenomena as oxidation of the base metal, evaporation of volatile elements in brazing of brass to steel were eliminated owing to the use of a special brazing technology and proper selection of the composition of a brazing alloy.

All the problems posed were solved and the brazing technology was optimised both under laboratory and factory conditions by the joint efforts of the Closed Joint-Stock Company «UKsnab» and the E.O. Paton Electric Welding Institute.

# EBW OF A FLAME TUBE CASE OF A STATIONARY GAS TURBINE

V.I. ZAGORNIKOV
E.O. Paton Electric Welding Institute, NASU, Kiev, Ukraine

Welding and assembly techniques, as well as peculiarities of manufacturing a serviceable unit, i.e. blocks of shells of output circuit of a gas turbine combustion chamber are described. Advantages of electron beam welding used to manufacture parts of heat-resistant nickel-base alloy 04KhN60VT over argon-arc and manual welding are shown.

***Keywords:*** *electron beam welding, nickel alloy, flame tube, microstructure, hot cracks*

Welded cases of flame tubes of gas turbines operate under the conditions of constant vibration and high temperature cycles (300–900 °C), which makes stringent requirements of the quality of their welded joints.

Producing reliable welded joints of high-temperature Ni-base alloys involves considerable difficulties. They are related primarily to the possibility of cracking in the HAZ during welding, heat treatment and high-temperature service [1–10].

In terms of improvement of the reliability of stationary gas turbines EBW application for fabrication of individual components seems to be promising. However, work in this direction still is in the embryo stage, so that the rationality of applying this welding process cannot be definitely stated so far. EBW application does not always provide sound welded joints of high-temperature nickel alloys and requires further investigations in this field. However, difficulties arising in EBW can be overcome at lower cost [2, 3, 5] than in arc welding. A favourable thermodeformational cycle of EBW enables avoiding the traditional for arc welding solidification cracks in the HAZ due to a low specific heat input and, as a result, lowering of the intensity of internal high-temperature deformation. In addition, high rates of heating and cooling above $A_{c_3}$ point limit grain growth in the weld and HAZ. This way the resistance of welded joints to hot cracking which is of intergranular nature, is increased [1].

It is anticipated that under the condition of observing the rules of design and fabrication of welded components, which eliminate design and technological stress raisers in an item, EBW will allow avoiding performance of postweld heat treatment. Experience of EBW of such items in ENERGOMASH plants did not yield any positive results, as in most of the cases they had hot cracks along the fusion line.

The first experiments, conducted at PWI on EBW application for making welds in shell blocks (Figure 1) showed that this process can significantly reduce residual deformations of the structure after welding. Technology was developed taking into account recommendations of the authors [2, 3, 7, 10], who determined the factors influencing crack initiation and propagation in EBW of high-temperature nickel alloys, and methods to reduce cracking by changing the welding modes [2, 3].

Technology is considered of EBW of a tube case, consisting of a block of complex-profile perforated shells of thickness $\delta$ = 1.5 mm, made of 04KhN60VT alloy. The alloy composition was as follows, wt.%: 0.04–0.05 C; 0.23–0.34 Mn; 0.22–0.34 Si; < 0.013 P; < 0.013 S; 24.7–25.4 Cr; < 0.01 Cu; 0.07–0.25 Al; 0.34–0.47 Ti; < 0.05 Ca; 13.2–13.9 W; 0.02–0.06 Mo; 0.23–0.42 Fe; Ni being the base.

From the structural viewpoint, welding should provide tight joining of the shell billets into a block by overlap welds (10 welds per a shell block).

Welding operations were conducted in UL-101 unit, fitted with ELA 60/60 power source, vacuum system, RASTR-5M butt following system, computerized system of controlling the mechanisms of displacement of the item and the welding beam. Electron beam gun at a working distance $L_g$ = 140 mm was positioned at an angle of 22.5° from the vertical (Figure 2).

Welding-assembly jig ensured the accuracy of shell mounting and their tightening into a block, as well as fast removal of the product after EBW. The

**Figure 1.** Appearance of a weldment

item assembled for welding was mounted on a rotator with a horizontal axis of revolution. When welding was performed in the downhand position, a uniform melting of the upper and lower edges of the circumferential joint was achieved. This allowed increasing the admissible inaccuracy of combining the electron beam with the butt of edges being welded at variation of the gaps or local thermal deformations (after additional tack welds have been made).

The quality and appearance of the welds were improved by preliminary cleaning of the butt surface by an electron beam scanning over a ring ($\varnothing \approx 6\delta$) and subsequent cosmetic treatment of the weld with a defocused beam. Before welding of the items, transverse macrosections from a test welded joint were made, which allowed selection of the range of EBW mode parameters, required to produce the necessary penetration shape (Table). Welding speed was constant ($v_w$ = 9 mm/s).

Tack welds were placed around the butt perimeter in diametrally opposite points. 4 tacks welds were usually applied, but with greater gap in the butts 8 and more tack welds were made. Total length of the

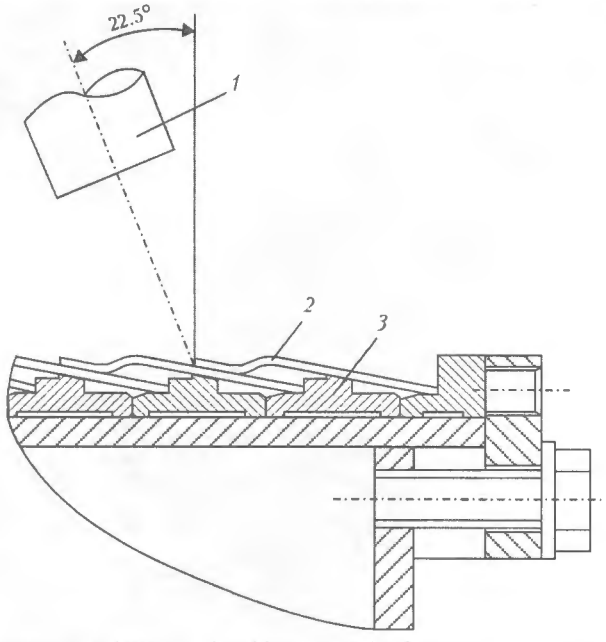


**Figure 2.** Schematic of welding a block of shells: *1* — electron beam gun; *2* — block of shells; *3* — assembly-welding device

Operational sequence and mode parameters of EBW of a test joint of 04KhN60VT alloy

| *Operational* | | *EBW mode parameters* | | *Macrosections* |
|---|---|---|---|---|
| | | $I_w$, mA | $I_f$, mA | |
| Mode No.1 | | | | |
| Making tack welds 30 mm long, 4 welds around the circumference | | 13 | 780 | 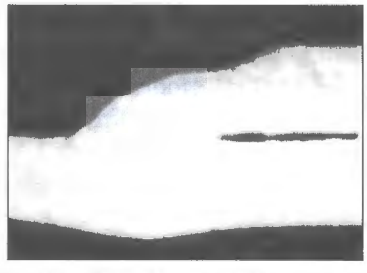 |
| Welding along the entire length $L = \pi D + 50$ mm | | 17 | 810 | |
| Cosmetic smoothing of the weld | | 19 | 808 | |
| Mode No.2 | | | | |
| Making tack welds 30–60 mm long, 8 welds | | 13 | 800 | 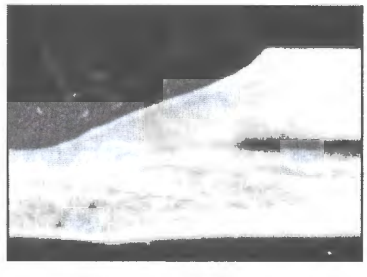 |
| Welding | 1 | 15 | 805 | |
| | 2 | 15 | 814 | |
| Cosmetic smoothing of the weld | | 19 | 800 | |
| Mode No.3 (repair mode, at > 0.15 mm gaps) | | | | |
| Making tack welds 30–60 mm long over ≥ 1.5 mm gap, overlap along the entire length | | 15 | 800 |  |
| Welding | 1 | 17 | 810 | |
| | 2 | 19 | 808 | |
| Cosmetic smoothing of the weld | | 19 | 816 | |
| | | 18 | 820 | |

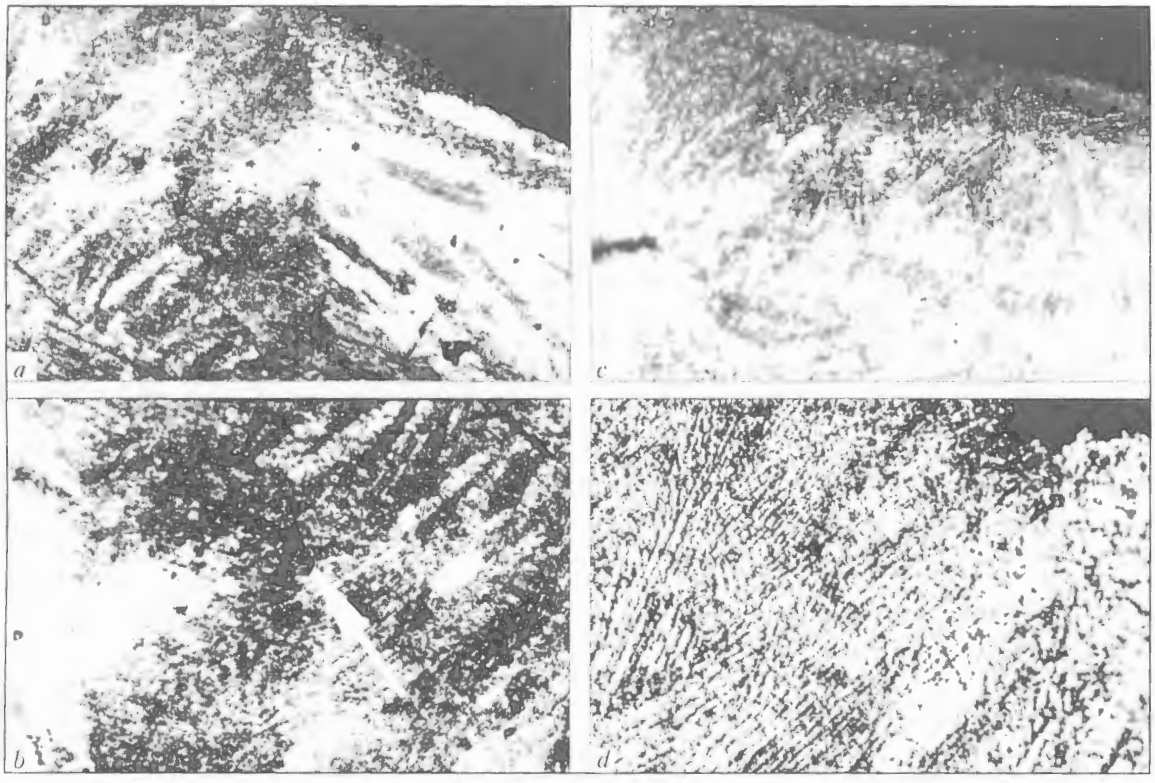

**Figure 3.** Microstructure of weld metal (*c*, *d*) and HAZ (*a*, *b*): *a* – mode No.1; *b* – mode No.3; *c*, *d* – mode No.2 (*a*, *c* – ×100; *b*, *d* – ×150)

tack welds was 30–60 mm, welding current was gradually switched on and switched off on 5 mm length. In the case of large gaps repeated passes were made at higher (by 10–15 %) welding currents, but without complete penetration of the shell wall.

Such considerable gaps for EBW (up to 1.5 mm) in shell assembly into a block are due to the fact that under the current requirements of manufacturing technology the manufacturer cannot ensure reproducibility of the diameter of the shell, on which the circumferential weld is made.

After applying the cosmetic pass, the cast zone of the weld from the face side became somewhat wider (up to 6 mm). Application of repeated passes to fill the gaps and cosmetic treatment of the weld (elimination of surface stress raisers) leads to coarser austenitic grain (Figure 3). However, crack initiation on the junction of three grains was observed only after 3–4 passes of circumferential overlap joints in shells with more than 0.15 mm excess width of the gap.

After multiple filling passes during welding of butt joints in shells with gaps exceeding the admissible values (see the Table, mode No.3), embryo cracks can develop on the weld–base metal boundary (see Figure 3, *b*). Duration of all the operations of welding a block of shells is 2–3 h. In this case, assembly-disassembly takes 0.5–1 h. Quality of welds and efficiency of EBW process are higher than with other processes of fusion welding, used earlier.

## CONCLUSIONS

1. Use of EBW is the optimum solution for alloy of 04KhN60VT grade, where the grain size has a strong influence on the processes of crack initiation.

2. EBW application allows producing minimum grain size in the HAZ metal with minor precipitation of impurities and eutectics along the grain boundaries.

3. Meeting of the requirements to preparation of joints for welding, assembly, as well as selection of EBW parameters allows avoiding cracking.


1. Zemzin, V.N. (1972) *High-temperature strength of welded joints*. Leningrad: Mashinostroenie.
2. Morochko, V.P., Zorin, N.Ya. (1977) Nature and causes of cracking in one-pass electron beam welding of nickel alloys. In: *Proc. of 5th All-Union Conf. on Electron Beam Welding*.
3. Morochko, V.P., Fyodorov, B.M., Andreev, V.D. (1985) Comparison of laser, electron beam and argon-arc welding of heat-resistant nickel alloy KhN68VMTYuK. *Svarochn. Proizvodstvo*, **5**, 13–16.
4. Sims, Ch.T. et al. (1987) *Superalloys II*. John Wiley&Sons.
5. Anik, S., Dorn, L. (1983) Metallphysikalische Vorgaenge beim Schweissen von Nickelwerkstoffen-Einfluss der Werkstoffzusammensetzung. *Schweissen und Schneiden*, **9**, 445–450.
6. Savchenko, V.S., Yushchenko, K.A., Savolej, N.I. et al. (1993) Some principles of hot cracking in welding of cast heat-resistant nickel alloys. *Avtomatich. Svarka*, **3**, 13–16.
7. Savchenko, V.S., Yushchenko, K.A., Savolej, N.I. (1987) Influence of strain rate on susceptibility of stable-austenitic welds to hot cracking in low-temperature brittleness range. *Ibid.*, **10**, 9–12.
8. Yushchenko, K.A., Lipodaev, V.N., Belchuk, M.V. et al. (1986) Resistance of welded joints on heat-resistant nickel alloy of Hastelloy N type to hot cracking. *Ibid.*, **9**, 10–12.
9. Kvasnitsky, V.F. (1985) Welding and brazing of heat-resistant alloys in shipbuilding. *Ibid.*, **10**, 26–30.
10. Slivinsky, A.A., Veit, P. (2003) Structure and properties of welded joints of nickel-based heat-resistant alloy. *The Paton Welding J.*, **5**, 6–12.

# FLUX-CORED WIRES FOR WELDING AND REPAIR OF DEFECTS IN 110G13L STEEL CASTINGS

L.N. ORLOV[1], A.A. GOLYAKEVICH[1], D.P. NOVIKOVA[2], V.N. PELESHKO[3] and V.V. SIMONENKO[3]
[1]TM. WELTECH, Ltd., Kiev, Ukraine
[2]E.O. Paton Electric Welding Institute, NASU, Kiev, Ukraine
[3]Central Ore-Blending Works, Krivoj Rog, Ukraine

Poor weldability of steel 110G13L, caused by a growth in heat input, is outlined. Electrodes, developed at different periods of time for welding Hadfield steel and its dissimilar joints, are described. Characteristic of flux-cored wires WELTECH-H220u and WELTECH-210u, developed by TM. WELTECH for the repair of 110G13L steel castings and welding of dissimilar joints of this steel with steel 20GSL, is given.

***Keywords:*** *arc welding, Hadfield steel, dissimilar joints, weldability, flux-cored wires*

The high-manganese steel 110G13L (C — 1.1; Mn — 13.0 wt.%), owing to its high capability to strain hardening of a manganese austenite [1, 2], has found a wide application for manufacture of products operating under the action of shock, shock-abrasive loads and high specific static pressures. Steel 110G13L possesses a poor weldability due to proceeding of processes of weakening, embrittlement and formation of hot cracks in HAZ metal under the influence of a welding thermal cycle. In this case, the redistribution of alloying elements in the fusion zone, formation of brittle interlayers and transformation of structure of HAZ metal, precipitation of carbides and fusible eutectics along the grain boundaries are observed. Exceeding of optimum values of heat input leads to the increase in thickness of the weakened layer of the HAZ metal that creates difficulties in repair of defects of castings, hardfacing of worn-out surfaces and welding of joints made from dissimilar steels (110G13L + 35GL, 110G13L + 20GSL). At definite concentrations of carbon and manganese the specifics of proceeding diffusion processes in high-manganese steels is manifested in instability of austenite, precipitation of grains of carbides along the grain boundaries and formation of a three-phase structure ($\gamma + \alpha + \varepsilon$) [1–6]. The carbide phase is characterized both by separate dispersed precipitations and also by solid interlayers along the grain boundaries with a different content of alloying elements and their ratio [1, 2, 7, 8].

At present there is a range of welding consumables for welding and repair of defects of castings of 110G13L steel, and also its welding with pearlitic steels 20GL and 35GL [8–10]. For welding critical products, the use of expensive low-carbon electrodes with systems of alloying on the base of Fe–Cr–Ni (OZL-6, NII48G), Fe–Cr–Mn–Ni (ANV-27), Fe–Cr–Mn (ANVM-2) are recommended. Over the recent years the sparsely-alloyed high-manganese electrodes (ANVM-1) have been developed [6, 10, 11].

Enterprise TM. WELTECH has fulfilled integrated works for the development of sparsely-alloyed flux-cored wires for a mechanized repair welding of defects of castings from high-manganese steels and their welding with pearlitic steels. The recent achievements in the field of metallurgy of production and welding of high-manganese steel were realized in the process of development. A special attention was paid to the decrease in content and neutralizing of harmful impurities (S, P, O) in weld metal. Realization of an integrated deoxidation of metal at the stage of drop and pool prevents the formation of fusible eutectics

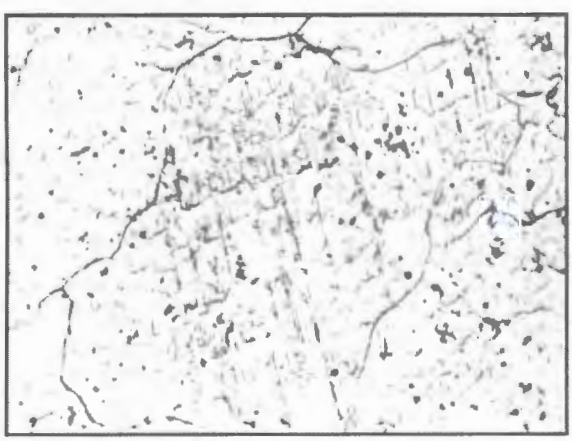

**Figure 1.** Microstructure of weld metal made by the flux-cored wire WELTECH-H220u (×320)

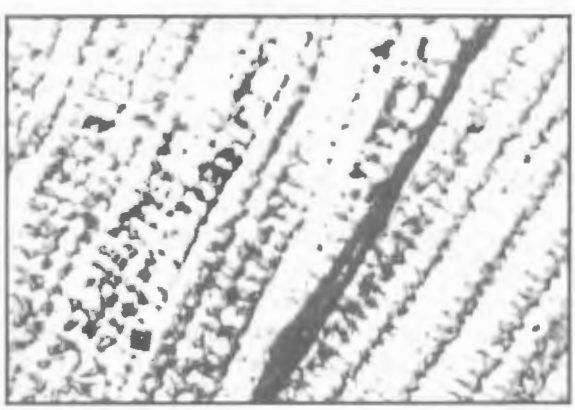

**Figure 2.** Subsolidus hot crack in weld metal with Fe–Mn–Cr alloying system

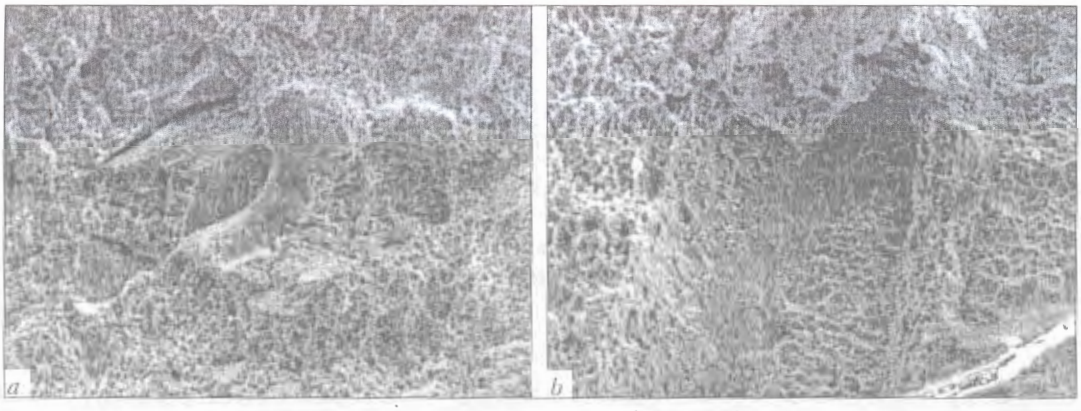

**Figure 3.** Fracture surface of samples at test temperature +20 °C, at tensile (*a* – ×320) and impact bend (*b* – ×400) tests

and iron-manganese oxide films $(MnO)_m(FeO)_n$ along the grain boundaries [2]. To repair the defects in steel 110G13L castings, a self-shielding flux-cored wire of WELTECH-H220u grade of 2.0–2.4 mm diameter has been developed, which provides high-manganese deposited metal with a high stability of austenite. The application of active desulphurizers in combination with a basic slag guarantees the sufficiently low content of harmful impurities ($S \leq 0.01$ and $P \leq 0.016$ %) in the deposited metal. The integrated alloying with manganese, titanium, vanadium, molybdenum and other alloying elements makes it possible to realize the structure of austenite hardened with dispersed carbides [1, 5]. Network of polygonizing boundaries is observed in the grain body (Figure 1). Globular non-metallic inclusions of 0.5–2.0 μm diameter are distributed uniformly in metal and represent complex oxysulphides. Weld metal possesses acceptable mechanical properties: $\sigma_t$ = 680–800 MPa, $\sigma_y$ = 400–500 MPa, $\delta$ = 24–30 %, $KCV$ = = 100–130 J/cm$^2$ at +20 °C. Repair welding of defects of 110G13L steel casting was realized using a standard technology.

As regards to welding of dissimilar steels (110G13L + 35GL, 110G13L + 20GSL) a self-shielding flux-cored wire WELTECH-210u of 2.4–2.6 mm diameter with Fe–Cr–Mn system of alloying has been developed. To produce a stable austenitic structure, the content of manganese, chromium, carbon and nitrogen was optimized [12]. Separate coarse carbides, chains or interlayers of carbides along the grain boundaries were not observed in metal of fusion zone and weld, the dispersed carbides and carbonitrides are distributed uniformly in the grain body and along the grain boundaries. At increased heat input a formation of subsolidus hot cracks are possible (Figure 2). Mechanical properties of weld metal are as follows: $\sigma_t$ = 680–800 MPa, $\sigma_y$ = 500–600 MPa, $\delta$ = = 28–36 %, $KCV$ = 120–150 J/cm$^2$ at + 20 °C. Brittle interlayers were not observed in the zone of fusion with a pearlitic steel. Fractographic analysis of fractures of samples of weld metal, made by flux-cored wires WELTECH-210u and WELTECH-H220u showed that a tough fracture by a mechanism of coalescence of pores independently of test type was characteristic in both cases (Figure 3, *a*, *b*).

The new flux-cored wires have good welding-technological characteristics: stable arc burning, negligible spattering of electrode metal, easy removal of slag crust even in a deep groove of edges, a good appearance of the weld surface. As compared with analogues, the content of manganese oxides in welding aerosol is by 30 % lower. Utilization factor of wire is within the ranges of $K_w$ = 1.15–1.20. The quality control of welded joints did not reveal the defects in the form of porosity and cracks in the deposited metal and welded joint. The flux-cored wires WELTECH-210u and WELTECH-H220u are used successfully at Central Ore-Blending Works (Krivoj Rog city) in manufacture of critical structures.


1. Goudremont, E. (1959) *Special steels*. Moscow: GNTI.
2. Zhitnov, S.V., Davydov, N.G., Bratchikov, S.G. (1995) *High-manganese steels*. Moscow: Metallurgiya.
3. Morozovskaya, E.N. (1967) Structure of near-weld zone in surfacing on G13L steel. *Avtomatich. Svarka*, **7**, 57–59.
4. Gotalsky, Yu.N. (1964) On problem of welding of dissimilar steels structures in long-term service at high temperature. *Ibid.*, **12**, 38–45.
5. Kondratyuk, S.E., Kasatkin, O.G. (1987) *Fracture of cast manganese steel*. Kiev: Naukova Dumka.
6. Lipodaev, V.N., Kakhovsky, N.I., Feldman, V.S. et al. (1977) New materials for welding of 110G13L and 30G steels. *Avtomatich. Svarka*, **9**, 71–73.
7. Malinov, L.S., Kharlanova, E.Ya. (1981) Influence of alloying and prestrain on phase composition and mechanical properties of Fe–Mn alloys. *Metally*, **6**, 141–147.
8. Berezovsky, A.V., Barmin, L.N., Shumyakov, V.I. (1987) Influence of electrode material composition on properties of 110G13L steel welded joints. *Svarochn. Proizvodstvo*, **7**, 26–27.
9. Snisar, V.V., Demchenko, E.L., Bredneva, O.I. et al. (2000) New electrodes for welding and surfacing of steel 110G13L. *The Paton Welding J.*, **5**, 45–47.
10. Gorpenyuk, V.N., Ignatchenko, P.V., Melichenko, S.S. et al. (1994) *Consumables for welding of steels and cast iron (electrodes, fluxes and wires)*. Refer. Book. Kiev.
11. Chejlyakh, A.P., Malinov, L.S. (1994) Properties and transformations of chrome-manganese corrosion-resistant steels. *Metalloved. i Termich. Obrab. Materialov*, **2**, 28–32.
12. Razikov, M.I., Kocheva, G.N., Tolstykh, L.G. (1968) Constitutional diagram of weld metal on chrome-manganese steels. *Avtomatich. Svarka*, **4**, 1–5.

# EUROPEAN PROGRAM NOMAD ON DEVELOPMENT OF A ROBOTIC CELL FOR HIGHLY-EFFICIENT WELDING OF SPECIALIZED STRUCTURES

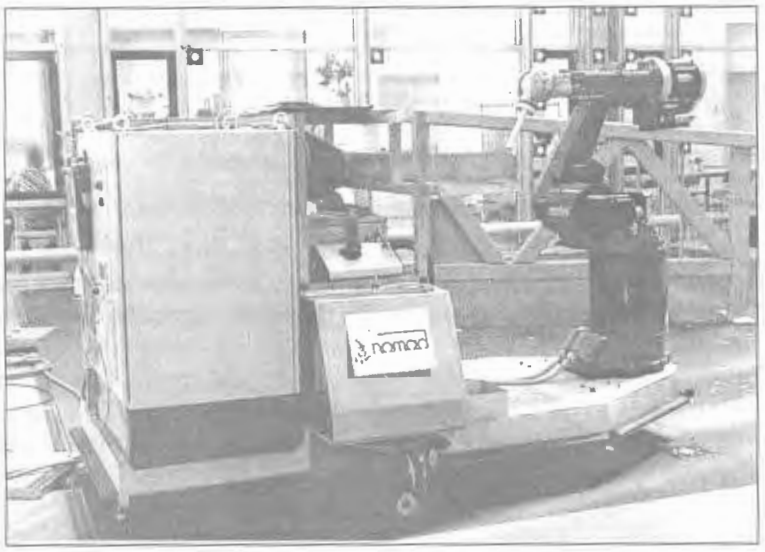


**Figure 1.** Robocar carrying the robot, welding equipment and control systems

NOMAD program is one of the five international programs, which are fulfilled within the European Commission. The aim of the program is development of robotic welding production cells of a new generation. The main point of difference of the cells being developed from the already existing cells consists in that the welding robot, mounted on a special carriage, can move freely inside the cell and perform welding of various structures in keeping with a preset program. In addition to the robot, the carriage also accommodates all the equipment, necessary for MAG welding, as well as blocks for controlling the welding process and carriage displacement (Figure 1). The carriage, which essentially is a robocar, can perform welding of separate structures of up to 50 t weight inside the cell, with the efficiency currently achieved in mass production.

Robocar navigation system finds the structure to be welded, determines its position inside the cell and controls robocar movement to the working position. The block of welding process control uses the database to identify the geometry of the item to be welded, position and geometrical dimensions of the welds and sends to the welding robot the parameters of the technology of structure welding (Figure 2).

Electronic models for welding two items are currently being developed: a fragment of a bridge for Nutsteel Structures Company and booms for Caterpillar excavating machine. The robocar carriage is also being designed. At completion of the project a demonstration robotic production welding unit of the new generation will be mounted in one of Caterpillar enterprises.

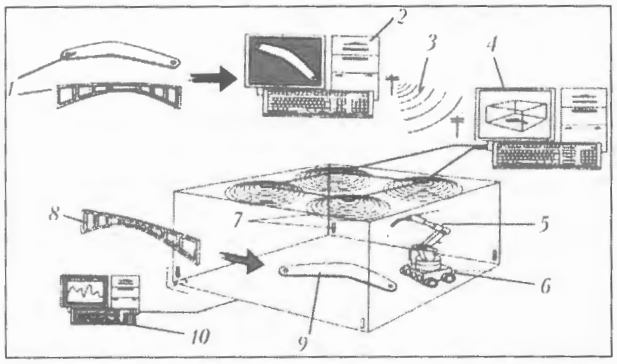


**Figure 2.** Basic elements of a robotic cell for highly-efficient welding: *1* — block of development of product specification; *2* — block of CAD of item welding technology; *3* — data transfer lines; *4* — block of controlling the welding process and carriage displacement; *5* — robotic arm; *6* — carriage; *7* — navigation system; *8* — part prepared for welding; *9* — part during welding; *10* — block of automatic monitoring of the process

Belgium (Caterpillar Company), Great Britain (The Welding Institute), Germany (Vraunhoffer Institute and Reis Company), Finland (Delfoi Company), France (Robosoft Company) and Sweden (ESAB) participate in the project. Project term is 3.5 years; its cost is EUR 4.8 mln, of which 50 % are provided by the European Commission and 50 % — by project partners.

*I.A. Ryabtsev*

# *INFORMATION FOR CONTRIBUTORS TO*
# THE PATON WELDING JOURNAL

THE PATON WELDING JOURNAL is a scientific journal publishing fundamental and applied papers and short notes in the area of

- *weldability of structural materials*
- *welding different types of steels and cast irons*
- *welding non-ferrous metals, including aluminium, titanium, etc.*
- *joining dissimilar and composite materials*
- *welding refractory metals and alloys*
- *welding cryogenic materials*
- *joining polymers*
- *arc welding*
- *flash-butt welding*
- *electron beam and laser welding*
- *explosion welding and cutting*
- *friction welding*
- *electroslag welding*
- *soldering and brazing*
- *advanced structural materials*
- *surfacing and coating*
- *cutting*
- *computer technologies in welding*
- *strength of welded joints and structures*
- *welding stresses and strains*
- *calculation and design of welded joints and structures*
- *automation of welding fabrication*
- *estimation of residual life of welded structures*
- *welding for fabrication of unique structures*
- *welding and repair in thermal and nuclear power engineering*
- *advances in underwater welding, cutting and repair*
- *welding in Space*

The journal accepts also advertisements and announcements of conferences and publications on related topics.

THE PATON WELDING JOURNAL is published monthly. Subscription requests should be sent to the Editorial Office.

Manuscripts should be submitted in duplicate in English, and supplemented with a text file and figures on a diskette. An electronic copy may be submitted by e-mail.

The rules for submission of electronic copies are as follows:

- an electronic copy should be submitted on a diskette or by e-mail simultaneously with sending a hard copy of the manuscript;
- acceptable text formats: MultiEdit (txt), MS Word'97 (rtf, doc);
- acceptable graphic formats for figures: EPS, TIFF, CDR. Figures created using software for mathematical and statistical calculations should be converted to one of these formats.

**Manuscripts should be sent to**

Aleksander T. Zelnichenko
Executive Director of Project
«The Paton Welding Journal»,
11, Bozhenko Str.,
03680, Kyiv, Ukraine
PWI, International Association «Welding»
Tel.: (38044) 227 67 57, Fax: 268 04 86
E-mail: journal@paton.kiev.ua
E-mail: tomik@mac.relc.com

***Manuscripts should be supplemented with***

- official letter signed by a chief manager of the institution where the work was performed. This rule does not apply to papers submitted by international groups of authors;
- publication permission: conclusion of a commission authorized to permit open publication of the paper (only for authors from Ukraine).

***Title Page:***

- title of the paper and name(s) of the author(s);
- name of affiliated institution, full address, telephone and fax numbers, e-mail addresses (if available) for each author.

***Abstract:*** up to 100 words, must be presented in English. Before the abstract text one should indicate in the same language: the paper title, surnames and initials of all authors.

***Key words:*** their amount must not exceed eight word units. In the specific cases it is acceptible to use two- or three-word terms. These words must be placed under the abstract and written in the same language.

***Text*** should be printed double-spaced on white paper (A4 format) with a 12-point font. Titles of the paper and sections should be typed with bold capitals.

***Tables*** should be submitted on separate pages in the format of appropriate text processors, or in the text format (with columns separated by periods, commas, semicolons, or tabulation characters). Use of pseudographic characters is not allowed.

***List of references*** should be double-spaced, with references numbered in order of their appearance in the text.

***Captions for figures and tables*** should be printed in the manuscript double-spaced after the list of references.

***Pictures*** will be scanned for digital reproduction. Only high-quality pictures can be accepted. Inscriptions and symbols should be printed inside. Negatives, slides and transparencies are accepted.

***Figures:*** each figure should be printed on a separate page of the manuscript and have a size not exceeding 160 × 200 mm. For text in figures, use 10-point fonts. All figures are to be numbered in order of their appearance in the text, with sections denoted as (a), (b), etc. Placing figure numbers and captions inside figures is not allowed. On the back side, write with a pencil the paper title, author(s) name(s) and figure number, and mark the top side with an arrow.

***Photographs*** should be submited as original prints.

Color printing is possible if its cost is covered by the authors or their sponsors. For information about the rules and costs, contact the Executive Director.

No author's fee is provided for.

Publication in TPWJ is free of charge.